

Phenomena in Gravitational Clustering

A thesis submitted to the
University of Pune
for the degree of
Doctor of Philosophy
(in Physics)
by
Sunu Engineer

Inter-University Centre for Astronomy and Astrophysics
Post Bag 4, Ganeshkhind, Pune 411 007, India

September 2003

Contents

Declaration	ix
Acknowledgements	x
Abstract	xi
1 Introduction	2
1.1 Background Cosmology	4
1.2 Dynamics of matter	9
1.3 Linear perturbation theory	12
1.4 Nonlinear approximations	13
1.4.1 Zeldovich approximation	13
1.4.2 Spherical model	15
1.5 N Body Simulations	18
1.6 Statistical indicators	26
1.7 Nonlinear scaling relations	29
2 Nonlinear gravitational clustering: Dreams of a paradigm	33
2.1 Introduction	33
2.2 General features of nonlinear evolution	36
2.2.1 <i>Formal solution</i>	37

2.2.2	<i>Critical indices</i>	39
2.3	Correlation functions, density profiles and stable clustering	40
2.4	Self-similar evolution	46
2.5	Units of the nonlinear universe	49
2.6	Results and Summary	59
3	A formal analysis of two dimensional gravity	62
3.1	Introduction	62
3.2	Formal $(D + 1)$ dimensional gravity	65
3.2.1	Poisson equation in D dimensions	66
3.2.2	Friedmann Universe in $(D + 1)$ dimensions	69
3.3	Structure formation in D dimensions	71
3.3.1	Equation for density perturbations in D dimensions	71
3.3.2	The Spherical Top Hat (STH) model	75
3.4	Summary of standard results in three dimensions	76
3.5	Two dimensional gravity	77
3.6	Results and Summary	82
4	Scaling Relations in Two Dimensions	83
4.1	Gravitational Clustering: Two vs Three Dimensions	83
4.1.1	Non-linear Scaling Relations	85
4.2	Simulations and Results	87
4.3	Summary	90
5	An improved spherical collapse model	95
5.1	Introduction	95
5.2	The Spherical Collapse Model	98

5.3	The $h_{\text{SC}}(\delta)$ function.	102
5.4	Detailed derivation of equation for h function	108
5.5	The virialization term	110
5.6	Results and Summary	121
6	Structure formation in QSSC	123
6.1	Introduction	123
6.2	The Basic Theory of the QSSC	125
6.2.1	Matter Creation	127
6.2.2	The Cosmological Solution	128
6.2.3	Observational Checks	129
6.3	A Toy Model for Formation of Structures	130
6.3.1	2D-Simulations	130
6.3.2	3D-Simulations	134
6.3.3	Simulations of QSSC Cycles	135
6.4	The Two Point Correlation Functions	136
6.5	Results and Summary	141
7	Conclusions	143

List of Figures

1.1	The Las Campanas Redshift Survey	3
1.2	The scale factor (solid line) for a $\Omega = 1$ universe with the solution for radiation dominated epoch (dashed line) and matter dominated epoch (dot dashed line) superposed on it.	8
1.3	N-body simulation at $a=0.25$ ($n=-1$. Power law spectrum).	15
1.4	Zeldovich approximation at $a=0.25$ ($n=-1$. Power law spectrum). The correspondence between structures in the full Nbody simulation is evident.	16
1.5	N-body simulation at $a=0.5$ ($n=-1$. Power law spectrum).	17
1.6	Zeldovich approximation at $a=0.5$ ($n=-1$. Power law spectrum). The thickening and dissolving of the structures formed is clear leading to breakdown of Zeldovich approximation.	18
1.7	The nonlinear density contrast versus the linear density contrast for the spherical collapse model	19
1.8	The flow field at $a=0.5$	24
1.9	The flow field at $a=1.5$. It can be seen that the velocity vectors flow along the caustics (filaments) towards the cluster centers	25
1.10	The flow field at very late times. The flow is almost completely con- centrated at the centers. The particles participating in these flows transfer power from large scales to small scales	26

1.11 Different statistical indicators such as the two point correlation function and $\Delta^2(k) = k^3 P(k)/(2\pi^2)$. ($\Delta(k)$ – dashed line, $\bar{\xi}$ – solid line, σ_{sph} – dotted line, σ_{gauss} – dash dot line for a standard CDM power spectrum with $k = 1/l$	29
1.12 The mass function plotted as the log of fraction of mass in structures more massive than M ($\ln(\Omega)$) as a function of $\sigma(M)$ for different redshifts $z=0,1,2,3,4,5$ from top to bottom.	30
1.13 The nonlinear scaling relation between nonlinear and linearly scaled two point correlation function.	31
1.14 The linearly scaled two point correlation function (solid line) and the nonlinear two point correlation function of CDM power spectrum at a late epoch ($a=1$)	32
2.1 The approximate solution to the functional equation determining the pseudo-linear profile.	54
2.2 The dot-dashed,dashed and two solid curves (upper one for $a^2 = 100$ and lower one for $a^2 = 900$) are for $a^2 = 1, 9, 100$ and 900 . The dotted straight line is of slope -1 and the solid one is of slope-2 showing both the $1/x$ and $1/x^2$ regions of the profile.	56
4.1 Two dimensional scaling relation for power law spectra	89

4.2 The correlation function $\bar{\xi}(x)$ as a function of x/x_{nl} for $n = 1$ model. Here $x_{nl} \propto a^{-2/(n+2)}$. Thick lines mark slopes expected from the non-linear scaling relations shown in fig. 4.1. The dashed line marks the expected slope of the correlation function in the stable clustering limit. The mismatch between the expected slope and the true slope in the intermediate regime may arise from the fact that the assumption of $\bar{\xi} \gg 1$ used in computing the slope is not valid at the lower end of the regime.	91
4.2 Similar plot for $n = 0$	92
4.2 $n = -0.4$	93
5.1 $y_q(x)$ for some values of q . The x axis has scaled time, x and the y axis is the scaled radius y	112
5.2 The parameters (R_{max}/r_{vir}) (broken line) and x_c (solid line) as a function of $q = B/A^2$. This clearly demonstrates that the single parameter description of the virialization term is constrained by the value that is chosen for the ratio r_{vir}/R_{max}	114
5.3 The h_{SC} function, obtained for various values of q . The values of q and $y_{max} \equiv R_{max}/r_{vir}$ for the curves are indicated at the top right hand corner. (Further discussion in text)	114
5.4 The best fit curve for the h function (dashed line) to the simulation data (solid line). The simulation results are obtained from Hamilton [19] and the fit is obtained by adjusting the value of q parameter until the curves coincide.	118

5.5 Plot of the scaled radius of the shell y_q as a function of scaled time x (solid line) and the fitting formula $y_q = (x+ax^3+bx^5)/(1+cx^3+bx^5)$, with $a = -3.6$, $b = 53$ and $c = -12$ (dashed line) (See text for discussion)	118
5.6 The non-linear density contrast in the SCM (solid line) and in the modified SCM (dashed line), plotted against the linearly extrapolated density contrast δ_L	119
6.1 The scale factor $S(t)$ of the QSSC in the upper panel against t to show how several oscillatory cycles of short period Q are accommodated in the longer e -folding time P of the exponential expansion. In the lower panel are sketched a few oscillations on an expanded timescale with our present epoch marked.	129
6.2 A cluster-void distribution generated in the $2D$ toy model for $N = 100,000$ initially randomly distributed particles, with typical separation parameter $x = 0.8$, and the number of iterations $n = 10$. Each particle resembles a galaxy. For further discussion see the text.	131
6.3 Schematic procedure for creating units in aligned direction for $n > 2$. Particle A is a representative of first generation units which are distributed randomly. B is a representative of the second generation units, being created in a random direction. Point C represents a third generation unit which has been created in the half plane lying away from A off the line perpendicular to AB . BC therefore makes an acute angle, φ , with the line ABB'	132

6.4 A computer simulated filament-void distribution with $n(> 2)$ iterations of aligned ejections having new points following the rule of Figure 6.3, for the same parameters of Figure 6.2.	133
6.5 A power law $2D$ simulation in the standard big bang cosmology for power index, $n = -0.4$ of density fluctuations.	134
6.6 A 3-dimensional version, adapted for the QSSC with $N = 1,000,000$, $x = 0.3$, $n = 10$, and $P/Q = 20$. Slice thickness in the Z direction is $\Delta Z = 0.001$. Evidently, voids are seen separated by filamentary structures. The left panel is for the case of isotropic distribution of particles, whereas the right panel shows the case of aligned ejections.	136
6.7 A FLAIR redshift survey in the direction of Hydra-Centaurus[54] . . .	137
6.8 The two point correlation function for the QSSC based model. Here, $N = 100,000$ and $x = 0.3$. As “time” goes on, the curve approaches more and more closely the slope of -1.8 . The solid curve shows the result after 10 iterations.	141

Declaration

CERTIFIED that the work incorporated in the thesis

Phenomena in Gravitational Clustering

submitted by **Sunu Engineer** was carried out by the candidate under my supervision. Such material as has been obtained from other sources has been duly acknowledged in the thesis.

Place: IUCAA, Pune

T. Padmanabhan

Date: September 2003

(Thesis supervisor)

Acknowledgments

A teacher affects eternity; he can never tell where his influence stops – Henry Adams

To paddy,

Akhandamandalakaram, vyaptham yena characharam

Tatpadam darshitam yena, tasmai shree gurave namah

Thanks to all my colleagues, who helped in this adventure of life, love and gravitation.

and to the people who started me off on this adventure and my friends who kept me on this songline until it was done.

Abstract

We can lick gravity but sometimes the paperwork is overwhelming – Werner von Braun

The problem of large scale structure formation in the universe is one of the core problems of cosmology today. This thesis discusses some of the issues involved in explaining how the observed large scale structure in the universe came to be.

This thesis has two distinct parts. The first part (chapters 1–5) discusses the issues of structure formation from the view point of standard model of structure formation. Chapter 6 discusses alternate cosmologies and structure formation scenarios in them.

In the standard approach we will explore the problem of structure formation through gravitational clustering in the universe. The sizes of numbers involved renders a microscopic viewpoint cumbersome. We have to adopt a statistical procedure which essentially averages over many particles and their individual behavior to give us some entities which we shall call “particles” whose behavior we can describe more easily. Alternatively we can replace the discrete structure of particles by a continuum approximation, thinking of the system of particles as a continuous fluid and apply the theoretical models of fluid mechanics to describe cosmological systems. In either of the approaches we run into a similar problem. When we frame the equations that describe the system, we find that the equation has terms which are highly nonlinear, leading to an analytically

intractable system of equations. An analytical solution to the relevant equations can be obtained only if one assumes that the system is linear, *i.e* one drops all the terms that are nonlinear in the parameter of interest. But the degree of nonlinearity associated with observed structures in the universe like galaxies is of the order of 10^3 . Thus we need to deal with the nonlinear terms in the equations to establish correspondence with observational results. The nonlinear terms elude a simple description, in that a general solution is not yet found. But since we have to study the behavior of this equation at highly nonlinear regions we try to model the behavior in a variety of ways.

1. Various approximation schemes such as Zeldovich approximation, frozen potential approximation, frozen flow approximation and adhesion approximation attempt to take us a little beyond linear theory.
2. Numerical simulation techniques attempt to integrate the equations either in terms of a particle based approach or a field based approach (or a combination of the two). N Body simulations form the mainstay of this approach.
3. An alternate technique treats evolution in time and space as a mapping problem and tries to find an appropriate map that takes us from one point in the history of the universe to another in a global sense. Scaling laws and other ansatzes fall under this category.

In this thesis we will be concerned with all the three approaches but with a preferential leaning towards the second and third approaches. Herein we explore the utility of the third method in various aspects of the study of structure formation and the insights it provides into dynamics of gravity in shaping the observed structures.

The first chapter gives a concise overview of the background.

Chapter 2 of this thesis uses the third approach to generate nonlinear quantities from their linear theory counterparts and applies it to the question of “universal” profiles in gravitational clustering. We addressed the problem by asking the following question: Is it possible to populate the nonlinear universe with structures such that the two point correlation function evolves as per linear theory in all regimes? We find that it is not possible to have strict linear evolution but it is possible to find functional forms such that approximate linear evolution to any desired order is possible. The earlier investigations had indicated that the evolution of density contrast can be separated into three regimes namely linear, quasilinear and nonlinear. We have found a functional form which evolves approximately linearly in quasilinear and nonlinear ends of the two point correlation function. It is also conjectured in this chapter that it should be possible to find basis functions which may be based on such approximately invariant forms such that the nonlinear density fields can be decoupled to a large extent if expanded in terms of these functions. We suggest that the functions that we have derived which evolve approximately linearly in all regimes might be a good candidate for the role of “units of nonlinear universe”. Another aspect of the analysis tries to discover universal aspects of the structures formed via gravitational clustering such as density profiles.

Chapter 3 critically examines the theoretical framework underlying two dimensional N body simulations. If one has to get requisite amount of dynamical range in force and mass one requires large grids and large number of particles which is not possible given the computing resources available. One attempts to get around this problem by trying to do the simulations in two dimensions which brings the computational requirements down by a considerable amount. So if it is

possible to extract fundamental principles which may be generalized to the case of three dimensional gravity from such simulations then they are a good way of exploring the fundamental features of gravity.

There are three ways in which we can define a two dimensional gravitational clustering scenario: (i) A set of point particles interacting by $1/r^2$ force but with a special set of initial conditions such that they are confined to a plane and have no velocity components orthogonal to the plane (ii) A set of infinite parallel “needles” in which each particle interacts with $1/r^2$ force but the “needles” interact with a $1/r$ force (iii) A description derived from Einstein’s equations in two dimensions.

Approach (i) is highly contrived and we will not discuss it. The second approach based on infinite “needles” suffers from the problem of manifest anisotropy because the universe is considered to be expanding in three dimensions while the clustering takes place only in two dimensions. In order to explore the third approach we developed the formal theory of gravity in $D + 1$ dimensions and considered $D = 2$ as a special case. The formal analysis of $D + 1$ dimensional gravity led us to the general expressions for scale factor and background density in the $D + 1$ dimensional universe.

Taking the usual Newtonian limit of the metric and writing down the equation describing the growth of density perturbations in the universe via a fluid approach made it possible to obtain the $D + 1$ dimensional analogue of the equation describing growth of density contrast. A corresponding formula for spherical collapse model is also derived in this work. We then specialize to the case of $D = 2$ and make the following observations. The linearized form of the density contrast equations only yield a constant or decaying solution. This is consistent with the result that perturbed gravitational potential does not couple to density contrast δ . The spherical collapse model solution yields a similar result in the

sense that it is not possible to have a gravitational clustering model that grows in time. It is possible to obtain clustering by an *ad hoc* approach by making some assumptions but they also lead to inconsistent results in that they give rise to singular solutions for the scale factor of the universe. Thus we conclude that the infinite “needle” based approach is the only viable way of simulating two dimensional gravity.

In Chapter 4 some of the issues involved in two dimensional gravitational simulations are discussed. Nonlinear scaling relations, which have been identified in three dimensional simulations, define a mapping from initial linear theory values of two point correlation function to the final nonlinear values at a different length scale. This allows us to immediately compute the nonlinear parameter at a specific length scale knowing the value of the linear one at some other length scale. We wish to check the theoretical prediction that similar nonlinear scaling relations hold in two dimensions. Another aspect of universal behavior of gravitational clustering that is conjectured is called “stable clustering”. This is the conjecture that at late times structures have their gravitational infall balanced by background expansion leading to a fixed profile. By applying this conjecture to the theoretical model for the NSR (nonlinear scaling relations) it is possible to derive the theoretical dependence of the NSR in two dimensions if it exists. Our conclusions regarding two dimensional gravitational clustering based on the simulations are as follows. (i) The prediction is verified and a form of nonlinear scaling relation exists for the two point correlation function in two dimensions as well. This NSR is independent of the spectrum for the spectra (power laws) considered in this study. (ii) In the quasilinear regime the theoretical model based on infall onto peaks predicts a dependence that is confirmed by the numerical experiments. (iii) In the highly nonlinear regime the results diverge from

that predicted by the “stable clustering” hypothesis. The “stable clustering” hypothesis demands that the ratio between infall velocity and expansion velocity go to unity but we find that it is driven towards 3/4. Thus we find that stable clustering is not a valid hypothesis in two dimensions.

Chapter 5 addresses the question: What happens at the late stages of clustering?. The hypothesis of stable clustering asserts that at some point the system ‘virialises’. We examine this process of virialisation and stabilization in more detail by analyzing what happens to a single spherically symmetric object as it goes through the cycle of expansion and collapse. By including a term that describes the asymmetries that are generated and enhanced during collapse we examine the final state of the system. We begin by writing a modified equation for the spherical collapse of a system which includes a term which takes into account the asymmetries that are generated during the process of collapse and we derive a functional form for this “asymmetry” term by an ansatz that this term depends only on density contrast δ . Since we have a relation connecting density contrast with the pairwise velocity function h , it is now possible to close the system of equations. We require the form of the h function before we can integrate this system of equations. By using the fact that the system must reach a constant value for h we obtain a functional form for the “asymmetry” term which allows us to integrate the equation and analyze the collapse of a single object. This leads us to conclude that the system reaches a constant value of 0.65 times the maximum radius which is not widely off the value of 0.5 that is usually stipulated. Thus we demonstrate that the growth of asymmetries can be used to stabilize the collapse.

In Chapter 6 the question of approaching the problem of structure formation from other alternate cosmological scenarios is discussed. To address this ques-

tion in the context of Quasi Steady state cosmology is the theme of the work discussed here. An algorithm was devised which mimicked the basic physical content of QSSC (Quasi Steady State Cosmology) model by the following geometrical method. We generate N random points and require that in the next cycle the volume becomes eight times the initial volume (due to the expansion) and the particles generate new mass particles in their vicinity. Then we select the central volume equal to the initial volume and repeat this scale and shrink process. To apply this algorithm in the context of QSSC model we use the fact that only a fraction of the particles given by $f = 3Q/P$ where Q and P are parameters of the QSSC model create new masses in the next generation. Consequently the scaling used is $\exp(f)$. We have succeeded in showing that this model reproduces the observed two point correlation function with a slope of -1.8 . Visual analysis shows clear indication of the clustering growing and the initial smooth distribution separating into voids and clumps. This approach is characterized by the fact that clustering in this model takes place without the help of gravity, *i.e* gravity plays no role in inducing clustering.

The final chapter of the thesis presents the conclusions and integrated discussion based on the previous chapters.

This thesis is based on the following publications.

1. T. Padmanabhan, **S. Engineer**, *Nonlinear gravitational clustering: dreams of a paradigm*, Ap.J **493**,(1998).
2. J.S.Bagla, **S. Engineer**,T. Padmanabhan, *Scaling Relations for gravitational clustering in two dimensions*, Ap.J **498**,(1998).
3. **S. Engineer**, K.Srinivasan, T. Padmanabhan, *A formal analysis of (2+1)-dimensional gravity*, Ap.J **512**,(1999).
4. Ali Nayeri, **S. Engineer**,Jayant Narlikar and F. Hoyle, *Structure formation in Quasi Steady State Cosmology: A toy model*, Ap.J **525**,(1999).
5. **S. Engineer**, Nissim Kanekar and T. Padmanabhan, *Nonlinear density evolution from an improved spherical collapse model*, MNRAS **314**,(2000).

Chapter 1

Introduction

Duct tape is like the force. It has a light side, a dark side and holds the universe together. – Carl Zwanzig

Observations of the universe in multiple wavelengths have revealed large aggregates of matter on all length scales. Figure 1.1 shows the distribution of galaxies from Las Campanas Redshift survey which clearly shows clustering in the distribution of galaxies. The formation and existence of large scale structures such as galaxy clusters and superclusters is an important problem in cosmology. In spite of the inhomogeneities on these scales it is also observed that on very large length scales ($> 300Mpc$) the universe appears homogeneous. This permits the universe to be modelled as being made up of statistically similar volumes of linear dimensions of about $300Mpc$ or more. Standard cosmological models based on General Theory of Relativity are derived from this assumption of statistical homogeneity and isotropy of the universe. The problem of large scale structure formation in these models thus involves explaining how the observed inhomogeneities and anisotropies were initially generated in this uniform background and how they grew into the observed structures. Once a mechanism for generating the initial perturbations of the smooth distribution of matter is postulated the transition from uniformity on large scales, to the highly non uniform structures at small scales, can be explained by gravitational clustering. Obser-

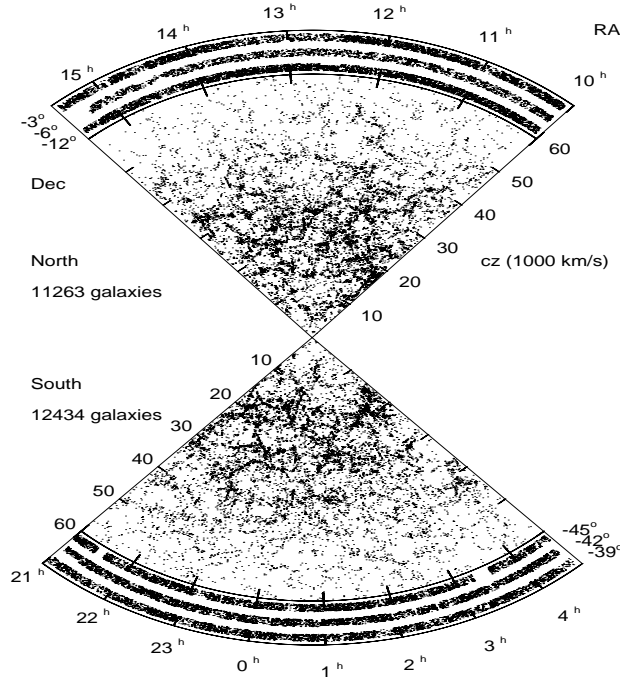


Figure 1.1: The Las Campanas Redshift survey (<http://www.lcgs.com>)

vations by space experiments (COBE, WMAP etc.) have revealed the presence of small inhomogeneities in the uniform density fields of matter at early times. It is assumed that these seeds evolved via gravitational clustering into the observed large scale structures and experienced a multitude of non gravitational phenomena at small scales (such as star formation) to evolve into the present day universe of clusters and galaxies.

This chapter introduces the basic framework of this model in brief. It is organized as follows. The first section 1.1 summarizes the main features of the smooth background cosmological models. The following section 1.2 discusses the equations governing the dynamics of matter in this expanding background cosmology in discrete and continuum approximations. Section 1.3 discusses the solutions of

this nonlinear system of equations in linearised regime. Nonlinear approximation schemes such as Zeldovich approximation and spherical top hat approximation are discussed in section 1.4. Section 1.5 deals with N body computer simulations as a way of modeling and studying some features of nonlinear structure formation. Various statistical measures used to quantify and analyze the formation of structures are discussed in section 1.6. Section 1.7 deals with an alternate approach to time evolution of some statistical quantities, thus obviating the need for expensive and time consuming full scale N body simulations.

1.1 Background Cosmology

A model appropriate for a universe dominated by gravity on large scales, is best formulated in the context of General theory of Relativity. This model, which will be referred to as the ‘background cosmology’, is described by the metric of the spacetime. The evolution of the metric is governed by the energy density distribution through Einstein’s equation given by

$$G_k^i = R_k^i - \frac{1}{2}\delta_k^i R = 8\pi G T_k^i \quad (1.1)$$

where G_k^i is the Einstein tensor, G the gravitational constant and T_k^i the energy momentum tensor. The ‘cosmological principle’ which assumes a statistically homogeneous and isotropic universe is further used to constrain the form of the metric of the universe to ([36],[38],[45],[46])

$$ds^2 = dt^2 - a^2(t) \left[\frac{dr^2}{1 - kr^2} + r^2(d\theta^2 + \sin^2 \theta d\phi^2) \right] \quad (1.2)$$

(we use the convention $c = 1$ consistently throughout unless explicitly indicated). This metric is completely characterized by a time dependent function *scale factor* $a(t)$ and *curvature* k . The constant k determines the geometry of the universe —

(the curvature of the spatial hypersurfaces of the Friedmann universe) — taking the values $k > 0$ in a closed universe, $k = 0$ in a flat universe and $k < 0$ in an open universe. The ‘fundamental observers’ to whom the universe appears isotropic and homogeneous remain at constant (r, θ, ϕ) with their physical separation increasing in proportion to scale factor $a(t)$ which determines the overall scale of the spatial metric. An observational consequence of expansion is that the light emitted by a source at time t is observed now, at $t = 0$ with a cosmological ‘redshift’ $z = a_0/a(t) - 1$ where $a_0 = a(t = 0)$. Another quantity of primary significance in observational cosmology is the ‘Hubble Constant’ H defined by $H = \dot{a}/a$, which measures the rate at which the universe is expanding at a given point in time. The value of ‘Hubble constant’ today is denoted by $H_0 = 100 h \text{km s}^{-1} \text{Mpc}^{-1}$ with $0.52 < h < 0.62$ [55].

The ‘cosmological principle’ also constrains the source term in Einstein’s equations, namely the energy momentum distribution, so as to make it consistent with the assumed homogeneity of the metric, leading to a diagonal form $T_\beta^\alpha = \text{dia}[\rho(t), -p(t), -p(t), -p(t)]$. This form is motivated by the assumption of the source to be an ideal fluid with pressure p and density ρ , whose stress tensor has the above form in the rest frame of the fluid. Under these assumptions, an extra equation of state connecting p and ρ allows the source to be completely determined.

When this source term is plugged into equation 1.1, the Friedmann equations

$$\frac{\dot{a}^2 + k}{a^2} = \frac{8\pi G}{3}\rho \quad (1.3)$$

$$\frac{2\ddot{a}}{a} + \frac{\dot{a}^2 + k}{a^2} = -8\pi Gp \quad (1.4)$$

for the scale factor $a(t)$ which determines the metric given the curvature k , are obtained.

From equation 1.3 we can define the value of curvature k by

$$\frac{k}{a_0^2} = \frac{8\pi G}{3}\rho_0 - H_0^2 = H_0^2(\Omega - 1) \quad (1.5)$$

where a_0 is the scale factor at present and $\Omega = \rho_0/\rho_c$ where ρ_0 is the present value of density and $\rho_c = 3H_0^2/8\pi G$ is called the critical density. Equation 1.5 shows that the universe will be open, closed or flat depending on the values of Ω being less than, more than or equal to one respectively.

We assume that the total ρ of the universe may be separated into contributions from the various constituents of the the cosmic fluid. Other than radiation and baryonic matter there is compelling evidence for the presence of a dominant component that does not interact with light and is consequently not directly observable, called the ‘dark matter’. There is also good observational evidence for the presence of a vaccum energy density ρ_v [3]. For each component of energy density ρ with an equation of state given by $p = p(\rho)$, the density varies with the scale factor according to energy conservation

$$d(\rho a^3) = -pd(a^3) \quad (1.6)$$

For a generic equation of state given by $p = w\rho$, equation 1.6 gives $\rho \propto a^{-3(1+w)}$. The equations of state for radiation component of the fluid is $p = \frac{1}{3}\rho$ and for the non relativistic pressureless dust, $p = 0$ [36]. Defining $\Omega_x = \rho_x/\rho_c$ where the subscript x is r for radiation, nr for nonrelativistic matter which has contributions from both baryonic matter ρ_B and ‘dark matter’ ρ_{DM} , v for the vaccum energy density, we can write the complete time dependence of the scale factor $a(t)$ as

$$\rho_{tot}(a) = \rho_{crit} \left[\Omega_r \left(\frac{a_0}{a} \right)^4 + (\Omega_B + \Omega_{DM}) \left(\frac{a_0}{a} \right)^3 + \Omega_v \right] \quad (1.7)$$

$$\frac{\dot{a}^2}{a^2} = H_0^2 \left[\Omega_r \left(\frac{a_0}{a} \right)^4 + \Omega_{nr} \left(\frac{a_0}{a} \right)^3 + (\Omega - 1) \left(\frac{a_0}{a} \right)^2 + \Omega_v \right] \quad (1.8)$$

The radiation density varies as a^{-4} whereas the matter density goes as a^{-3} . This has the interesting consequence that although radiation density is much smaller than matter density today, in the past the radiation field dominated. The point in time where the densities were equal is defined as the ‘matter-radiation equality’. The dynamics of the universe from this epoch is dominated by matter, and we speak of ‘radiation dominated epoch’ as opposed to ‘matter dominated epoch’. The redshift of equality z_{eq} and the value of Hubble constant at equality H_{eq} are defined by, (neglecting curvature and radiation components)

$$\frac{a_0}{a_{eq}} = \frac{\Omega_{nr}}{\Omega_r} = (1 + z_{eq}) \quad (1.9)$$

$$H_{eq}^2 = 2H_0^2\Omega_{nr}(1 + z_{eq})^4 \quad (1.10)$$

Since the curvature term and the vacuum energy terms do not contribute significantly in early times [36], analytical solutions to 1.7 valid for $t \gg t_{eq}$ and $t < t_{eq}$ may be obtained, where t_{eq} is the time of equality.

$$\frac{a}{a_{eq}} \approx \left(\frac{3}{2\sqrt{2}} \right)^{2/3} (H_{eq}t)^{2/3} \quad (\text{for } t \gg t_{eq}) \quad (1.11)$$

$$\frac{a}{a_{eq}} \approx \left(\frac{3}{\sqrt{2}} \right)^{1/2} (H_{eq}t)^{1/2} \quad (\text{for } t \ll t_{eq}) \quad (1.12)$$

Figure 1.2 shows the complete evolution for the scale factor $a(t)$ (obtained by integrating Eq.(1.8)with Ω_v and $(\Omega - 1)$ terms neglected) with the solutions in the matter dominated and radiation dominated regimes superposed.

In the standard model, the initially hot universe whose evolution is dominated by radiation energy transitions to a matter dominated structure at $z \sim 10^4$. In this hot universe, electrons and photons couple to each other via scattering processes such as Thompson scattering. At $z \sim 1100$ the temperature cools enough for neutral hydrogen to form and the photons and matter decouple. The photons then travel freely, cooling adiabatically, until they are observed at the present time

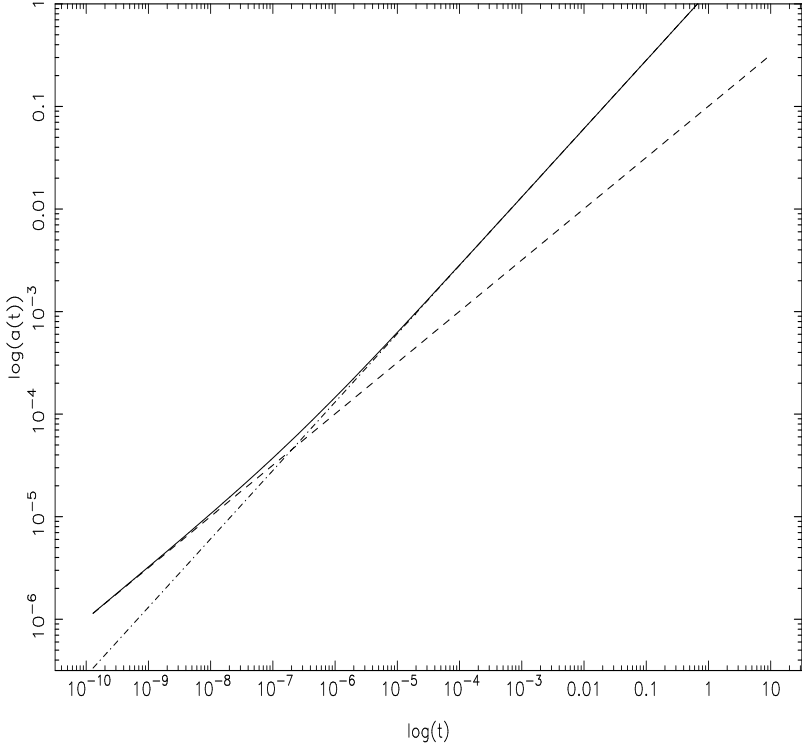


Figure 1.2: The scale factor (solid line) for a $\Omega = 1$ universe with the solution for radiation dominated epoch (dashed line) and matter dominated epoch (dot dashed line) superposed on it.

as the $2.73K$ cosmic microwave background (CMB) radiation. The observations of CMB ([1],[2]) show that the universe at the time of formation of neutral hydrogen (last scattering surface) was extremely uniform with fractional fluctuations in energy density (and consequently in gravitational potential) of approximately 10^{-5} . These small fluctuations, are the seeds of the large scale structures seen today. They are amplified through gravitational interaction, eventually leading to the formation of galaxies and stars.

1.2 Dynamics of matter

To analyse the evolution of matter in this expanding background a dynamical model which describes how matter aggregates under the influence of force of gravity in an expanding universe is required.

If the system has to be described in its full generality one must use a general relativistic description. But one can use a ‘Newtonian’ approximation valid for certain regimes by finding the effective ‘Newtonian limit’ of the Friedmann metric [38]. Applying the transformation to new variables R and T defined by

$$R = ra(t) \quad (1.13)$$

$$T = t - t_0 + \frac{1}{2}a\dot{a}r^2 + \mathcal{O}(r^4) \quad (1.14)$$

on eq 1.2 we get

$$\begin{aligned} ds^2 \approx & (1 - \frac{\ddot{a}}{a}R^2)dT^2 - (1 + \frac{k}{a^2}R^2 + \frac{\dot{a}^2}{a^2}R^2)dR^2 - \\ & R^2(d\theta^2 + \sin^2\theta d\phi^2) \end{aligned} \quad (1.15)$$

Near $R = 0$ one can assume a locally inertial coordinate system if one restricts to quadratic order in R/d_H where $d_H = cH^{-1}$ is the ‘Hubble Radius’. In the weak field limit, we know that $g_{00} = (1 + 2\phi_N)$ where ϕ_N is the Newtonian potential. Hence the equivalent Newtonian potential of the FRW metric is

$$\phi_{FRW}(R, t) = -\frac{1}{2}\frac{\ddot{a}}{a}R^2 \quad (1.16)$$

To proceed further one has to investigate how particles move in a self consistent manner in universe described by a perturbed Friedmann metric, with the perturbations introduced by the potential ϕ of the particles. Since in the limit of weak gravity, the perturbed metric can be written as a linear superposition of the

effective gravitational potential of the unperturbed metric and the perturbation ϕ due to matter, the effective Newtonian potential of the perturbed metric is

$$\phi_N = \phi_{FRW} + \phi \quad (1.17)$$

In the transformed coordinate system we can write the equation of motion for a particle in the Newtonian limit as

$$\frac{d^2 R_i}{dT^2} = \frac{d^2}{dT^2}(a\mathbf{x}_i) = -\nabla_R \phi_N \quad (1.18)$$

where \mathbf{x}_i is the coordinate of the particle i . This equations when expanded, and the contribution from the effective Newtonian potential of the FRW metric cancelled, leads to

$$a \frac{d^2}{dT^2} \mathbf{x}_i + 2\dot{a}\dot{\mathbf{x}}_i = -\frac{1}{a} \nabla_x \phi \quad (1.19)$$

where ϕ is the perturbed potential which satisfies Poisson's equation

$$\nabla_x^2 \phi = 4\pi G a^2 \rho_{bm} \delta \quad (1.20)$$

ρ_{bm} is the smoothed density of the background and $\delta = (\rho/\rho_{bm}) - 1$ is the density contrast which defines the perturbations on the smooth background.

To the same order accuracy, we can replace d^2/dT^2 by d^2/dt^2 in the equation of motion leading to

$$\ddot{\mathbf{x}}_i + 2\frac{\dot{a}}{a}\dot{\mathbf{x}}_i = -\frac{1}{a^2} \nabla_x \phi \quad (1.21)$$

as the equation of motion governing the trajectory of a particle moving in an expanding universe in a potential created by the perturbation δ .

The density field $\rho(\mathbf{x}, t)$ of a set of point particles may be defined by the following expression

$$\rho(\mathbf{x}) = \frac{m}{a^3(t)} \sum_i \delta_{Dirac}(\mathbf{x} - \mathbf{x}_i(t)) \quad (1.22)$$

$$(1.23)$$

Taking derivatives, Fourier transforming to get the density modes in Fourier space $\delta_{\mathbf{k}}(t)$ and using the equation of motion for \mathbf{x} we get [38]

$$\ddot{\delta}_{\mathbf{k}} + 2\frac{\dot{a}}{a}\dot{\delta}_{\mathbf{k}} = 4\pi G \rho_{bm} \delta_{\mathbf{k}} + A_{\mathbf{k}} - B_{\mathbf{k}} \quad (1.24)$$

where the $A_{\mathbf{k}}$ and $B_{\mathbf{k}}$ terms are given by

$$A_{\mathbf{k}} = 2\pi G \rho_{bm} \sum_{\mathbf{k}' \neq 0, \mathbf{k}} \delta_{\mathbf{k}'} \delta_{\mathbf{k}-\mathbf{k}'} \left[\frac{\mathbf{k} \cdot \mathbf{k}'}{k'^2} + \frac{\mathbf{k} \cdot (\mathbf{k} - \mathbf{k}')}{|\mathbf{k} - \mathbf{k}'|^2} \right] \quad (1.25)$$

$$B_{\mathbf{k}} = \frac{m}{M} \sum_j (\mathbf{k} \cdot \dot{\mathbf{x}}_j)^2 \exp[i\mathbf{k} \cdot \mathbf{x}_j(t)] \quad (1.26)$$

The two terms $A_{\mathbf{k}}$ and $B_{\mathbf{k}}$ are the nonlinear mode coupling terms which cause the evolution to have a nonlinear structure. The summation in term $B_{\mathbf{k}}$ is over all the particles in the system. Neglecting $A_{\mathbf{k}}$ and $B_{\mathbf{k}}$ when δ is small leads to a linear equation that has a solution that grows as well as a solution that decays in time.

The equations that govern the mechanics of the fluid in the continuum are the *continuity equation*, the *Euler equation* and the *Poisson equation* which governs the evolution of the potential.

$$\frac{\partial \rho_m}{\partial t} + \nabla_r \cdot (\rho_m \mathbf{U}) = 0 \quad (1.27)$$

$$\frac{\partial \mathbf{U}}{\partial t} + (\mathbf{U} \cdot \nabla) \mathbf{U} = -\nabla \phi_{tot} = -\nabla \phi_{FRW} - \nabla \phi \quad (1.28)$$

$$\nabla_r^2 \phi = 4\pi G(\rho_m - \rho_{bm}) = 4\pi G \rho_{bm} \delta \quad (1.29)$$

Using a different time parameter $b(t)$ defined as growing mode solution of the linearised equation for density contrast and the corresponding peculiar velocity $u = v/(ab)$ where $v = a\dot{\mathbf{x}}$ is the original peculiar velocity, results in a second order equation which governs the growth of density contrast δ [38]

$$\frac{d^2 \delta}{db^2} + \frac{3A}{2b} \frac{d\delta}{db} - \frac{3A}{2b^2} \delta(1 + \delta) = \frac{4}{3} \frac{1}{(1 + \delta)} \left(\frac{d\delta}{db} \right)^2 + (1 + \delta)(\sigma^2 - 2\Omega^2) \quad (1.30)$$

in the fluid approximation. σ and Ω represent the shear and rotation of the peculiar velocity field of the fluid given by $\sigma^2 = \sigma^{ab}\sigma_{ab}$ and $\Omega^2 = \Omega_a\Omega^a$. and $A = (\rho_{bm}/\rho_{crit})(\dot{a}b/a\dot{b})^2$.

Solutions to these formal mathematical equations are rather difficult except in special cases, due to the presence of the highly nonlinear terms. Understanding the nonlinear terms is the key to understanding structure formation, since many of the observed structures are highly nonlinear entities with the parameters of interest such as density contrast of the order of a thousand or more.

1.3 Linear perturbation theory

Solutions to the equation governing the growth of δ may be obtained in the framework of linear perturbation theory [36]. In this approach the nonlinear terms A_k and B_k are assumed to be zero due to the small values of δ and velocities.

The equation that governs the growth of δ_k in the linear regime is

$$\ddot{\delta}_k + 2\frac{\dot{a}}{a}\dot{\delta}_k = 4\pi G\rho_{bm}\delta_k \quad (1.31)$$

This equation as discussed before yields solutions which describe growth as well as decay of density contrast. The growing mode solution shows that δ in matter dominated phase evolves proportional to scale factor a in an $\Omega = 1$ universe. The solutions for time dependence of potential and velocity field indicate that the gravitational potential remains constant in time and the velocity field in linear regime is proportional to the gradient of potential given by

$$\mathbf{v} = -\frac{2f}{3H\Omega}\frac{\nabla\phi}{a} \quad (1.32)$$

where $f \approx \Omega^{0.6}$.

Since the regimes of interest are highly nonlinear, we require insight into the behaviour of the nonlinear terms. One of the important physical effects

that can be readily mapped into the nonlinear terms is obvious from equation (1.25). This equation clearly shows that mathematically speaking the nonlinear terms couple various Fourier modes of density contrast field in that it causes evolution of one mode to be dependent on the other. This gives an equivalent way of identifying the linear regime as the period of evolution of a mode, where it evolves independently of the others. The slow growth of nonlinearity causes this independence to be broken until the strong coupling at highly nonlinear scales links together many modes of the system.

1.4 Nonlinear approximations

1.4.1 Zeldovich approximation

The approximation schemes attempt to either extend the linear theory results such as constancy of potential, into nonlinear regimes or model the universe by analytically tractable structures such as spheres. The most fruitful of the approximation schemes of the first kind is the Zeldovich approximation [58]. This is a simplistic yet effective approximation which assumes that the particles move in inertial trajectories, with their initial velocities given by the initial potential. These trajectories cross, leading to caustic surfaces where high density aggregates of matter are produced. The shapes of the caustic surfaces of the initial potential/density field determine the shapes of the large scale structures, which are formed in this approach. Thus this approximation scheme is a simple one time map from Lagrangian space \mathbf{q} to the Eulerian space \mathbf{x} , given by

$$\mathbf{x}(t) = \mathbf{q} + b(t)\mathbf{f}(\mathbf{q}) \quad (1.33)$$

where $b(t)$ is the growing mode solution from linear perturbation theory and \mathbf{f} is the initial velocity field $\propto \nabla\phi$. The density in Eulerian space

$$\frac{\rho(\mathbf{x})}{\rho_0} = [(1 - b(t) \alpha)(1 - b(t) \beta)(1 - b(t) \gamma)]^{-1} \quad (1.34)$$

where $(-\alpha, -\beta, -\gamma)$ are the eigenvalues of $\partial^2\mathbf{f}/\partial\mathbf{q}^2$. This expression clearly shows that the collapse will take place along the axis defined by the largest negative eigenvalue. The distribution function of the eigenvalues for a gaussian random field indicates that collapse along one dimension in that has a much higher probability of occurring since $\alpha \gg \beta, \gamma$. Thus the first structures that form will be sheet like structures that are likely to be highly warped.

The following figures (Fig.1.3 – 1.6) show a slice of a full N body simulation and a corresponding scenario generated by the Zeldovich approximation. It is visually evident that Zeldovich approximation is fairly accurate. The point of breakdown of this approximation comes when the particles after having reached the caustics start moving away from it, *i.e* the shells start crossing and passing through each other leading to a thickening and dissolution of the structures that form (Fig 1.6). This approximation when supplemented by an artificial viscosity term (the ‘adhesion approximation’) is more faithful to the N Body simulation even at late times. There are many variants on the basic Zeldovich approximation such as the truncated Zeldovich approximation which are all consistent with N body simulations to various degrees. Some of the other approximation schemes driven by physical considerations are frozen potential approximation, frozen flow approximation and so on which extend the linear theory results related to density, velocity and potential field growth in various ways. Nonlinear growth of a single object is also of interest because the universe at late stages can be modelled as a set of highly collapsed objects whose overall configuration in the universe is

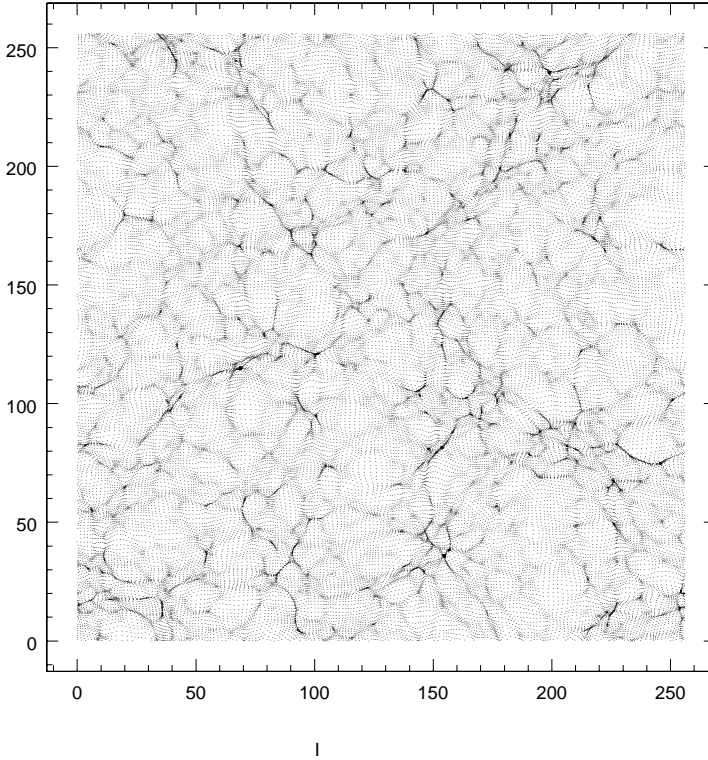


Figure 1.3: N-body simulation at $a=0.25$ ($n=-1$. Power law spectrum).

determined by the large scales in the power spectrum of perturbations. Spherical collapse is an approach in this direction. This model has been successfully used to derive evolution of mass spectrum, non linear scaling relations and so on.

1.4.2 Spherical model

A single virialised structure such as a galaxy or a cluster in the universe is modeled as a spherically symmetric density perturbation in this approximation. The assumption of spherical symmetry allows the system to be analytically solved [4] and the whole history of evolution from initial conditions till the collapse and stabilization to be dealt with analytically. The system is modeled as consisting of concentric spherical shells of radius $R_i(t)$. It can be seen that this overdense/underdense sphere can be modeled as an embedded closed/open uni-

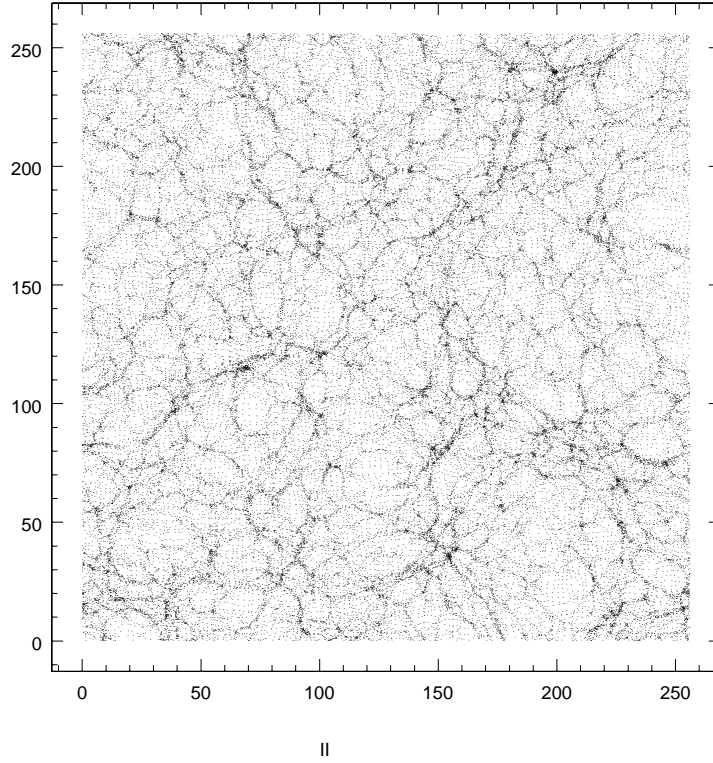


Figure 1.4: Zeldovich approximation at $a=0.25$ ($n=-1$. Power law spectrum). The correspondence between structures in the full Nbody simulation is evident.

verse and the equation of motion for the shell can be identified with the equation of growth of scale factor. This analogy permits the solution for time evolution of a shell to be written in a parametric form as

$$R_i = A(1 - \cos \theta) \quad (1.35)$$

$$t = B(\theta - \sin \theta) \quad (1.36)$$

where $A^3 = GM B^2$ (M is the total mass inside R_i). Defining the density contrast in terms of the average density within the sphere δ , its time dependence may be approximated as

$$\delta \simeq \frac{3}{20} \left(\frac{6t}{B} \right)^{2/3} \quad (1.37)$$

Comparing with the linear theory results in an $\Omega = 1$ universe it can be seen

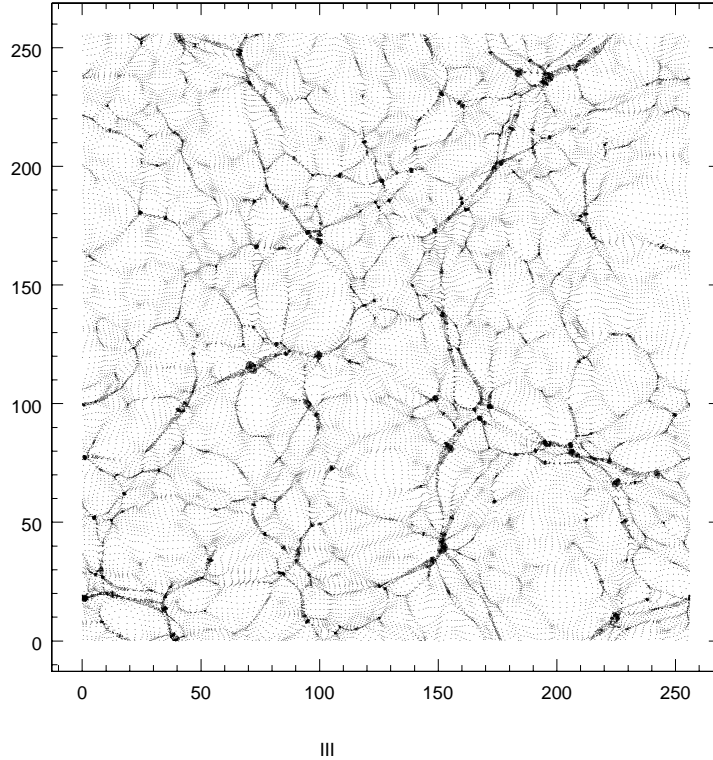


Figure 1.5: N-body simulation at $a=0.5$ ($n=-1$. Power law spectrum).

that the sphere will breakaway from the general expansion and reach a maximum radius at $\theta = \pi$. At this point the linear theory result for density contrast is $\delta_{lin} = 1.06$ where as the nonlinear density contrast is $\delta_{sph} = 5.6$. The final fate of the sphere will be an uninterrupted collapse towards a single point at $\theta = 2\pi$. The linear density contrast at this time is $\delta_{lin} = 1.68$ where as the actual nonlinear density contrast essentially shoots up towards infinity (Figure 1.7).

To prevent the model from being driven towards a singularity one has to invoke a physical mechanism referred to as ‘virialisation’. This involves an *ad hoc* principle of introducing a stability criterion such that when the potential energy is equal to twice the kinetic energy the collapse will stop and the system will reach a final density contrast of about 180.

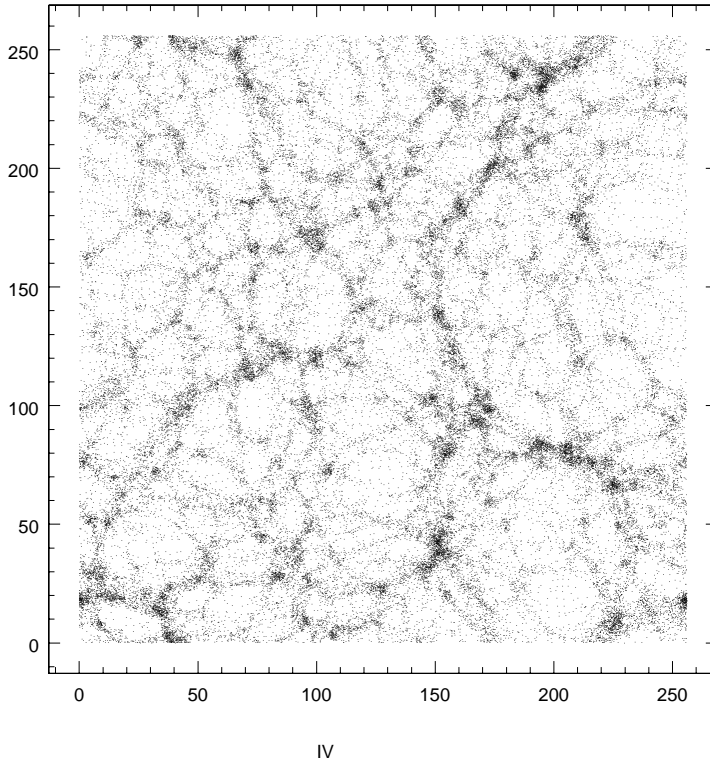


Figure 1.6: Zeldovich approximation at $a=0.5$ ($n=-1$. Power law spectrum). The thickening and dissolving of the structures formed is clear leading to breakdown of Zeldovich approximation.

This approximation has proved to very effective, despite its highly restrictive assumptions, in quantitatively describing measures such as mass functions and in theoretically modeling nonlinear scaling relations. However spherical symmetry is a restrictive assumption and a model which is more representative of the observed structures is to be sought.

1.5 N Body Simulations

An effective model of the phenomena so that the process can be better understood must have the following three components (1) a representation of the basic entities that are being modeled (2) a set of initial conditions (3) a dynamical system of

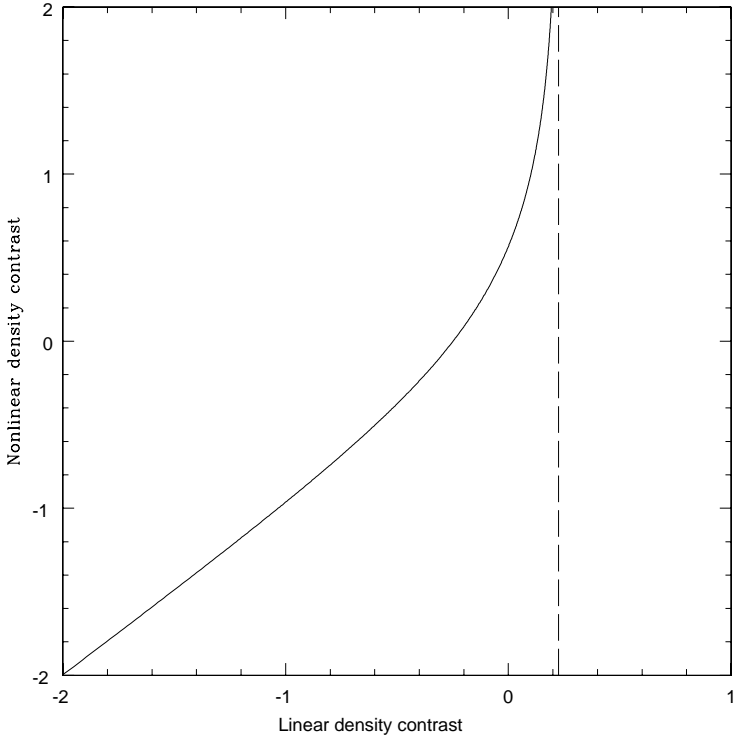


Figure 1.7: The nonlinear density contrast versus the linear density contrast for the spherical collapse model

equations to evolve the system. The various models differ in the ways in which these three requisites are met. Truly speaking, they also differ in the domain of the problem that they address but it can be traced down to the way in which they implement the above conditions.

(1) The basic entities must be chosen such that the high degree of detail afforded by computer simulations is not detrimental to understanding these structures better. A complete model of the universe taking into account all the fundamental interactions between the particles is therefore ruled out. A more feasible and productive approach is to treat large mass aggregates as the “particles” of the system and describe the universe in terms of the dynamics of these massive “particles” which are governed by gravity. This approach forms the basis of N

body simulations. An alternate approach involves averaging over the local velocities of the particles in a small volume and treating the volume itself as a fluid element and describe the system in terms of dynamics of a fluid. Analytic approaches usually favor this picture. Observationally all the matter in the universe consists of that which is inferred from the various signals that we receive via the electromagnetic spectrum. Some observations such as rotation curves of galaxies as well as velocities of galaxies in clusters indicate that there is a large, dominant component of matter in the universe, that has no interaction with light. This matter is referred to as ‘dark matter’. Many observational problems such as the observed flat rotation curves of galaxies and so on can be explained by a judicious invocation of this invisible “matter” whose constituents and interactions other than gravitational, is yet to be discovered. Since it is indicated that more than 90% of the observed universe consists of dark matter, the models incorporate the dynamics of the dark matter prior to that of visible matter. Thus the computer simulation model has three core components. The Friedmann metric, the dark matter and the visible matter. The dark matter forms the major component as far as gravitation is concerned.

The various forms of dark matter that have been used are (1) CDM [Cold dark matter] (2) HDM [Hot dark matter] and a mixture of the two. The hot dark matter and the cold dark matter differ in the way power is distributed in various modes. The most notable physical difference is due to ‘free streaming’ which causes small scale power to be suppressed in the case of hot dark matter. This qualitatively and quantitatively changes the way hierarchies of structures form in the two models. The next set of entities which are baryons (or the components of visible matter) are dealt with separately since their gravitational contribution is much smaller than that of dark matter but they have interactions which are

non gravitational which govern their dynamics. Thus the basic entities and their interactions are as follows. The dark matter gravitationally clusters in an universe with an expanding background. The baryonic particles collect in the deep dark matter potentials with their structure and state dominated by additional non gravitational processes such as heating, cooling and so on.

(2) The initial conditions: The universe that is observed is considered to be a single realization of an underlying gaussian random field which is predicted by various theories of early universe and has been observationally supported by the COBE data. The gaussian random field is wholly described by the power spectrum defined as follows.

$$P(\mathbf{k}, \mathbf{k}') = |\delta_{\mathbf{k}}|^2 \quad (1.38)$$

where $\delta_{\mathbf{k}}$) is k th Fourier mode of random field δ .

The quantities that are used to describe the structure of the universe are also statistical in nature. This implies that exact structure of the universe as observed today cannot be modeled by these approaches, but rather allows us to describe a statistical model of the universe.

(3) The dynamics; The dynamical equations that describe the growth of the system when it is treated as a set of interacting particles consist of the equation of motion for the trajectory of a single particle in an expanding background and an equation which allows us to evaluate the force on a particle due to all other particles. N Body simulations essentially define a number of particles and generate a phase space configuration for them based on the chosen initial conditions which are usually specified by the initial cosmological model, *ie* the parameters that describe the background universe such as density of matter, density of vacuum energy, Hubble's constant etc and the power spectrum of the initial perturbation

field. The initial conditions also specify the epoch at which these conditions are given. This epoch is usually chosen to be the epoch of recombination at a redshift of approximately 1000.

The initial conditions can be evolved analytically to a point where the non-linear effects start to increase in importance and from there the system is allowed to evolve according to the full system of equations until the desired point in time. This approach is detailed in the following review [9].

N Body approach is complete but not feasible to a high degree of accuracy owing to the computational limitations that exist. The limitations are usually caused due to resource (memory and disk storage) and computational (CPU power, time) requirements being inadequately met by existing technology. The large number of theoretical models and the continually increasing accuracy of observational data require that the system be modeled more and more accurately. In addition the outputs of simulations which consist of the phase space of all the particles in the system are too detailed and a large amount of further computation has to be performed before statistical measures are derived from them which may be used to effect the comparisons.

These limitations led to attempts to model the system under study by techniques which either bypass the simulation strategy (analytic and semi analytic techniques) or use some physically motivated ansatz to arrive at a final configuration from an initial one, essentially by bypassing some of the steps in the simulation. The second category of approaches include the various numerical approximation schemes such as Zeldovich approximation, frozen potential approximation and so on. The other approach leads to perturbative techniques for exploring the quasi and nonlinear regimes as well as some nonperturbative techniques that attempt to look at the problem of evolution in time as a one

shot time dependent mapping which gives some of the statistical measures computable from the final configuration in terms of the measures computed over the initial configuration at one go. Thus the three approaches, the complete N body approach, the approximation schemes and the mapping approach, all attempt to explain the formation of structure in a complimentary sense.

The algorithms for N body simulations have been discussed in the references. The different categories of simulations are essentially based on the force computation method. This thesis will be primarily using a PM (particle mesh) code developed by Bagla and Padmanabhan [9]. The N body experiments and some of their results are discussed in this section. There are two kinds of PM N body simulations discussed here: the two dimensional simulations and the three dimensional simulations. The 2D simulations allow us to explore a much higher dynamic range in the given computational resources and consequently many experiments are conducted in two dimensions. The 3D simulations correspond to full scale models for the universe at hand. The essential nature of gravitational clustering in terms of how the “particles” of the system respond is easily visualized in two dimensions. The following results reveal that initially the particles are distributed in a random manner according to chosen power spectrum. Then the clustering proceeds forming filamentary structures whose intersections serve as the points to which matter flows along the filaments to form clusters. In three dimensions this phenomenon is essentially repeated with sheets, filaments and clusters.

Figures(1.8 – 1.10) which show the results visually for a set of 2D simulations clearly reveal the initial peaks and the formation of long filamentary structures and the later collapse into the peaks themselves. To the first approximation one can clearly understand the fact that the initial peaks in the system serve

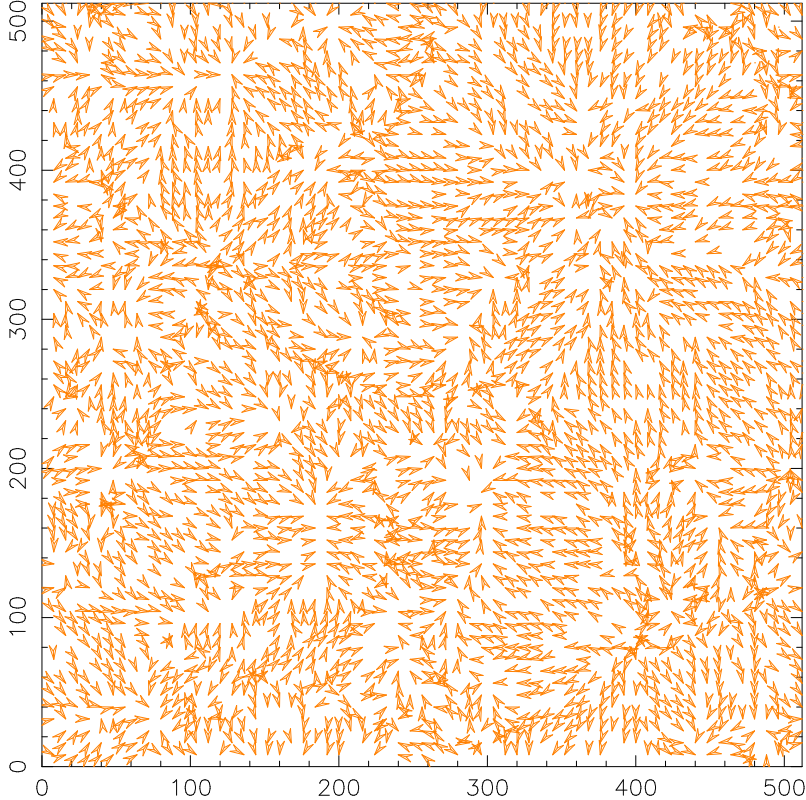


Figure 1.8: The flow field at $a=0.5$

as the nucleation centres for structure formation and these nucleation centres themselves do move due to the power existing at length scales corresponding to their mean separation. The question of first structures that form, whether they are filamentary or sheet like in 3D and it's analogue in 2D has partial answer in terms of the Zeldovich approximation. This approximation scheme which essentially places the particles in inertial motion with their initial velocities given by the initial conditions indicates that the initial structures are sheet like (string like in 2D) which is roughly concordant with what the simulations indicate. Observationally too we see the presence of very large structures (100 Mpc) which may be sheet like or filamentary. A simple analysis based on the Zeldovich approximation which is a valid approximation until shell crossing takes place

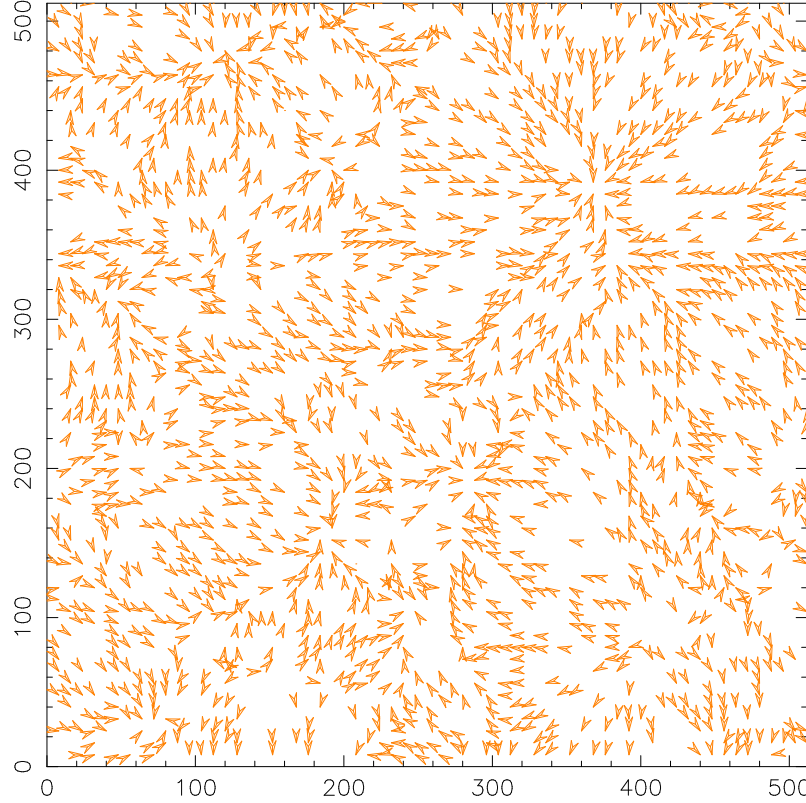


Figure 1.9: The flow field at $a=1.5$. It can be seen that the velocity vectors flow along the caustics (filaments) towards the cluster centers

gives the statistical answer, that for a gaussian random field it is more probable that sheets would form rather than filaments in 3D and correspondingly in 2D. The pictures below clearly reveal the initial formation of filamentary structures (the arrows indicate the direction of velocity) and the damping of the velocity transverse to the filament. This causes the matter to flow along the filaments into the junctions where filaments meet which are essentially where the roughly spherically symmetric clusters form. This picture is expected to hold good in three dimensions also.

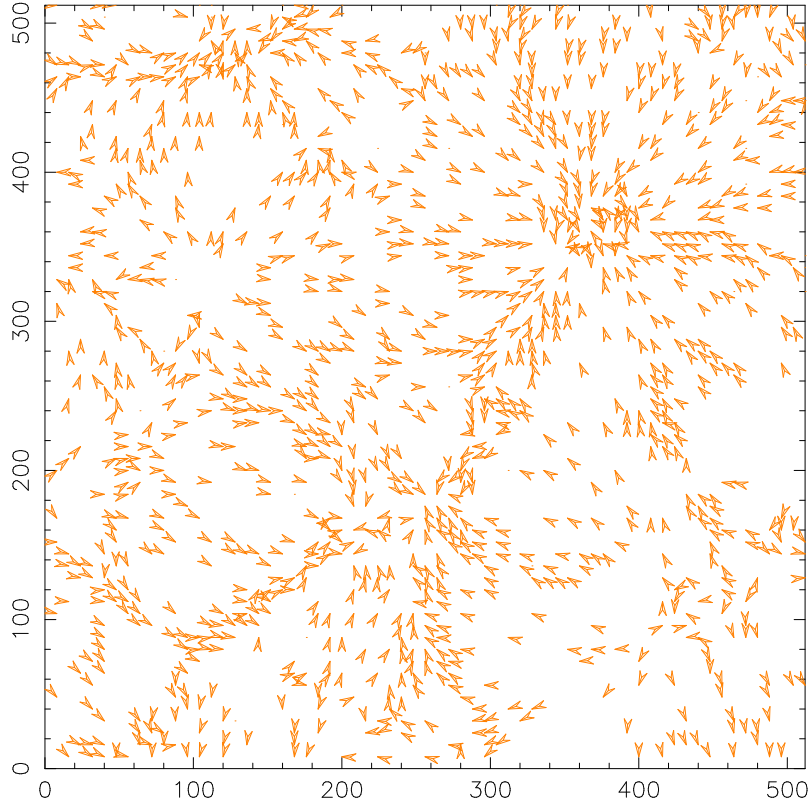


Figure 1.10: The flow field at very late times. The flow is almost completely concentrated at the centers. The particles participating in these flows transfer power from large scales to small scales

1.6 Statistical indicators

In developing the framework discussed in the earlier sections, we have made some simplifying assumptions regarding homogeneity, Newtonian limit of the metric and so on. Since these approximations are valid only at different length scales (homogeneity on large length scales and Newtonian approximation on small length scales) it is clear that our models for the universe as a whole is built from smaller models at different length scales. To extend the results derived from the smaller models to the universe as a whole as well as correlate them with observations, we need to use statistical approaches. Thus the models allow us to predict various statistical quantities which may be compared to observations.

The statistical quantities that are used to analyse and compare the N body data with other simulations (as well as with observations) are computed from the positions and velocities. The statistical quantities are usually measures of deviation from the assumed smoothness and distributions of such quantities such as two point correlation function, power spectrum and higher moments of the distribution functions. Another approach followed when models are being compared to observational data, is to constrain the parameters of the model by using statistical goodness of fit and other tests of significance. In this section we shall briefly discuss some of the quantities relevant to later discussions.

The underlying gaussian field is completely characterised by the power spectrum $P(k)$ defined by

$$P(\mathbf{k}) = |\delta_{\mathbf{k}}|^2 = P(k)$$

One can further define other related quantities such as two point correlation function in terms of the power spectrum

$$\xi(\mathbf{x}) = \int \frac{d^3\mathbf{k}}{(2\pi)^3} P(\mathbf{k}) e^{i\mathbf{k}\cdot\mathbf{x}} = \int_0^\infty \frac{dk}{k} \left(\frac{k^3 P(k)}{2\pi^2} \right) \left(\frac{\sin kx}{kx} \right) \quad (1.39)$$

$$\bar{\xi}(r) = \frac{3}{r^3} \int_0^r dx x^2 \xi(x) \quad (1.40)$$

The assumed statistical isotropy of the universe implies that the two point correlation function and power spectrum are functions of magnitude of r and k respectively and is independent of direction. Some of the other measures of departures from homogeneity are the variance of the density field after an appropriate smoothing using a window function such as

$$W_{sph}(k, R) = \frac{3}{k^3 R^3} [\sin kR - kR \cos kR] \quad (1.41)$$

$$W_{gauss}(k, R) = \exp\left(-\frac{1}{2} k^2 R^2\right) \quad (1.42)$$

giving

$$\sigma_{sph}^2(R) = \int \frac{d^3k}{(2\pi)^3} P(k) W_{sph}(k, R)^2 \quad (1.43)$$

$$\sigma_{gauss}^2(R) = \int_0^\infty \frac{dk}{k} \frac{k^3 P(k)}{2\pi^2} W_{gauss}(k, R)^2 \quad (1.44)$$

Figure 1.11 shows the quantities discussed above computed for a standard COBE normalized CDM power spectrum given by

$$P(k) = \frac{Ak^n}{(1 + Bk + Ck^{1.5} + Dk^2)^2} \quad (1.45)$$

where the parameters A, B, C, D, n are equal to $(24/h)^4 Mpc^4$, $1.77/(\Omega h^2) Mpc$, $9(\Omega h^2)^{-1.5} Mpc^{3/2}$, $(\Omega h^2)^{-2} Mpc^2$ and 1 respectively ($h = 0.65$)[36].

A more complex quantity is the Press Schechter mass function (Fig.1.12) which gives the number of collapsed objects of mass M as a function of redshift

$$N(M)dM = -\frac{\bar{\rho}}{M} \left(\frac{2}{\pi}\right)^{1/2} \frac{\delta_c}{\sigma^2} \left(\frac{\partial\sigma}{\partial M}\right) \exp\left(-\frac{\delta_c^2}{2\sigma^2}\right) dM \quad (1.46)$$

As has been indicated, all these different measures which are low order moments of the underlying distributions are not independent of each other. Higher order moments contain more detailed information which is required to discriminate between models for instance when the lower order correlations are unable to do so. There exist statistical measures such as minimum spanning tree, percolation statistics and so on which attempt to deal with the whole hierarchy of moments in a holistic manner. They can be used to characterise complementary aspects in the statistical description of large scale structure. Various other quantities are also used to quantify morphologies and topological properties of large scale structure such as minkowski functionals which are related to the moments of the distributions.

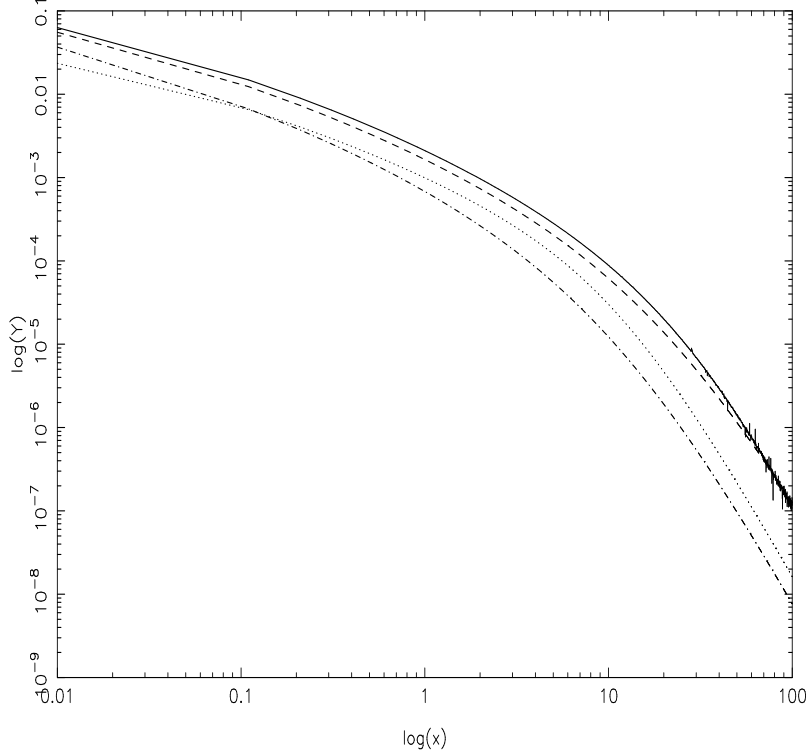


Figure 1.11: Different statistical indicators such as the two point correlation function and $\Delta^2(k) = k^3 P(k)/(2\pi^2)$. ($\Delta(k)$ – dashed line, $\bar{\xi}$ – solid line, σ_{sph} – dotted line, σ_{gauss} – dash dot line for a standard CDM power spectrum with $k = 1/l$

1.7 Nonlinear scaling relations

The N body approaches form an expensive way of arriving at the statistical properties of the late universe given the statistical quantities describing the early universe. An alternate approach which is a one time mapping approach to nonlinear evolution is referred to as ‘Nonlinear scaling relations’. It was demonstrated empirically from simulations by Hamilton *et al* [19] that the averaged two point correlation function in the nonlinear regime may be obtained from the initial average two point correlation function via a non local map given by

$$\bar{\xi}_{NL}(x) = f_{NL}(\bar{\xi}_L(l)) \quad (1.47)$$

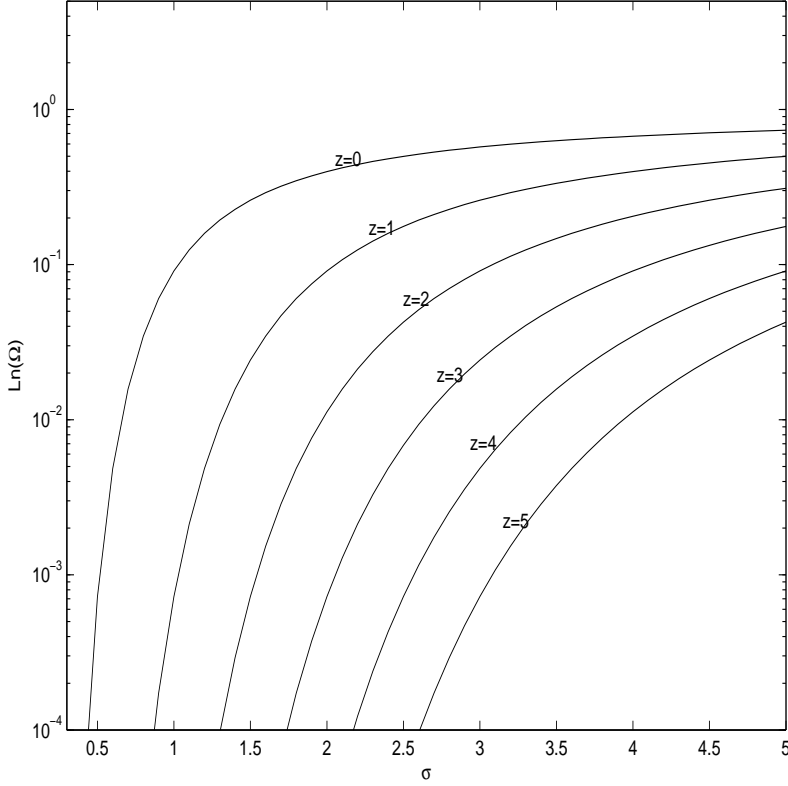


Figure 1.12: The mass function plotted as the log of fraction of mass in structures more massive than M ($\ln(\Omega)$) as a function of $\sigma(M)$ for different redshifts $z=0,1,2,3,4,5$ from top to bottom.

where x and l are related by $l^3 = (1 + \bar{\xi}_{NL}(x))x^3$. The functional form for f_{NL} proposed by Hamilton *et al* [19] is as follows

$$f_{NL}(z) = \frac{z + 0.358 z^3 + 0.0236 z^6}{1 + 0.0134 z^3 + 0.0020 z^{9/2}} \quad (1.48)$$

It is possible to give a theoretical explanation for the existence of such a mapping [34] through an argument based on the pair conservation equation which leads to the result that the universal mapping function for the two point correlation function may be obtained from the behaviour of $h = -v/(\dot{a}r)$, ratio of average pair velocity to Hubble velocity $\dot{a}r$ under an assumed closure condition. This allows us to express the mapping function as an integral over the h function.

A theoretical modeling of the mapping based on infall on to high peaks in the

intermediate regimes [37] allows the empirical relation to be well approximated by a discontinuous powerlaw approximation with three different values for the power law indices in the three regimes, linear, quasilinear and nonlinear. The power law index in the nonlinear regime is related to the value of h in the highly nonlinear end which might not be unity as is implied by the stable clustering hypothesis. This approach permits the notion of a more generalised stable clustering to be introduced with a corresponding slope for the nonlinear end of the mapping. The power law representation in three dimensions is

$$f_{NL}(z) = \begin{cases} 1 & (z \ll 1) \\ z^3 & (1 \lesssim z \lesssim 200) \\ z^{3/2} & (200 \ll z) \end{cases} \quad (1.49)$$

Figure 1.13 shows the mapping function in three dimensions and power law approximations to the same. Figure 1.14 shows the evolution of average two point correlation function for a CDM power spectrum at a late epoch and the linearly evolved two point correlation function at the same time. The nonlinear evolution of the two point correlation function may be seen at small scales.

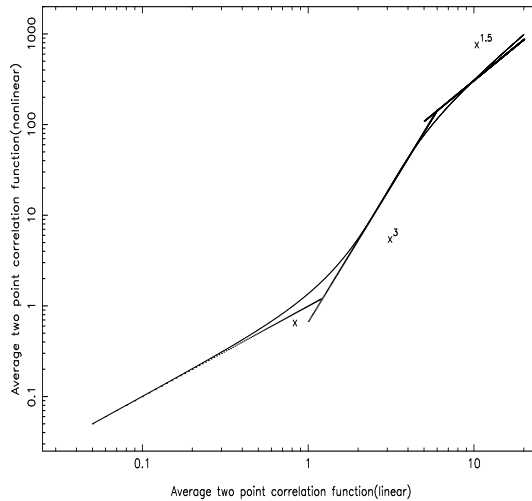


Figure 1.13: The nonlinear scaling relation between nonlinear and linearly scaled two point correlation function.

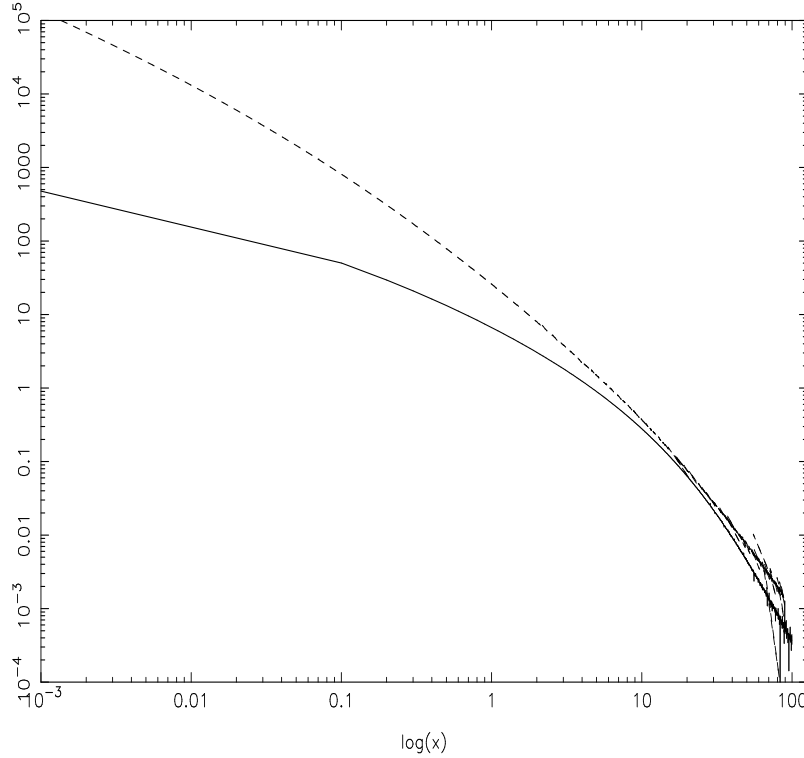


Figure 1.14: The linearly scaled two point correlation function (solid line) and the nonlinear two point correlation function of CDM power spectrum at a late epoch ($a=1$)

In brief the approach taken towards studying structure formation in the universe is a) a model for the underlying smooth background universe b) a model for the seed perturbations c) a system of equations for describing the growth of these perturbations, their linear approximations and analytical solutions d) statistical quantities to describe the various uncertainties and selection effects e) nonlinear approximations of various kinds to obtain physical insight and f) full scale N body simulations in an expanding background.

The following chapters detail the approaches we have taken and progress made, using the theoretical model sketched herein.

Chapter 2

Nonlinear gravitational clustering: Dreams of a paradigm

Humor is the only test of gravity and gravity of humor – Aristotle

2.1 Introduction

As is clear from the first chapter the evolution of large number of particles under their mutual gravitational influence is a well-defined mathematical problem. But, if such a system occupies a finite region of phase space at an initial instant, and evolves via Newtonian gravity, then it does not reach any sensible ‘equilibrium’ state. The core region of the system will keep on shrinking and will be eventually be dominated by a few ‘hard binaries’. Rest of the particles will evaporate away to large distances, gaining kinetic energy from the shrinking core [for a discussion of such systems, see [35]].

The situation is drastically different in the presence of an expanding background universe characterised by an expansion factor $a(t)$. Firstly, the expansion tends to keep particles apart thereby exerting a civilising influence against Newtonian attraction. Secondly, it is now possible to consider an infinite region of space filled with particles. The average density of particles will contribute to the

expansion of the background universe and the deviations from the uniformity will lead to clustering. Particles evaporating from a local overdense cluster cannot escape to “large distances” but necessarily will encounter other deep potential wells. Naively, one would expect the local overdense regions to eventually form gravitationally bound objects, with a hotter distribution of particles hovering uniformly all over. As the background expands, the velocity dispersion of the second component will keep decreasing and they will be captured by the deeper potential wells. Meanwhile, the clustered component will also evolve dynamically and participate in, e.g mergers. If the background expansion and the initial conditions have no length scale, then it is likely that the clustering will continue in a hierarchical manner *ad infinitum*.

Most of the practising cosmologists will broadly agree with the above picture of gravitational clustering in an expanding universe. It is, however, not easy to translate these concepts into a well-defined mathematical formalism and provide a more quantitative description of the gravitational clustering. One of the key questions regarding this system which needs to be addressed is the following: Can one make any general statements about the very late stage evolution of the clustering ? For example, does the power spectrum at late times ‘remember’ the initial power spectrum or does it possess some universal characteristics which are reasonably independent of initial conditions ? [This question is closely related to the issue of whether gravitational clustering leads to density profiles which are universal. [32]].

In this chapter we address some of the above issues and show that it is possible to provide (at least partial) answers to these questions based on a simple paradigm. The key assumption we shall make is the following: Let ratio between mean relative pair velocity $v(a, x)$ and the negative hubble velocity ($-\dot{a}x$) be

denoted by $h(a, x)$ and let $\bar{\xi}(a, x)$ be the mean correlation function averaged over a sphere of radius x . *We shall assume that $h(a, x)$ depends on a and x only through $\bar{\xi}(a, x)$; that is, $h(a, x) = h[\bar{\xi}(a, x)]$.* With such a minimal assumption, we will be able to obtain several conclusions regarding the evolution of power spectrum in the universe. Such an assumption was originally introduced — in a different form — by Hamilton [19]. The present form, as well as its theoretical implications were discussed in [34], and a theoretical model for the scaling was attempted by Padmanabhan [37]. It must be noted that simulations indicate a dependence of the relation $h(a, x) = h[\bar{\xi}(a, x)]$ on the initial spectrum and also on cosmological parameters ([43],[44],[42], [30]). Most of our discussion is independent of this fact or can be easily generalised to such cases. When we need to use an explicit form for h we shall use the original ones suggested by Hamilton [19] because of its simplicity.

Since this chapter addresses several independent but related questions, we provide here a brief summary of how it is organised. Section 2.1 studies some aspects of nonlinear evolution based on the assumption mentioned above. We begin by summarising some previously known results in subsection 2.2.1 to set up the notation and collect together in one place the formulas we need later. Subsection 2.2.2 makes a brief comment about the critical indices in gravitational dynamics so as to motivate later discussion. In section 2.3, we discuss the relation between density profiles of halos and correlation functions and derive the conditions under which one may expect universal density profiles in gravitational clustering. In section 2.4 we show that gravitational clustering does *not* admit self similar evolution except in a very special case. We also discuss the conditions for approximate self-similarity to hold. Section 2.5 discusses the question as whether one can expect to find power spectra which evolve preserving their shape, even in

the nonlinear regime. We first show, based on the results of section 2.4, that such *exact* solutions cannot exist. We then discuss the conditions for the existence of some *approximate* solutions. We obtain one prototype approximate solution and discuss its properties. The solution also allows us to understand the connection between statistical mechanics of gravitating systems in the small scale and evolution of correlation functions on the large scale. Finally, section 2.6 discusses the results.

2.2 General features of nonlinear evolution

Consider the evolution of the system starting from a gaussian initial fluctuations with an initial power spectrum, $P_{in}(k)$. The fourier transform of the power spectrum defines the correlation function $\xi(a, x)$ where $a \propto t^{2/3}$ is the expansion factor in a universe with $\Omega = 1$. It is more convenient to work with the average correlation function inside a sphere of radius x , defined by

$$\bar{\xi}(a, x) \equiv \frac{3}{x^3} \int_0^x \xi(a, y) y^2 dy \quad (2.1)$$

This quantity is related to the power spectrum $P(a, k)$ by

$$\bar{\xi}(x, a) = \frac{3}{2\pi^2 x^3} \int_0^\infty \frac{dk}{k} P(a, k) [\sin(k x) - k x \cos(k x)] \quad (2.2)$$

with the inverse relation

$$P(a, k) = \frac{4\pi}{3k} \int_0^\infty dx x \bar{\xi}(a, x) [\sin(k x) - k x \cos(k x)] \quad (2.3)$$

In the linear regime we have $\bar{\xi}_L(a, x) \propto a^2 \bar{\xi}_{in}(a_i, x)$.

We now recall that the conservation of pairs of particles gives an exact equation satisfied by the correlation function [45]:

$$\frac{\partial \xi}{\partial t} + \frac{1}{ax^2} \frac{\partial}{\partial x} [x^2(1 + \xi)v] = 0 \quad (2.4)$$

where $v(a, x)$ denotes the mean relative velocity of pairs at separation x and epoch a . Using the mean correlation function $\bar{\xi}$ and a dimensionless pair velocity $h(a, x) \equiv -(v/\dot{a}x)$, equation (2.4) can be written as

$$\left(\frac{\partial}{\partial \ln a} - h \frac{\partial}{\partial \ln x} \right) (1 + \bar{\xi}) = 3h(1 + \bar{\xi}) \quad (2.5)$$

This equation can be simplified by introducing the variables

$$A = \ln a, \quad X = \ln x, \quad D(X, A) = \ln(1 + \bar{\xi}) \quad (2.6)$$

in terms of which we have [34]

$$\frac{\partial D}{\partial A} - h(A, X) \frac{\partial D}{\partial X} = 3h(A, X) \quad (2.7)$$

At this stage we shall introduce our key assumption, viz. that h depends on (A, X) only through $\bar{\xi}$ (or, equivalently, D). Given this single assumption, several results follow which we shall now summarise.

2.2.1 Formal solution

Given that $h = h[\bar{\xi}(a, x)]$, one can easily integrate the equation (2.5) to find the general solution [34]. The characteristics of this equation (2.5) satisfy the condition

$$x^3(1 + \bar{\xi}) = l^3 \quad (2.8)$$

where l is another length scale. When the evolution is linear at all the relevant scales, $\bar{\xi} \ll 1$ and $l \approx x$. As clustering develops, $\bar{\xi}$ increases and x becomes considerably smaller than l . The behaviour of clustering at some scale x is then determined by the original *linear* power spectrum at the scale l through the “flow of information” along the characteristics. This suggests that *we can express the true correlation function $\bar{\xi}(a, x)$ in terms of the linear correlation function $\bar{\xi}_L(a, l)$*

evaluated at a different point. This is indeed true and the general solution can be expressed as a nonlinear scaling relation (NSR, for short) between $\bar{\xi}_L(a, l)$ and $\bar{\xi}(a, x)$ with l and x related by equation(2.8). To express this solution we define two functions $\mathcal{V}(z)$ and $\mathcal{U}(z)$ where $\mathcal{V}(z)$ is related to the function $h(z)$ by

$$\mathcal{V}(z) = \exp\left(\frac{2}{3} \int^z \frac{dz}{h(z)(1+z)}\right) \quad (2.9)$$

and $\mathcal{U}(z)$ is the inverse function of $\mathcal{V}(z)$. Then the solution to the equation (2.5) can be written in either of two equivalent forms as:

$$\bar{\xi}(a, x) = \mathcal{U}\left[\bar{\xi}_L(a, l)\right]; \quad \bar{\xi}_L(a, l) = \mathcal{V}\left[\bar{\xi}(a, x)\right] \quad (2.10)$$

where $l^3 = x^3(1 + \bar{\xi})$ [34]. Given the form of $h(\bar{\xi})$ this allows one to relate the nonlinear correlation function to the linear one.

From general theoretical considerations [37] it can be shown that $\mathcal{V}(z)$ has the form:

$$\mathcal{V}(z) = \begin{cases} 1 & (z \ll 1) \\ z^{1/3} & (1 \lesssim z \lesssim 200) \\ z^{2/3} & (200 \ll z) \end{cases} \quad (2.11)$$

In these three regions $h(z) \approx [(2z/3), 2, 1]$ respectively. We shall call these regimes, linear, intermediate and nonlinear respectively. More exact fitting functions to $\mathcal{V}(z)$ and $\mathcal{U}(z)$ have been suggested in literature. ([19],[30],[43]). When needed in this chapter, we shall use the one given in Hamilton [19]:

$$\mathcal{V}(z) = z \left(\frac{1 + 0.0158 z^2 + 0.000115 z^3}{1 + 0.926 z^2 - 0.0743 z^3 + 0.0156 z^4} \right)^{1/3} \quad (2.12)$$

$$\mathcal{U}(z) = \frac{z + 0.358 z^3 + 0.0236 z^6}{1 + 0.0134 z^3 + 0.0020 z^{9/2}} \quad (2.13)$$

Equations (2.10) and (2.12,2.13) implicitly determine $\bar{\xi}(a, x)$ in terms of $\bar{\xi}_L(a, x)$.

2.2.2 Critical indices

These NSR already allow one to obtain some general conclusions regarding the evolution. To do this most effectively, let us define a local index for rate of clustering by

$$n_a(a, x) \equiv \frac{\partial \ln \bar{\xi}(a, x)}{\partial \ln a} \quad (2.14)$$

which measures how fast $\bar{\xi}(a, x)$ is growing. When $\bar{\xi}(a, x) \ll 1$, then $n_a = 2$ irrespective of the spatial variation of $\bar{\xi}(a, x)$ and the evolution preserves the shape of $\bar{\xi}(a, x)$. However, as clustering develops, the growth rate will depend on the spatial variation of $\bar{\xi}(a, x)$. Defining the effective spatial slope by

$$-[n_{eff}(a, x) + 3] \equiv \frac{\partial \ln \bar{\xi}(a, x)}{\partial \ln x} \quad (2.15)$$

one can rewrite the equation (2.5) as

$$n_a = h\left(\frac{3}{\bar{\xi}(a, x)} - n_{eff}\right) \quad (2.16)$$

At any given scale of nonlinearity, decided by $\bar{\xi}(a, x)$, there exists a critical spatial slope n_c such that $n_a > 2$ for $n_{eff} < n_c$ [implying rate of growth is faster than predicted by linear theory] and $n_a < 2$ for $n_{eff} > n_c$ [with the rate of growth being slower than predicted by linear theory]. The critical index is fixed by setting $n_a = 2$ in equation (2.16) at any instant. This feature will tend to “straighten out” correlation functions towards the critical slope. [We are assuming that $\bar{\xi}(a, x)$ has a slope that is decreasing with scale, which is true for any physically interesting case]. From the fitting function it is easy to see that in the range $1 \lesssim \bar{\xi} \lesssim 200$, the critical index is $n_c \approx -1$ and for $200 \lesssim \bar{\xi}$, the critical index is $n_c \approx -2$ [10]. This clearly suggests that the local effect of evolution is to drive the correlation function to have a shape with $(1/x)$ behaviour at nonlinear regime and $(1/x^2)$ in the intermediate regime. Such a correlation function will have $n_a \approx 2$ and hence will grow at a rate close to a^2 .

2.3 Correlation functions, density profiles and stable clustering

Now that we have a NSR giving $\bar{\xi}(a, x)$ in terms of $\bar{\xi}_L(a, l)$ we can ask the question: How does $\bar{\xi}(a, x)$ behave at highly nonlinear scales or, equivalently, at any given scale at large a ?

To begin with, it is easy to see that we must have $v = -\dot{a}x$ or $h = 1$ for sufficiently large $\bar{\xi}(a, x)$ if we assume that the evolution gets frozen in proper coordinates at highly nonlinear scales. Integrating equation (2.5) with $h = 1$, we get $\bar{\xi}(a, x) = a^3 F(ax)$; we shall call this phenomenon “stable clustering”. There are two points which need to be emphasised about stable clustering:

- (1) At present, there exists some evidence from simulations [42] that stable clustering does *not* occur in a $\Omega = 1$ model. In a *formal* sense, numerical simulations cannot disprove [or even prove, strictly speaking] the occurrence of stable clustering, because of the finite dynamic range of any simulation.

(2). Theoretically speaking, the “naturalness” of stable clustering is often overstated. The usual argument is based on the assumption that at very small scales — corresponding to high nonlinearities — the structures are “expected to be” frozen at the proper coordinates. However, this argument does not take into account the fact that mergers are not negligible at *any scale* in an $\Omega = 1$ universe. In fact, stable clustering is more likely to be valid in models with $\Omega < 1$ — a claim which seems to be again supported by simulations [42].

If stable clustering *is* valid, then the late time behaviour of $\bar{\xi}(a, x)$ *cannot* be independent of initial conditions. In other words the two requirements: (i) validity of stable clustering at highly nonlinear scales and (ii) the independence of late time behaviour from initial conditions, are mutually exclusive. This is

most easily seen for initial power spectra which are scale-free. If $P_{in}(k) \propto k^n$ so that $\bar{\xi}_L(a, x) \propto a^2 x^{-(n+3)}$, then it is easy to show that $\bar{\xi}(a, x)$ at small scales will vary as

$$\bar{\xi}(a, x) \propto a^{\frac{6}{n+5}} x^{-\frac{3(n+3)}{n+5}}; \quad (\bar{\xi} \gg 200) \quad (2.17)$$

if stable clustering is true. Clearly, the power law index in the nonlinear regime “remembers” the initial index. The same result holds for more general initial conditions.

What does this result imply for the profiles of individual halos? To answer this question, let us start with the simple assumption that the density field $\rho(a, \mathbf{x})$ at late stages can be expressed as a superposition of several halos, each with some density profile; that is, we take

$$\rho(a, \mathbf{x}) = \sum_i f(\mathbf{x} - \mathbf{x}_i, a) \quad (2.18)$$

where the i -th halo is centered at \mathbf{x}_i and contributes an amount $f(\mathbf{x} - \mathbf{x}_i, a)$ at the location \mathbf{x} [We can easily generalise this equation to the situation in which there are halos with different properties, like core radius, mass etc by summing over the number density of objects with particular properties; we shall not bother to do this. At the other extreme, the exact description merely corresponds to taking the f 's to be Dirac delta functions]. The power spectrum for the density contrast, $\delta(a, \mathbf{x}) = (\rho/\rho_b - 1)$, corresponding to the $\rho(a, \mathbf{x})$ in (2.18) can be expressed as

$$P(\mathbf{k}, a) \propto \left(a^3 |f(\mathbf{k}, a)| \right)^2 \left| \sum_i \exp -i\mathbf{k} \cdot \mathbf{x}_i(a) \right|^2 \quad (2.19)$$

$$\propto \left(a^3 |f(\mathbf{k}, a)| \right)^2 P_{\text{cent}}(\mathbf{k}, a) \quad (2.20)$$

where $P_{\text{cent}}(\mathbf{k}, a)$ denotes the power spectrum of the distribution of centers of the halos.

If stable clustering is valid, then the density profiles of halos are frozen in proper coordinates and we will have $f(\mathbf{x} - \mathbf{x}_i, a) = f(a(\mathbf{x} - \mathbf{x}_i))$; hence the fourier

transform will have the form $f(\mathbf{k}, a) = f(\mathbf{k}/a)$. On the other hand, the power spectrum at scales which participate in stable clustering must satisfy $P(\mathbf{k}, a) = P(\mathbf{k}/a)$ [This is merely the requirement $\bar{\xi}(a, x) = a^3 F(ax)$ re-expressed in Fourier space]. From equation (2.20) it follows that we must have $P_{\text{cent}}(\mathbf{k}, a) = \text{constant}$ independent of \mathbf{k} and a at small length scales. This can arise in the special case of random distribution of centers or — more importantly — because we are essentially probing the interior of a single halo at sufficiently small scales. [Note that we must *necessarily* have $P_{\text{cent}} \approx \text{constant}$, for length scales smaller than typical halo size, by definition]. We can relate the halo profile to the correlation function using (2.20). In particular, if the halo profile is a power law with $f \propto r^{-\epsilon}$, it follows that the $\bar{\xi}(a, x)$ scales as $x^{-\gamma}$ ([29],[53]) where

$$\gamma = 2\epsilon - 3 \quad (2.21)$$

Now if the *correlation function* scales as $[-3(n+3)/(n+5)]$, then we see that the halo density profiles should be related to the initial power law index through the relation

$$\epsilon = \frac{3(n+4)}{n+5} \quad (2.22)$$

So clearly, the halos of highly virialised systems still “remember” the initial power spectrum.

Alternatively, one can try to “reason out” the profiles of the individual halos and use it to obtain the scaling relation for correlation functions. One of the favourite arguments used by cosmologists to obtain such a “reasonable” halo profile is based on spherical, scale invariant, collapse. It turns out that one can provide a series of arguments, based on spherical collapse, to show that — under certain circumstances — the *density profiles* at the nonlinear end scale as $[-3(n+3)/(n+5)]$. The simplest variant of this argument runs as follows: If we

start with an initial density profile which is $r^{-\alpha}$, then scale invariant spherical collapse will lead to a profile which goes as $r^{-\beta}$ with $\beta = 3\alpha/(1+\alpha)$ [37]. Taking the intial slope as $\alpha = (n+3)/2$ will immediately give $\beta = 3(n+3)/(n+5)$. [Our definition of the stable clustering in the last section is based on the scaling of the correlation function and gave the slope of $[-3(n+3)/(n+5)]$ for the *correlation* function. The spherical collapse gives the same slope for *halo profiles*.] In this case, when the halos have the slope of $\epsilon = 3(n+3)/(n+5)$, then the correlation function should have slope

$$\gamma = \frac{3(n+1)}{n+5} \quad (2.23)$$

Once again, the final state “remembers” the initial index n .

Is this conclusion true? Unfortunately, simulations do not have sufficient dynamic range to provide a clear answer but there are some claims[32] that the halo profiles are “universal” and independent of initial conditions. The theoretical arguments given above are also not very rigourous (in spite of the popularity they seem to enjoy!). The argument for correlation function to scale as $[-3(n+3)/(n+5)]$ is based on the assumption of $h = 1$ asymptotically, which may not be true. The argument, leading to density profiles scaling as $[-3(n+3)/(n+5)]$, is based on scale invariant spherical collapse which does not do justice to nonradial motions. Just to illustrate the situations in which one may obtain final configurations which are independent of initial index n , we shall discuss two possibilities:

(i) As a first example we will try to see when the slope of the correlation function is universal and obtain the slope of halos in the nonlinear limit using our relation (2.21). Such an interesting situation can develop *if we assume that h reaches a constant value asymptotically which is not necessarily unity*. In that case, we can integrate our equation (2.5) to get $\bar{\xi}(a, x) = a^{3h} F[a^h x]$ where h now denotes the constant asymptotic value of of the function. For an initial spectrum

which is scale-free power law with index n , this result translates to

$$\bar{\xi}(a, x) \propto a^{\frac{2\gamma}{n+3}} x^{-\gamma} \quad (2.24)$$

where γ is given by

$$\gamma = \frac{3h(n+3)}{2+h(n+3)} \quad (2.25)$$

We now notice that one can obtain a γ which is independent of initial power law index provided h satisfies the condition $h(n+3) = c$, a constant. In this case, the nonlinear correlation function will be given by

$$\bar{\xi}(a, x) \propto a^{\frac{6c}{(2+c)(n+3)}} x^{-\frac{3c}{2+c}} \quad (2.26)$$

The halo index will be independent of n and will be given by

$$\epsilon = 3 \left(\frac{c+1}{c+2} \right) \quad (2.27)$$

Note that we are now demanding the asymptotic value of h to *explicitly depend* on the initial conditions though the *spatial* dependence of $\bar{\xi}(a, x)$ does not. In other words, the velocity distribution — which is related to h — still “remembers” the initial conditions. This is indirectly reflected in the fact that the growth of $\bar{\xi}(a, x)$ — represented by $a^{6c/((2+c)(n+3))}$ — does depend on the index n .

As an example of the power of such a — seemingly simple — analysis note the following: Since $c \geq 0$, it follows that $\epsilon > (3/2)$; invariant profiles with shallower indices (for e.g with $\epsilon = 1$) are not consistent with the evolution described above.

(ii) For our second example, we shall make an ansatz for the halo profile and use it to determine the correlation function. We assume, based on small scale dynamics, that the density profiles of individual halos should resemble that of isothermal spheres, with $\epsilon = 2$, irrespective of initial conditions. Converting this halo profile to correlation function in the *nonlinear* regime is straightforward and

is based on equation (2.21): If $\epsilon = 2$, we must have $\gamma = 2\epsilon - 3 = 1$ at small scales; that is $\bar{\xi}(a, x) \propto x^{-1}$ at the nonlinear regime. Note that this corresponds to the critical index at the nonlinear end, $n_{eff} = n_c = -2$ for which the growth rate is a^2 — same as in linear theory. [This is, however, possible for initial power law spectra, only if $\epsilon = 1$, i.e $h(n+3) = 1$ at very nonlinear scales. Testing the conjecture that $h(n+3)$ is a constant is probably a little easier than looking for invariant profiles in the simulations but the results are still uncertain].

The corresponding analysis for the intermediate regime, with $1 \lesssim \bar{\xi}(a, x) \lesssim 200$, is more involved. This is clearly seen in equation (2.20) which shows that the power spectrum [and hence the correlation function] depends *both* on the Fourier transform of the halo profiles as well as the power spectrum of the distribution of halo centres. In general, both quantities will evolve with time and we cannot ignore the effect of $P_{cent}(k, a)$ and relate $P(k, a)$ to $f(k, a)$. The density profile around a *local maxima* will scale approximately as $\rho \propto \xi$ while the density profile around a *randomly* chosen point will scale as $\rho \propto \xi^{1/2}$. [The relation $\gamma = 2\epsilon - 3$ expresses the latter scaling of $\xi \propto \rho^2$]. There is, however, reason to believe that the intermediate regime (with $1 \lesssim \bar{\xi} \lesssim 200$) is dominated by the collapse of high peaks [37]. In that case, we expect the correlation function and the density profile to have the same slope in the intermediate regime with $\bar{\xi}(a, x) \propto (1/x^2)$. Remarkably enough, this corresponds to the critical index $n_{eff} = n_c = -1$ for the intermediate regime for which the growth is proportional to a^2 .

We thus see that if: (i) the individual halos are isothermal spheres with $(1/x^2)$ profile and (ii) if $\xi \propto \rho$ in the intermediate regime and $\xi \propto \rho^2$ in the nonlinear regime, we end up with a correlation function *which grows as a^2 at all scales*. Such an evolution, of course, preserves the shape and is a good candidate for the late stage evolution of the clustering.

While the above arguments are suggestive, they are far from conclusive. It is, however, clear from the above analysis and it is not easy to provide *unique* theoretical reasoning regarding the shapes of the halos. The situation gets more complicated if we include the fact that all halos will not all have the same mass, core radius etc and we have to modify our equations by integrating over the abundance of halos with a given value of mass, core radius etc. This brings in more ambiguities and depending on the assumptions we make for each of these components [e.g, abundance for halos of a particular mass could be based on Press-Schechter or Peaks formalism], and the final results have no real significance. It is, therefore, better [and probably easier] to attack the question based on the evolution equation for the correlation function rather than from “physical” arguments for density profiles as done next.

2.4 Self-similar evolution

Since the above discussion motivates us to look for correlation functions of the form $\bar{\xi}(a, x) = a^2 L(x)$, we will start by asking a more general question: Does equation (2.5) possess self-similar solutions of the form

$$\bar{\xi}(a, x) = a^\beta F\left(\frac{x}{a^\alpha}\right) = a^\beta F(q) \quad (2.28)$$

where $q \equiv xa^{-\alpha}$? Defining $Q = \ln q = X - \alpha A$ and changing independent variables to from (A, X) to (A, Q) we can transform our equation (2.5) to the form:

$$\left(\frac{\partial \bar{\xi}}{\partial A}\right)_Q - (h + \alpha) \left(\frac{\partial \bar{\xi}}{\partial Q}\right)_A = 3(1 + \bar{\xi}) h(\bar{\xi}) \quad (2.29)$$

Using the relations $(\partial \bar{\xi}/\partial A)_Q = \beta \bar{\xi}$, $(\partial \bar{\xi}/\partial Q)_A = (\bar{\xi}/F)(dF/dQ)$ we can rewrite this equation as

$$\frac{\beta \bar{\xi} - 3(1 + \bar{\xi})h(\bar{\xi})}{[\alpha + h(\bar{\xi})]\bar{\xi}} = \frac{1}{F} \frac{dF}{dQ} \equiv K(Q) \quad (2.30)$$

The right hand side of this equation depends only on Q and hence will vanish if differentiated with respect to A at constant Q . Imposing this condition on the left hand side and noticing that it is a function of $\bar{\xi}(a, x)$ we get

$$\left(\frac{\partial \bar{\xi}}{\partial A} \right)_Q \frac{d}{d\bar{\xi}} (\text{Left Hand Side}) = 0 \quad (2.31)$$

To satisfy this condition we either need (i) $(\partial \bar{\xi} / \partial A)_Q = \beta \bar{\xi} = 0$ implying $\beta = 0$ or (ii) the left hand side must be a constant. Let us consider the two cases separately.

(i) The simpler case corresponds to $\beta = 0$ which implies that $\bar{\xi}(a, x) = F(Q)$.

Setting $\beta = 0$ in equation (2.30) we get

$$\left(\frac{d\bar{\xi}}{dQ} \right) = -\frac{3(1 + \bar{\xi})h(\bar{\xi})}{[\alpha + h(\bar{\xi})]} \quad (2.32)$$

which can be integrated in a straightforward manner to give a relation between $q = \exp Q$ and $\bar{\xi}$:

$$\begin{aligned} q &= q_0(1 + \bar{\xi})^{-1/3} \exp \left(-\frac{\alpha}{3} \int \frac{d\bar{\xi}}{(1 + \bar{\xi})h(\bar{\xi})} \right) \\ &= q_0(1 + \bar{\xi})^{-1/3} \mathcal{V}(\bar{\xi})^{-\alpha/2} \end{aligned}$$

Given the form of $h[\bar{\xi}(a, x)]$, this equation can be in principle inverted to determine $\bar{\xi}$ as a function of $q = xa^{-\alpha}$.

To understand when such a solution will exist, we should look at the limit of $\bar{\xi} \ll 1$. In this limit, when linear theory is valid, we know that $h \approx (2/3)\bar{\xi}$ [45].

Using this in equation (2.33) we get the solution to be $\ln \bar{\xi} = -(2/\alpha) \ln q$ or

$$\bar{\xi} \propto q^{-\frac{2}{\alpha}} \propto x^{-\frac{2}{\alpha}} a^2 \propto a^2 x^{-(n+3)} \quad (2.33)$$

with the definition $\alpha \equiv 2/(n+3)$. This clearly shows that our solution is valid, *if and only if* the linear correlation function is a scale-free power law. In this

case, of course, it is well known that solutions of the type $\bar{\xi}(a, x) = F(q)$ with $q = xa^{-\frac{2}{(n+3)}}$ exists. [Equation (2.33) gives the explicit form of the function $F(q)$]. This result shows that this is the *only* possibility. It should be noted that, even though we have no explicit length scale in the problem, the function $\bar{\xi}(q)$ — determined by the above equation — does exhibit different behaviour at different scales of nonlinearity. Roughly speaking, the three regimes in equation (2.11) translates into nonlinear density contrasts in the ranges $\delta < 1$, $1 < \delta < 200$ and $\delta > 200$ and the function $\bar{\xi}(q)$ has different characteristics in these three regimes. This shows that gravity can intrinsically select out a density contrast of $\delta \approx 200$ which, of course, is well-known from the study of spherical tophat collapse.

(ii) Let us next consider the second possibility, *viz.* that the left hand side of equation (2.30) is a constant. If the constant is denoted by μ , then we get $F = F_0 q^\mu$ and

$$\beta \bar{\xi} - 3(1 + \bar{\xi}) h(\bar{\xi}) = \mu \alpha \bar{\xi} + \mu h \bar{\xi} \quad (2.34)$$

which can be rearranged to give

$$h = \frac{(\beta - \alpha\mu)\bar{\xi}}{3 + (\mu + 3)\bar{\xi}} \quad (2.35)$$

This relation shows that solutions of the form $\bar{\xi}(a, x) = a^\beta F(x/a^\alpha)$ with $\beta \neq 0$ is possible only if $h[\bar{\xi}(a, x)]$ has a *very specific* form given by (2.35). In this form, h is a monotonically increasing function of $\bar{\xi}(a, x)$. There is, however, firm theoretical and numerical evidence [19],[37] to suggest that h increases with $\bar{\xi}(a, x)$ first, reaches a maximum and then decreases. In other words, the h for actual gravitational clustering is *not* in the form suggested by equation (2.35). *We, therefore, conclude that solutions of the form in equation (2.28) with $\beta \neq 0$ cannot exist in gravitational clustering.*

By a similar analysis, we can prove a stronger result: There are no solutions

of the form $\bar{\xi}(a, x) = \bar{\xi}(x/F(a))$ except when $F(a) \propto a^\alpha$. So self-similar evolution in clustering is a very special situation.

This result, incidentally, has an important implication. It shows that power-law initial conditions are very special in gravitational clustering and may not represent generic behaviour. This is because, for power laws, we have a strong constraint that the correlations etc can only depend on $q = xa^{-2/(n+3)}$. For more realistic — non-power law — initial conditions the shape can be distorted in a generic way during evolution.

All the discussion so far was related to finding *exact* scaling solutions. It is however possible to find *approximate* scaling solutions which are of practical interest. Note that we normally expect constants like α, β, μ etc to be of order unity while $\bar{\xi}(a, x)$ can take arbitrarily large values. If $\bar{\xi}(a, x) \gg 1$ then equation (2.35) shows that h is approximately a constant with $h = (\beta - \alpha\mu)/(\mu + 3)$. In this case

$$\bar{\xi}(a, x) = a^\beta F(q) \propto a^\beta q^\mu \propto a^{(\beta - \alpha\mu)} x^\mu \propto a^{h(\mu+3)} x^\mu \quad (2.36)$$

which has the form $\bar{\xi}(a, x) = a^{3h} F(a^h x)$ which was obtained earlier by directly integrating equation (2.5) with constant h . We shall say more about such approximate solutions in the next section.

2.5 Units of the nonlinear universe

Having reached the conclusion that *exact* solutions of the form $\bar{\xi}(a, x) = a^2 G(x)$ are not possible, we will ask the question: Are there such *approximate* solutions? And if so, how do they look like? We will see that such profiles — which we shall call “pseudo-linear profiles” — that evolve very close to the above form indeed exist. In order to obtain such a solution and check its validity, it is better to use the results of section 2.2.1 and proceed as follows:

We are trying to find an approximate solution of the form $\bar{\xi}(a, x) = a^2 G(x)$ to equation (2.5). Since the linear correlation function $\bar{\xi}_L(a, x)$ does grow as a^2 at fixed x , continuity demands that $\bar{\xi}(a, x) = \bar{\xi}_L(a, x)$ for all a and x . [This can be proved more formally as follows: Let $\bar{\xi} = a^2 G(x)$ and $\bar{\xi}_L = a^2 G_1(x)$ for some range $x_1 < x < x_2$. Consider a sufficiently early epoch $a = a_i$ at which all the scales in the range (x_1, x_2) are described by linear theory so that $\bar{\xi}(a_i, x) = \bar{\xi}_L(a_i, x)$. It follows that $G_1(x) = G(x)$ for all $x_1 < x < x_2$. Hence $\bar{\xi}(a, x) = \bar{\xi}_L(a, x)$ for all a in $x_1 < x < x_2$. By choosing a_i sufficiently small, we can cover any range (x_1, x_2) . So $\bar{\xi} = \bar{\xi}_L$ for any arbitrary range. *QED*]. Since we have a formal relation (2.10) between nonlinear and linear correlation functions, we should be able to determine the form of $G(x)$.

To do this we shall invert the form of the linear correlation function $\bar{\xi}_L(a, l) = a^2 G(l)$ and write $l = G^{-1}(a^{-2}\bar{\xi}_L) \equiv F(a^{-2}\bar{\xi}_L)$ where F is the inverse function of G . We also know that the linear correlation function $\bar{\xi}_L(a, l)$ at scale l can be expressed as $\mathcal{V}[\bar{\xi}(a, x)]$ in terms of the true correlation function $\bar{\xi}(a, x)$ at scale x where

$$l = x(1 + \bar{\xi}(a, x))^{1/3} \quad (2.37)$$

So we can write

$$l = F\left[\frac{\bar{\xi}_L(a, l)}{a^2}\right] = F\left[\frac{\mathcal{V}[\bar{\xi}(a, x)]}{a^2}\right] \quad (2.38)$$

But x can be expressed as $x = F[\bar{\xi}_L(a, x)/a^2]$; Substituting this in (2.37) we have

$$l = F\left[\frac{\bar{\xi}_L(a, x)}{a^2}\right] [1 + \bar{\xi}]^{1/3} \quad (2.39)$$

From our assumption $\bar{\xi}_L(a, x) = \bar{\xi}(a, x)$; therefore this relation can also be written as

$$l = F\left[\frac{\bar{\xi}(a, x)}{a^2}\right] (1 + \bar{\xi})^{1/3} \quad (2.40)$$

Equating the expressions for l in (2.38) and (2.40) we get an implicit functional equation for F :

$$F \left[\frac{\mathcal{V}[\bar{\xi}]}{a^2} \right] = F \left[\frac{\bar{\xi}}{a^2} \right] (1 + \bar{\xi})^{1/3} \quad (2.41)$$

which can be rewritten as

$$\frac{F \left[\mathcal{V}(\bar{\xi})/a^2 \right]}{F \left[\bar{\xi}/a^2 \right]} = (1 + \bar{\xi})^{1/3} \quad (2.42)$$

This equation should be satisfied by the function F if we need to maintain the relation $\bar{\xi}(a, x) = \bar{\xi}_L(a, x)$.

To see what this implies, note that the left hand side should not vary with a at fixed $\bar{\xi}$. This is possible only if F is a power law:

$$F(\bar{\xi}) = A\bar{\xi}^m \quad (2.43)$$

which in turn constrains the form of $\mathcal{V}(\bar{\xi})$ to be

$$\mathcal{V}(\bar{\xi}) = \bar{\xi} (1 + \bar{\xi})^{1/3m} \quad (2.44)$$

Knowing the particular form for \mathcal{V} we can compute the corresponding $h(\bar{\xi})$ from the relation

$$\frac{d \ln \mathcal{V}}{d \bar{\xi}} = \frac{2}{3} \frac{1}{(1 + \bar{\xi}) h(\bar{\xi})} \quad (2.45)$$

For the $\mathcal{V}(\bar{\xi})$ considered in equation (2.44) we get

$$h = \frac{2\bar{\xi}}{3 + (3 + 1/m)\bar{\xi}} \quad (2.46)$$

which is the same result obtained by putting $\beta = 2$, $\alpha = 0$ in equation (2.28).

We thus recover our old result — as we should — that *exact* solutions of the form $\bar{\xi}(a, x) = \bar{\xi}_L(a, x) = a^2 G(x)$ are *not* possible because the correct $\mathcal{V}(\bar{\xi})$ and $h(\bar{\xi})$ do not have the forms in equations (2.44) and (2.46) respectively. But, as in the last section, we can look for approximate solutions.

We note from equation (2.44) that for $\bar{\xi} \gg 1$, we have

$$\mathcal{V}(\bar{\xi}) = \bar{\xi}^{(1+1/3m)}; \quad F(\bar{\xi}) \propto \bar{\xi}^m; \quad G(\bar{\xi}) \propto \bar{\xi}^{1/m} \quad (2.47)$$

This can be rewritten as

$$\mathcal{V}(\bar{\xi}) = \bar{\xi}^\nu; \quad F(\bar{\xi}) \propto \bar{\xi}^{1/3(\nu-1)}; \quad G(\bar{\xi}) \propto \bar{\xi}^{3/(\nu-1)} \quad (2.48)$$

In other words if $\mathcal{V}(\bar{\xi})$ can be approximated as $\bar{\xi}^\nu$, we have an approximate solution of the form

$$\bar{\xi}(a, x) = a^2 G(x) = a^2 x^{3(\nu-1)} \quad (2.49)$$

Since the \mathcal{V} in equation (2.12) is well approximated by the power laws in (2.11) so that

$$\mathcal{V}(\bar{\xi}) \propto \bar{\xi}^{1/3} \quad (1 \lesssim \bar{\xi} \lesssim 200) \quad (2.50)$$

$$\propto \bar{\xi}^{2/3} \quad (200 \lesssim \bar{\xi}) \quad (2.51)$$

we can take $\nu = 1/3$ in the intermediate regime and $\nu = 2/3$ in the nonlinear regime. It follows from (2.48) that the approximate solution should have the form

$$F(\bar{\xi}) \propto \frac{1}{\sqrt{\bar{\xi}}} \quad (1 \lesssim \bar{\xi} \lesssim 200) \quad (2.52)$$

$$\propto \frac{1}{\bar{\xi}} \quad (200 \lesssim \bar{\xi}) \quad (2.53)$$

This gives the approximate form of a pseudo-linear profile which will grow as a^2 at all scales.

There is another way of looking at this solution which is probably more physical and throws light on the scalings of pseudo-linear profiles. We recall that, in the study of finite gravitating systems made of point particles and interacting via Newtonian gravity, isothermal spheres play an important role. They can be shown to be the local maxima of entropy [35] and hence dynamical evolution drives the

system towards an $(1/x^2)$ profile. Since one expects similar considerations to hold at small scales, during the late stages of evolution of the universe, we may hope that isothermal spheres with $(1/x^2)$ profile may still play a role in the late stages of evolution of clustering in an expanding background. However, while converting the profile to correlation, we have to take note of the issues discussed in section 2. In the intermediate regime, dominated by scale invariant radial collapse [37], the density will scale as the correlation function and we will have $\bar{\xi} \propto (1/x^2)$. On the other hand, in the nonlinear end, we have the relation $\gamma = 2\epsilon - 3$ [see equation (2.21)] which gives $\bar{\xi} \propto (1/x)$ for $\epsilon = 2$. Thus, if isothermal spheres are the generic contributors, then we expect the correlation function to vary as $(1/x)$ and nonlinear scales, steepening to $(1/x^2)$ at intermediate scales. Further, since isothermal spheres are local maxima of entropy, a configuration like this should remain undistorted for a long duration. This argument suggests that a $\bar{\xi}$ which goes as $(1/x)$ at small scales and $(1/x^2)$ at intermediate scales is likely to be a candidate for pseudo-linear profile. It was found that this is indeed the case.

To go from the scalings in two limits given by equation (2.52) to an actual profile, we can use some fitting function. By making the fitting function sufficiently complicated, we can make the pseudo-linear profile more exact. We shall, however, choose the simplest interpolation between the two limits and try the ansatz:

$$F(z) = \frac{A}{\sqrt{z} (\sqrt{z} + B)} \quad (2.54)$$

where A and B are constants. Using the original definition $l = F[\bar{\xi}_L/a^2]$ and the condition that $\bar{\xi} = \bar{\xi}_L$, we get

$$\frac{A}{\sqrt{\bar{\xi}/a^2} (\sqrt{\bar{\xi}/a^2} + B)} = l \quad (2.55)$$

This relation implicitly fixes our pseudo-linear profile. Solving for $\bar{\xi}$, we get

$$\bar{\xi}(a, x) = \left(\frac{Ba}{2} \left(\sqrt{1 + \frac{L}{x}} - 1 \right) \right)^2 \quad (2.56)$$

with $L = 4A/B^2$. Since this profile is not a pure power law, this will satisfy the equation (2.42) only approximately. We choose B such that the relation

$$F\left(\frac{\mathcal{V}(\bar{\xi})}{a^2}\right) = F\left(\frac{\bar{\xi}}{a^2}\right) (1 + \bar{\xi})^{1/3} \quad (2.57)$$

is satisfied to greatest accuracy at $a = 1$. This approximate profile works rea-

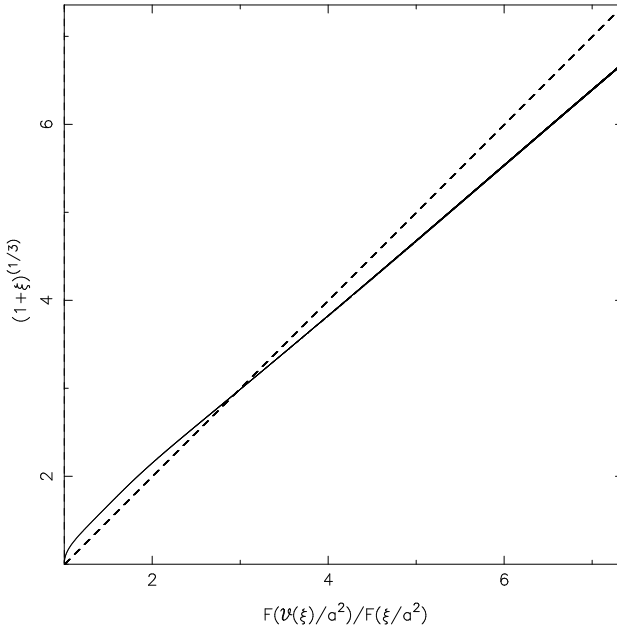


Figure 2.1: The approximate solution to the functional equation determining the pseudo-linear profile.

sonably well. Figures 2.1 and 2.2 show this result. In figure 2.1 we have plotted the ratio $F(\mathcal{V}(\bar{\xi})/a^2)/F(\bar{\xi}/a^2)$ on the x-axis and the function $(1 + \bar{\xi})^{1/3}$ on the y-axis. If the function in (2.56) satisfies equation (2.42) exactly, we should get a

45-degree line in the figure which is shown by a dashed line. The fact that our curve is pretty close to this line shows that the ansatz in (2.56) satisfies equation (2.42) fairly well. The optimum value of B chosen for this figure is $B = 38.6$. When a is varied from 1 to 10^3 , the percentage of error between the 45-degree line and our curve is less than about 20 percent in the worst case. It is clear that our profile in (2.56) satisfies equation (2.57) quite well for a dynamic range of 10^6 in a^2 .

Figure 2.2 shows this result more directly. We evolve the pseudo linear profile form $a^2 = 1$ to $a^2 \approx 1000$ using the NSR, and plot $[\bar{\xi}(a, x)/a^2]$ against x . The dot-dashed, dashed and two solid curves (upper one for $a^2 = 100$ and lower one for $a^2 = 900$) are for $a^2 = 1, 9, 100$ and 900 respectively. The overlap of the curves show that the profile does grow approximately as a^2 . Also shown are lines of slope -1 (dotted) and -2 (solid); clearly $\bar{\xi} \propto x^{-1}$ for small x and $\bar{\xi} \propto x^{-2}$ in the intermediate regime.

We emphasize that we have chosen in equation (2.56) the simplest kind of ansatz combining the two regimes and we have used only two parameters A and B . It is quite possible to come up with more elaborate fitting functions which will solve our functional equation far more accurately but we have not bothered to do so for two reasons: (i) Firstly, the fitting functions in equation (2.11) for $\mathcal{V}(z)$ itself is approximate and is probably accurate only at 10-20 percent level. There has also been repeated claims in literature that these functions have weaker dependence on n which we have ignored for simplicity. (ii) Secondly, one must remember that only those $\bar{\xi}$ which correspond to positive definite $P(k)$ are physically meaningful. This happens to be the case our choice [which can be verified by explicit numerical integration with a cutoff at large x] but this may not be true for arbitrarily complicated fitting functions. Incidentally, another

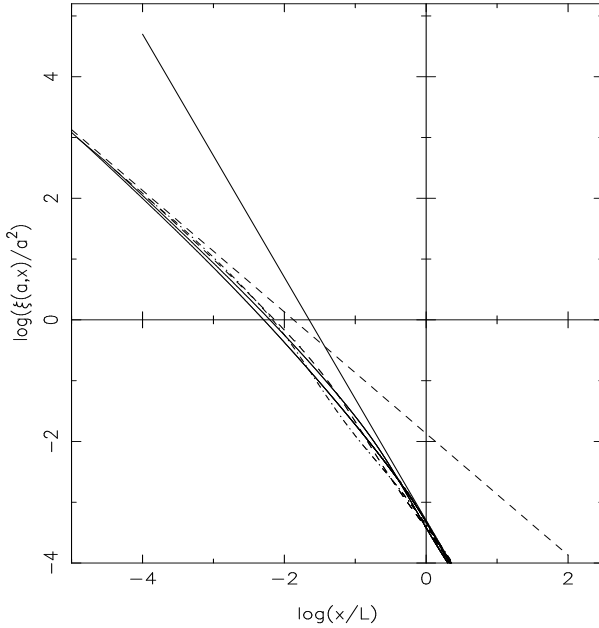


Figure 2.2: The dot-dashed,dashed and two solid curves (upper one for $a^2 = 100$ and lower one for $a^2 = 900$) are for $a^2 = 1, 9, 100$ and 900 . The dotted straight line is of slope -1 and the solid one is of slope-2 showing both the $1/x$ and $1/x^2$ regions of the profile.

simple fitting function for the pseudo-linear profile is

$$\bar{\xi}(a, x) = a^2 \frac{A'}{(x/L')[((x/L') + 1]} \quad (2.58)$$

with $A' = B^2$ and $L' = L/4$.

If a more accurate fitting is required, one can obtain it more directly from equation (2.16). Setting $n_a = 2$ in that equation predicts the instantaneous spatial slope of $\bar{\xi}(a, x)$ to be

$$\frac{\partial \ln \bar{\xi}(a, x)}{\partial \ln x} = \frac{2}{h[\bar{\xi}(a, x)]} - 3\left(1 + \frac{1}{\bar{\xi}(a, x)}\right) \quad (2.59)$$

which can be integrated to give

$$\ln \frac{x}{L} = \int_{\bar{\xi}[L]}^{\bar{\xi}[x]} \frac{hd\bar{\xi}}{\bar{\xi}(2-3h)-3h} \quad (2.60)$$

at $a = 1$ with L being an arbitrary integration constant. Numerical integration of this equation will give a profile which varies as $(1/x)$ at small scales and goes over to $(1/x^2)$ and then to $(1/x^3), (1/x^4), \dots$ etc with an asymptotic logarithmic dependence. In the regime $\bar{\xi}(a, x) > 1$, this will give results reasonably close to our fitting function.

It should be noted that equation (2.42) reduces to an identity for any F , in the limit $\bar{\xi} \rightarrow 0$ since, in this limit $\mathcal{V}(z) \approx z$. This shows that we are free to modify our pseudo-linear profile at large scales into any other form [essentially determined by the input linear power spectrum] without affecting any of our conclusions.

Finally, we will discuss a different way of thinking about pseudolinear profiles. In studying the evolution of the density contrast $\delta(a, \mathbf{x})$, it is conventional to expand in term of the plane wave modes as

$$\delta(a, \mathbf{x}) = \sum_{\mathbf{k}} \delta(a, \mathbf{k}) \exp(i\mathbf{k} \cdot \mathbf{x}) \quad (2.61)$$

In that case, the *exact* equation governing the evolution of $\delta(a, \mathbf{k})$ is given by [45]

$$\frac{d^2\delta_{\mathbf{k}}}{da^2} + \frac{3}{2a} \frac{d\delta_{\mathbf{k}}}{da} - \frac{3}{2a^2} \delta_{\mathbf{k}} = \mathcal{A} \quad (2.62)$$

where \mathcal{A} denotes the terms responsible for the nonlinear coupling between different modes. The expansion in equation (2.61) is, of course, motivated by the fact that in the linear regime we can ignore \mathcal{A} and each of the modes evolve independently. For the same reason, this expansion is not of much value in the highly nonlinear regime.

This prompts one to ask the question: Is it possible to choose some other set of basis functions $Q(\alpha, \mathbf{x})$, instead of $\exp i\mathbf{k} \cdot \mathbf{x}$, and expand $\delta(a, \mathbf{x})$ in the form

$$\delta(a, \mathbf{x}) = \sum_{\alpha} \delta_{\alpha}(a) Q(\alpha, \mathbf{x}) \quad (2.63)$$

so that the nonlinear effects are minimised? Here α stands for a set of parameters describing the basis functions. This question is extremely difficult to answer, partly because it is ill-posed. To make any progress, we have to first give meaning to the concept of “minimising the effects of nonlinearity”. One possible approach we would like to suggest is the following: We know that when $\delta(a, \mathbf{x}) \ll 1$, then $\delta(a, \mathbf{x}) \propto a F(\mathbf{x})$ for *any* arbitrary $F(\mathbf{x})$; that is all power spectra grow as a^2 in the linear regime. In the intermediate and nonlinear regimes, no such general statement can be made. But it is conceivable that there exists certain *special* power spectra for which $P(\mathbf{k}, a)$ grows (at least approximately) as a^2 even in the nonlinear regime. For such a spectrum, the left hand side of (2.62) vanishes (approximately); hence the right hand side should also vanish. *Clearly, such power spectra are affected least by nonlinear effects.* Instead of looking for such a special $P(k, a)$ we can, equivalently look for a particular form of $\bar{\xi}(a, x)$ which evolves as closely to the linear theory as possible. Such correlation functions and corresponding power spectra [which are the pseudo-linear profiles] must be capable of capturing most of the essence of nonlinear dynamics. In this sense, we can think of our pseudo-linear profiles as the basic building blocks of the nonlinear universe. The fact that the correlation function is closely related to isothermal spheres, indicates a connection between local gravitational dynamics and large scale gravitational clustering.

2.6 Results and Summary

It seems reasonable to hope that the late stage evolution of collisionless point particles, interacting via Newtonian gravity in an expanding background, should be understandable in terms of a simple paradigm. This chapter tries to realise this within some well defined framework. It should be viewed as a first step in a new direction.

There are three key points which emerge from this analysis. The first is the fact that we have been able to find approximate correlation functions which evolve preserving their shapes. We achieved this by looking at the structure of an exact equation which obeys certain nonlinear scaling relations. As we emphasised before, the existence of such special class of solutions to the equations of gravitational dynamics is an important feature.

Secondly, we should take note of the role played by the “isothermal” profile ($1/x^2$) in our solution. Such a profile can lead to correlation functions which go as $(1/x)$ at small scales and $(1/x^2)$ in the intermediate scales. If this profile is indeed “special” then one expects it to lead to a pseudo-linear profile for the correlation function. Our analysis shows that there is indeed good evidence for this feature. If one accepts this evidence, then the next level of enquiry would be to ask why $(1/x^2)$ profiles are “special”. In the statistical mechanics of gravitating systems, one can show that these profiles arise as end stages of violent relaxation which operates at dynamical time scales. Whether a similar reasoning holds in an expanding background, independent of the index for power spectrum, is open to question. We emphasise that our equations, along with NSR, naturally lead to a pseudo-linear profile, which can be interpreted and understood in terms of isothermal density profiles for halos; we did not have to assume anything a priori

regarding the halo profiles.

In a more pragmatic way, one can understand the pseudo-linear profile from the dependence of the rate of growth of the correlation function on the local slope. The NSR suggest that $\bar{\xi}$ grows (approximately) as $a^{6/(n_{eff}+4)}$ in the intermediate regime and as $a^{6/(n_{eff}+5)}$ in the nonlinear regime. This scaling shows that $n_{eff} = -1$ grows as a^2 in the intermediate regime and $n_{eff} = -2$ grows as a^2 in the nonlinear regime. This is precisely the form our pseudo-linear profile has. Also, in the intermediate regime, the correlation grows faster than a^2 if $n_{eff} < -1$ and slower than a^2 if $n_{eff} > -1$. The net effect is, of course, to straighten out a curved correlation and drive it to $n = -1$. Similar effect drives the correlations to $n = -2$ in the nonlinear regime.[see [10] for a more detailed discussion of this aspect in the intermediate regime]. Of course, one still needs to understand the dependence of growth rate on the n_{eff} from more physical considerations to get the complete picture. We have not addressed what is the timescale over which clustering can lead to the psuedo-linear profile assuming that it does.

The last aspect has to do with what one can achieve using the pseudo-linear profiles. In principle, one would like to build the nonlinear density field through a superposition of pseudo-linear profiles but this is a mathematically complex problem. As a first step one should understand why the nonlinear term in equation (2.62) is subdominant for such a profile. This itself is complicated since we have only fixed the power spectrum — but not the phases of the density modes — while the nonlinear terms do depend on the phase.

High resolution numerical simulations serve to test the framework presented in this chapter but resource limitations hamper such experiments. The following chapter discusses the general theory of two dimensional simulations which may be used to explore these issues in greater detail by bypassing the resource constraints

plaguing 3-D simulations.

Chapter 3

A formal analysis of two dimensional gravity

Computers make it easy to do a lot of things but most of the things they make it easier to do don't need to be done – Andy Rooney

3.1 Introduction

The analytical explorations of the previous chapter has clearly shown that the equations describing the growth of density perturbations in the highly nonlinear stage are analytically intractable and hence large scale numerical simulations are resorted to for exploration of this regime.

These N–Body simulations require large amount of computing resources (CPU, memory and storage space) if one is to get the requisite amount of dynamical range, *i.e.* good resolution in force and mass, large range in values of density etc. Time and resource constraints usually limit our ability to probe structure formation issues more deeply using computers, once the required resources are at the limits of technological feasibility. The key parameter which decides the feasibility level of numerical simulations is the size of a simulation, which — in turn — is characterised by: (i) The number of particles in the simulation volume, which is generally specified as N^D , where D is the dimensionality of the simu-

lation (usually 2 or 3) and (ii) The number of mesh points (M) along any axis which determines the minimum length scale at which the results can be treated as reliable indicators of physical phenomena. In order to create a simulation volume that is a fair sample of the universe one needs about 10^7 particles and in order to have a high enough force resolution one needs to increase the number of grid points adequately [9]. Let us suppose we have 160^3 particles in three dimensions and our grid is 160 units on a side. Then, for the same amount of computational resources one can simulate a two dimensional situation with 2048^2 particles on a 2048^2 grid ($160^3 \approx 2048^2$). So, if we can extract useful (i.e. generalisable to the three dimensional case) physical insights from results in two dimensions, then simulations of two dimensional gravity will be helpful. This hope has led to a large number of two dimensional simulations in the field of gravitational clustering ([7], [56], [50], [6], [51]).

There are three ways in which two dimensional gravity can be operationally defined and corresponding numerical simulations undertaken: (i) Consider a system of point particles in a three dimensional (expanding) background with the force of interaction being given by Newton's law of gravitation (*i.e* $F \propto 1/r^2$). The initial positions and velocities of the particles are such that they all lie in the same plane and all the velocities are in the plane *i.e* there are no velocity components orthogonal to the plane. This system will evolve with the particles being confined to the plane with clustering occurring in the plane. Thus, we have a two dimensional clustering scenario. (ii) Another system we can consider consists of infinite, thin 'needles' located parallel to each other. The mass elements in the 'needles' still interact through the $1/r^2$ force, but the interaction between 'needles' (obtained by summing over the mass elements) is given by a $1/r$ force. In this case as well, the background space expands uniformly in three dimensions.

The two dimensional clustering that we study is the clustering of these ‘needles’, examined by taking a slice orthogonal to the ‘needles’. (iii) The third possibility involves writing down the Einstein’s equations in two dimensions, finding the homogeneous and isotropic cosmological solution, taking the Newtonian limit (in which the potentials due to density perturbations and background metric can be superposed), finding the corresponding perfect fluid equations and solving them. In this case, we will have a background spacetime expanding in *two* dimensions unlike the other two cases. (There is yet another, fourth possibility, which can be defined only in an *ad hoc* manner discussed towards the end of the chapter.)

The first case is not of much interest for cosmological simulations since the system is anisotropic, confined to a single plane and the clustering takes place in a specific plane *only because the initial conditions were specifically selected* to give this result. Hence we will not discuss it and it is mentioned here only for completeness. The way simulations in two dimensions are carried out usually is by simulating the second case and then defining the ‘particles’ as the intersection of the ‘needles’ with any plane orthogonal to them. In this case – as in the first case – the background spacetime expands in three dimensions (for a flat dust dominated universe the scale factor $a(t)$ goes as $t^{2/3}$). The clustering that we observe and quantify in two dimensions, is basically the clustering of these needles in three dimensions. But this is also an anisotropic situation since the background spacetime is expanding in three dimensions. As an alternative we may try to write down the equations derived from Einstein’s equations in two dimensions and examine how a system of particles interacting in a two dimensional expanding background spacetime is to be simulated.

In the rest of this chapter we shall examine the third alternative. We will take a very general approach by developing the formal theory of $(D + 1)$ gravity

and considering $D = 2$ as a special case [15].

The basic layout of the chapter is as follows: In section (3.2) we first define the analogue of Einstein's gravity in $(D + 1)$ dimensions, discuss the Newtonian limit and its corresponding Poisson's equation and then go on to analyse the Friedmann metric in $(D+1)$ dimensions for a flat universe with dust. In section (3.3) we write down the D dimensional fluid equations and obtain the equation governing the density perturbations. This equation is then solved in the linear approximation and using the Spherical Top Hat model. Then in section (3.4) and section (3.5) we specialise to the cases $D = 3$ and $D = 2$ respectively. Finally, in section (3.6) we summarise and discuss the implications of the results obtained in the earlier sections.

3.2 Formal $(D + 1)$ dimensional gravity

We start our analysis of $(D + 1)$ dimensional (1 time dimension and D space dimensions) gravity from the action principle which we assume has the same form as that used in $(3 + 1)$ dimensions. Using this action we construct the corresponding $(D+1)$ dimensional Einstein equations which will be subsequently used to study structure formation and spherical collapse. Thus, we begin with the action principle,

$$\mathcal{S} = \mathcal{S}_g + \mathcal{S}_m = -\frac{c^4}{2\kappa(D)} \int d^{(D+1)}x R\sqrt{|g|} + \int d^{(D+1)}x \mathcal{L}_m \quad (3.1)$$

where \mathcal{S}_g is the action for the gravitational field, \mathcal{S}_m is the action for the matter fields, g is the determinant of the metric tensor g_{ik} , R is the Ricci scalar, $\kappa(D)$ is a suitable constant which can be, in general, a function of D (when $D = 3$, $\kappa = 8\pi G$, G being the usual gravitational constant) and \mathcal{L}_m is the lagrangian density for the matter fields. The metric signature we adopt is $(+, -, -, -, \dots, -)$.

We adopt the following convention regarding indices. Latin alphabets $i, j, k \dots$ are used to represent $(D + 1)$ dimensional indices which take on the values $(0, 1, 2, \dots, D)$ while greek letters are used to denote D dimensional indices taking on the values $(1, 2, \dots, D)$. Varying the total action \mathcal{S} with respect to g_{ik} we obtain Einstein's equations,

$$G_{ik} \equiv R_{ik} - \frac{1}{2} g_{ik} R = \frac{\kappa(D)}{c^4} T_{ik} \quad (3.2)$$

where T_{ik} is the energy momentum tensor of the matter fields and is defined by

$$\frac{1}{2} \sqrt{|g|} T_{ik} = \frac{\partial(\sqrt{|g|} \mathcal{L}_m)}{\partial g^{ik}} - \frac{\partial}{\partial x^l} \left(\frac{\partial(\sqrt{|g|} \mathcal{L}_m)}{\partial (\partial g^{ik}/\partial x^l)} \right) \quad (3.3)$$

G_{ik} is the Einstein tensor and R_{ik} is the usual Ricci tensor. Note that the $(1/2)$ that appears in Einstein's equations arises due to the square root in the term $\sqrt{|g|}$ and has nothing to do with the dimension of the spacetime.

We will use the above equations in the subsections to follow. In subsection (3.2.1), we will study the Newtonian limit of the metric tensor and then construct the corresponding Poisson equation that relates the Newtonian gravitational field ϕ to the matter density ρ . Then, in subsection (3.2.2), we analyse the Friedmann metric in $(D + 1)$ dimensions and the corresponding Newtonian limit of this metric is derived.

3.2.1 Poisson equation in D dimensions

In this section, we derive the Poisson equation relating the gravitational potential ϕ to the matter density ρ . We keep all factors of c since the Newtonian limit involves the limit $c \rightarrow \infty$. The analysis here follows closely the treatment in [28]. Consider the metric.

$$ds^2 = \left(1 + \frac{2\phi}{c^2}\right) c^2 dt^2 - dl^2 \quad (3.4)$$

where ϕ is a function of space and time with dimensions of velocity square. The term dl^2 is the D dimensional spatial line element given by the formula

$$dl^2 = \sum_{\alpha=1}^D (dx^\alpha)^2 \quad (3.5)$$

We will now show that the metric written above is the Newtonian limit of Einstein's gravitational equations. We do this by showing that, in the Newtonian limit, the equation of motion of a particle follows Newton's force law with the force $-m\nabla\phi\dots$. In relativistic mechanics, the motion of a particle of mass m is determined by the action function S

$$S = -mc \int ds = -mc \int c dt \sqrt{\left(1 + \frac{2\phi}{c^2} - \frac{v^2}{c^2}\right)} \quad (3.6)$$

where v^2 is the square of the magnitude of the particle's velocity in D dimensions. In arriving at the second equality we have used the form of the metric in equation (3.4). In the limit $c \rightarrow \infty$, the action S can be approximated as

$$S \approx -mc^2 \int dt \left(1 + \frac{2\phi - v^2}{2c^2}\right) = \int dt \left(-mc^2 + \frac{1}{2}mv^2 - m\phi\right) \quad (3.7)$$

The equation of motion for the particle can be immediately written down and we obtain

$$m \frac{d\mathbf{v}}{dt} = -m\nabla\phi \quad (3.8)$$

where \mathbf{v} is the velocity vector in D space dimensions. Thus, Newton's force law is recovered in the non-relativistic limit and from this we conclude that the metric given in equation (3.4) is the Newtonian limit of Einstein's gravitational equations with ϕ acting as the Newtonian gravitational potential.

The relation between ϕ and the mass density ρ is found by taking the $c \rightarrow \infty$ limit of Einstein's equations. This procedure, in $(3+1)$ gravity, determines the constant $\kappa(D)$ since the Poisson equation is explicitly known. In other dimensions

however, a definite criterion, like Gauss's law for example, must be imposed in order to determine $\kappa(D)$. We now consider the limit $c \rightarrow \infty$ of Einstein's equations in the following manner. First, we use the line element given in equation (3.4) to calculate the Ricci tensor component R_{00}

$$R_{00} = \frac{1}{c^2} \frac{1}{c^2 + 2\phi} (\partial_\mu \phi)(\partial^\mu \phi) - \frac{1}{c^2} \partial_\mu \partial^\mu \phi \quad (3.9)$$

where the summation convention has been invoked in the above equation and the sum over μ is only over the *spatial* dimensions. Then, using equation (3.2), we obtain,

$$R = -\frac{2\kappa(D)}{c^4(D-1)} T \quad (3.10)$$

where we have used the fact that $g_{ik}g^{ik} = D + 1$ and assumed $D \neq 1$. Thus, Einstein's equations can be written in the equivalent form,

$$R_{ik} = \frac{\kappa(D)}{c^4} \left(T_{ik} - \frac{1}{D-1} g_{ik} T \right). \quad (3.11)$$

where T is the trace of T_{ik} . The energy momentum tensor of point particles is $T_{ik} = \rho c^2 u_i u_k$ where ρ is the mass density and u_i is the four velocity. Since, in the non-relativistic limit, the macroscopic motion is slow, the space components of u_i can be neglected and only the time component should be retained. Therefore, $u_0 = \sqrt{g_{00}}$ and $u_\mu \approx 0$ for all μ . Consequently, only $T_{00} = g_{00}\rho c^2$ is non-zero. Substituting for T_{ik} into equation (3.11) and using the expression in equation (3.9) for R_{00} , we get,

$$\frac{1}{c^2} \partial_\mu \partial^\mu \phi = - \left(\frac{D-2}{D-1} \right) \left(1 + \frac{2\phi}{c^2} \right) \frac{\kappa(D)}{c^4} \rho c^2 \approx - \left(\frac{D-2}{D-1} \right) \frac{\kappa(D)}{c^2} \rho \quad (3.12)$$

That is,

$$\nabla^2 \phi = \left(\frac{D-2}{D-1} \right) \kappa(D) \rho \quad (3.13)$$

where ∇^2 is the usual Laplacian operator in D dimensions. This equation is the Poisson equation in D dimensions. Note that when substituting for the value

of R_{00} from equation (3.9), we neglected the first term in comparison with the second since the former is of order c^{-4} while the latter is only of order c^{-2} .

3.2.2 Friedmann Universe in $(D + 1)$ dimensions

Let us next consider the maximally symmetric Robertson-Walker metric in $(D+1)$ dimensions, specialising to flat space with $k = 0$ (we set $c = 1$ in this and in subsequent sections),

$$ds^2 = dt^2 - a^2(t)dl^2 \quad (3.14)$$

where $a(t)$ is the scale factor and dl^2 is the D dimensional line element given in equation (3.5). Calculating the components of the Einstein tensor, we obtain,

$$\begin{aligned} G_{00} &= \frac{D(D-1)\dot{a}^2}{2a^2} \\ G_{11} = G_{22} = \dots = G_{DD} &= (1-D)a\ddot{a} + \\ &\left(1 - \frac{D}{2}\right)(D-1)\dot{a}^2 \end{aligned} \quad (3.15)$$

where \dot{a} stands for $da(t)/dt$ and similarly \ddot{a} is the second derivative of $a(t)$ with respect to time. All the other components are zero. For consistency, the energy momentum tensor must have the form $T_k^i = \text{diag}(\rho, -p, -p, -p, \dots)$ where ρ is the matter density and p is the pressure.

Substituting in Einstein's equations, we obtain,

$$\frac{D(D-1)\dot{a}^2}{2a^2} = \kappa(D)\rho \quad (3.16)$$

$$\frac{\ddot{a}}{a} + \frac{D-2}{2}\frac{\dot{a}^2}{a^2} = -\frac{\kappa(D)p}{D-1} \quad (3.17)$$

The above two equations, together with the equation of state in the form $p = p(\rho)$ completely specify the system. Solving these three equations, we can determine $a(t)$, $\rho(t)$ and subsequently $p(t)$. Combining equations (3.16,3.17), we get the

single equation,

$$\frac{\ddot{a}}{a} = -\frac{\kappa(D)}{D(D-1)} [(D-2)\rho + Dp]. \quad (3.18)$$

We now specialise to the case of pressureless dust with the equation of state $p = 0$. Using the principle of conservation of energy and momentum expressed by the relation

$$T^k_{i;k} = 0 \quad (3.19)$$

we derive the following relation,

$$\begin{aligned} T^k_{i;k} &= \frac{1}{\sqrt{|g|}} \frac{\partial}{\partial x^k} \left(\sqrt{|g|} T^k_i \right) - \frac{1}{2} \frac{\partial g_{kl}}{\partial x^i} T^{kl} \\ &= \frac{1}{a^D} \frac{\partial}{\partial x^k} \left(a^P T^k_i \right) - \frac{1}{2} \frac{\partial g_{kl}}{\partial x^i} T^{kl} = 0 \end{aligned} \quad (3.20)$$

Noting that the only non-zero component of T^i_k is $T^0_0 = \rho$ we finally get

$$\rho a^D = \text{constant} = C_1 \quad (3.21)$$

Substituting the above relation into equation (3.16), and solving for $a(t)$ and subsequently for $\rho(t)$, we obtain the solutions,

$$a(t) = \left(\frac{D\kappa(D)C_1}{2(D-1)} \right)^{1/D} t^{2/D} \quad ; \quad \rho(t) = \left(\frac{2(D-1)}{D\kappa(D)} \right) t^{-2} \quad (3.22)$$

Let us next consider the Newtonian limit of the Friedmann metric. This limit is important because the length scales of interest in structure formation are small compared to the Hubble radius and the velocities in the system are also much smaller than c . This permits us to study the formation of large scale structures in the universe in a Newtonian framework where the effective potential due to the expanding background universe, Φ_{FRW} , and the potential due to the density perturbations, φ , can be simply superposed. In order to obtain Φ_{FRW} , we first recast the Friedmann metric in equation (3.14) into the more convenient form

$$ds^2 = dt^2 - a^2(t) (dX^2 + X^2 d\Omega^2) \quad (3.23)$$

where X is the radial distance in D dimensions and Ω is the corresponding solid angle. We then apply the transformations (see [38], pg 80,346)

$$r = Xa(t) \quad , \quad T = t - t_0 + \frac{1}{2}a\dot{a}X^2 + \mathcal{O}(X^4) \quad (3.24)$$

where only terms up to quadratic in X are retained. Direct calculations, correct upto this order, transforms the Friedmann line element to the form,

$$ds^2 \approx \left(1 - \frac{\ddot{a}}{a}r^2\right) dT^2 - dr^2 - r^2 d\Omega^2 \quad (3.25)$$

which upon comparison with the metric in equation (3.4) gives the equivalent Newtonian potential Φ_{FRW} in D dimensions as

$$\Phi_{\text{FRW}} = -\frac{1}{2}\frac{\ddot{a}}{a}r^2 \quad (3.26)$$

We will now use the results developed in the last two subsections to study structure formation and spherical collapse using the STH model.

3.3 Structure formation in D dimensions

Having determined the form of the Poisson equation in the Newtonian limit and analysed the Friedmann equations in $(D + 1)$ dimensions, we proceed to derive the equation for the growth of inhomogeneities in the expanding universe. After this we consider a specific model, the STH model, to study spherical collapse of matter.

3.3.1 Equation for density perturbations in D dimensions

Let us assume that matter in the universe is a perfect, pressureless fluid with density ρ_m and flow velocity \mathbf{U} . We can formally write down the D dimensional fluid equations describing a perfect fluid in an external potential field Φ_{tot} in a

proper coordinate system labelled by the D dimensional vector \mathbf{r} . Therefore, we have,

$$\left(\frac{\partial \rho_m}{\partial t} \right)_r + \nabla_r \cdot (\rho_m \mathbf{U}) = 0 \quad (3.27)$$

$$\left(\frac{\partial \mathbf{U}}{\partial t} \right)_r + (\mathbf{U} \cdot \nabla_r) \mathbf{U} = -\nabla_r \Phi_{\text{tot}} \quad (3.28)$$

where equation (3.27) is the usual continuity equation while equation (3.28) is the Euler equation for the fluid. The potential in equation (3.28), Φ_{tot} , is the total external Newtonian potential

$$\Phi_{\text{tot}} = \Phi_{\text{FRW}} + \varphi \quad (3.29)$$

where Φ_{FRW} is the background potential associated with the smooth background matter density ρ_{bm} and is given in equation (3.26) while φ is the potential caused by density perturbations ($\rho_m - \rho_{\text{bm}}$). The potential φ satisfies the Poisson equation given in equation (3.13). Thus,

$$\nabla_r^2 \varphi = \left(\frac{D-2}{D-1} \right) \kappa(D) (\rho_m - \rho_{\text{bm}}) = \left(\frac{D-2}{D-1} \right) \kappa(D) \rho_{\text{bm}} \delta \quad (3.30)$$

where δ is the density contrast defined by

$$\delta = \frac{\rho_m - \rho_{\text{bm}}}{\rho_{\text{bm}}} \quad (3.31)$$

We now transform to comoving coordinates defined by $\mathbf{x} = \mathbf{r}/a(t)$ and define the peculiar velocity \mathbf{v} by the relation

$$\mathbf{U} = H(t) \mathbf{r} + \mathbf{v} = \dot{a} \mathbf{x} + \mathbf{v} \quad (3.32)$$

where $\mathbf{v} = a \dot{\mathbf{x}}$ and $H(t) = (\dot{a}/a)$. Then, equation (3.27) and equation (3.28) become

$$\left(\frac{\partial \rho_m}{\partial t} \right)_x + D H \rho_m + \frac{1}{a} \nabla_x \cdot (\rho_m \mathbf{v}) = 0 \quad (3.33)$$

$$\left(\frac{\partial \mathbf{v}}{\partial t} \right)_x + H \mathbf{v} + \frac{1}{a} (\mathbf{v} \cdot \nabla_x) \mathbf{v} = -\frac{1}{a} \nabla_x \varphi \quad (3.34)$$

where we have used equation (3.26) to substitute for Φ_{FRW} . Similarly, in co-moving co-ordinates, equation (3.30) reduces to

$$\nabla_{\mathbf{x}}^2 \varphi = \left(\frac{D-2}{D-1} \right) \kappa(D) a^2 \rho_{\text{bm}} \delta \quad (3.35)$$

Using $\rho_m = \rho_{\text{bm}}(1+\delta)$, transforming the time variable from t to $a(t)$ and defining a new velocity variable \mathbf{u} by

$$\mathbf{u} = \frac{d\mathbf{x}}{da} = \frac{\mathbf{v}}{a\dot{a}} \quad (3.36)$$

we can obtain equations for $\delta(a)$ and $\mathbf{u}(a)$. Therefore, using equation (3.21) and performing the transformations, equation (3.33) and equation (3.34) further reduce to,

$$\frac{\partial \delta}{\partial a} + \nabla_{\mathbf{x}} \cdot [\mathbf{u}(1+\delta)] = 0 \quad (3.37)$$

$$\dot{a}^2 \frac{\partial \mathbf{u}}{\partial a} + \left(\ddot{a} + 2 \frac{\dot{a}^2}{a} \right) \mathbf{u} + \dot{a}^2 (\mathbf{u} \cdot \nabla_{\mathbf{x}}) \mathbf{u} = -\frac{1}{a^2} \nabla_{\mathbf{x}} \varphi \quad (3.38)$$

Now, we use the Friedmann equations in equations (3.16,3.17) with ρ replaced by ρ_{bm} and with $p = 0$ to substitute for \ddot{a} in the above equation. Further, we define a new potential Ψ by the relation

$$\Psi = \left(\frac{D(D-1)}{6-D} \right) \frac{1}{\kappa(D) \rho_{\text{bm}} a^3} \varphi \quad (3.39)$$

so that, upon using equation (3.35), one obtains,

$$\nabla_{\mathbf{x}}^2 \Psi = \left(\frac{D(D-2)}{6-D} \right) \frac{\delta}{a} \quad (3.40)$$

where all reference to $\kappa(D)$ has disappeared. Hence the final system of equations we need to tackle are,

$$\frac{\partial \delta}{\partial a} + \nabla_{\mathbf{x}} \cdot [\mathbf{u}(1+\delta)] = 0 \quad (3.41)$$

$$\frac{\partial \mathbf{u}}{\partial a} + (\mathbf{u} \cdot \nabla_{\mathbf{x}}) \mathbf{u} = -\frac{6-D}{2a} A [\nabla_{\mathbf{x}} \Psi + \mathbf{u}] \quad (3.42)$$

where A is given by the relation

$$A = \left(\frac{2\kappa(D)}{D(D-1)} \right) \frac{a^2}{\dot{a}^2} \rho_{\text{bm}} = \frac{\rho_{\text{bm}}(t)}{\rho_c(t)} ; \quad \rho_c \equiv \left(\frac{D(D-1)}{2\kappa(D)} \right) \frac{\dot{a}^2}{a^2} \quad (3.43)$$

For the $k = 0$ universe, we will set $A = 1$.

To proceed further and determine the equation satisfied by δ , we decompose the term $\partial_\alpha u_\beta$ (where u_β is the β th covariant component of the vector \mathbf{u} and ∂_α is short for $\partial/\partial x^\alpha$) as

$$\partial_\alpha u_\beta = \sigma_{\alpha\beta} + \Omega_{\alpha\beta} + \frac{1}{D} \delta_{\alpha\beta} \theta \quad \alpha, \beta = (1, 2, \dots, D) \quad (3.44)$$

where $\sigma_{\alpha\beta}$ is the traceless, symmetric shear tensor, $\Omega_{\alpha\beta}$ is the antisymmetric rotation tensor, θ is the (trace) expansion and $\delta_{\alpha\beta}$ is the Kronecker delta symbol. Then, equation (3.41) and equation (3.42) are combined by taking the divergence of equation (3.42) and using the above decomposition of $\partial_\alpha u_\beta$ to obtain a single equation for δ . Straightforward algebra gives,

$$\frac{d^2\delta}{da^2} + \left(\frac{6-D}{2a} \right) \frac{d\delta}{da} - \left(\frac{D(D-2)}{2a^2} \right) \delta(1+\delta) = \left(\frac{D+1}{D} \right) \frac{1}{(1+\delta)} \left(\frac{d\delta}{da} \right)^2 + (1+\delta)(\sigma^2 - 2\Omega^2) \quad (3.45)$$

where $\sigma^2 = \sigma_{\alpha\beta}\sigma^{\alpha\beta}$ and $\Omega^2 = (1/2)\Omega_{\alpha\beta}\Omega^{\alpha\beta}$. This equation is the full non-linear equation for δ . Apart from the obvious nonlinear terms containing δ^2 and $(d\delta/da)^2$, the term $(1+\delta)(\sigma^2 - 2\Omega^2)$, which is the contribution from the shear and rotation, is also non-linear. The non-linear terms in δ in the above equation render the equation unsolvable in general. Ignoring these non-linear terms to a first approximation, we can get a linear equation for $\delta(a)$,

$$\frac{d^2\delta}{da^2} + \left(\frac{6-D}{2a} \right) \frac{d\delta}{da} - \left(\frac{D(D-2)}{2a^2} \right) \delta = 0. \quad (3.46)$$

Assuming a power law solution for delta in the form $\delta \propto a^p$, we get,

$$p = \frac{D-4}{4} \pm \frac{1}{4} \sqrt{9D^2 - 24D + 16} \quad (3.47)$$

as the required values for p . Notice that δ has a growing mode as well as a decaying mode in general. The above solutions hold for all values of $D > 1$ in the linear regime.

Though the full non-linear equation is not solvable, by neglecting the contribution from the shear and rotation terms and by using a suitable ansatz for δ , the resulting non-linear equation *can* be solved. We proceed to do this within the framework of the STH model in the next section.

3.3.2 The Spherical Top Hat (STH) model

In the STH (spherical collapse) model, we assume spherical symmetry by neglecting the shear and rotation terms in the equation for δ . With this assumption the δ equation can be exactly solved.

Transforming equation (3.45) by changing the independent variable back to t , dropping the rotation and shear terms and using the Friedmann equations given in equations (3.16,3.17), we get,

$$\frac{d^2\delta}{dt^2} + 2\frac{\dot{a}}{a}\frac{d\delta}{dt} - \left(\frac{D+1}{D}\right)\frac{1}{(1+\delta)}\left(\frac{d\delta}{dt}\right)^2 = \left(\frac{D-2}{D-1}\right)\kappa(D)\rho_{\text{bm}}\delta(1+\delta) \quad (3.48)$$

We now define a function $R(t)$ by the relation

$$1 + \delta = \frac{\rho}{\rho_{\text{bm}}} = \frac{M}{C_D R^D(t) \rho_{\text{bm}}} \quad (3.49)$$

where $C_D = 2\pi^{D/2}/(D\Gamma[D/2])$ is the volume of a unit sphere in D dimensions introduced for later convenience and M is a constant. The expression for δ above can be rewritten using the relation $\rho_{\text{bm}}a^D = \rho_0 a_0^D$ from equation (3.21):

$$1 + \delta = \frac{M}{C_D \rho_0 a_0^D} \left[\frac{a}{R}\right]^D = \lambda \frac{a^D}{R^D} \quad (3.50)$$

where ρ_0 and a_0 are the matter density and scale factor at some (arbitrarily chosen) “present” epoch t_0 . Substituting equation (3.50) in equation (3.48), we

get an equation for the growth of $R(t)$ as,

$$\frac{d^2R}{dt^2} = -\frac{D-2}{D(D-1)} \frac{\kappa(D)}{C_D} \frac{M}{R^{D-1}} \quad (3.51)$$

[As an aside we may note that if the universe contains matter or fields with equations of state other than $p = 0$, the equation for $R(t)$ becomes

$$\frac{d^2R}{dt^2} = -\frac{D-2}{D(D-1)} \frac{\kappa(D)}{C_D} \frac{M}{R^{D-1}} - \frac{\kappa(D)}{D(D-1)} ((D-2)\rho + Dp)_{\text{rest}} R \quad (3.52)$$

where the term $((D-2)\rho + Dp)_{\text{rest}}$ comes from the smoothly distributed component with $p \neq 0$.]

From the form of the equation of motion of $R(t)$ we can give the following interpretation. Since the entire system considered above is spherically symmetric, we interpret R as the radius of a D dimensional spherical region containing a mass M . The equation of motion of R determines the motion of the surface of this region. In general, a spherical overdense region will be expected to initially expand because of the expansion of the background universe till the excess gravitational force due to the overdensity of enclosed matter stops the expansion and causes the region to collapse back on itself. We will discuss the cases $D = 3$ and $D = 2$ in the subsequent sections and determine the differences in the behaviour of the growth of inhomogeneities.

3.4 Summary of standard results in three dimensions

When $D = 3$, all the standard equations are recovered. First the Poisson equation satisfied by the Newtonian gravitational potential given by equation(3.13) reduces to the standard form,

$$\nabla^2\phi = 4\pi G\rho \quad (3.53)$$

where we have defined G by relating it to $\kappa(3)$ by $\kappa(3) = 8\pi G$. Similarly, equations (3.41) and equation (3.42) reduce to (with $A = 1$),

$$\frac{\partial \delta}{\partial a} + \nabla_{\mathbf{x}} \cdot [\mathbf{u}(1 + \delta)] = 0 \quad (3.54)$$

$$\frac{\partial \mathbf{u}}{\partial a} + (\mathbf{u} \cdot \nabla_{\mathbf{x}})\mathbf{u} = -\frac{3}{2a} [\nabla_{\mathbf{x}}\Psi + \mathbf{u}] \quad (3.55)$$

while the equation for Ψ becomes,

$$\nabla_{\mathbf{x}}^2\Psi = \frac{\delta}{a}. \quad (3.56)$$

In a similar manner, the δ equation reduces to,

$$\frac{d^2\delta}{da^2} + \frac{3}{2a} \frac{d\delta}{da} - \frac{3}{2a^2}\delta(1 + \delta) = \frac{4}{3(1 + \delta)} \left(\frac{d\delta}{da} \right)^2 + (1 + \delta)(\sigma^2 - 2\Omega^2) \quad (3.57)$$

and the solutions to the linear perturbation equation which is obtained by dropping the nonlinear terms and the $(\sigma^2 - 2\Omega^2)$ term, are

$$\delta \propto a^p, \quad p = 1, -\frac{3}{2} \quad (3.58)$$

which are well known. The STH model for $D = 3$ also reduces to the standard form

$$\frac{d^2R}{dt^2} = -\frac{GM}{R^2} - \frac{4\pi G}{3}(\rho + 3p)_{\text{rest}} R \quad (3.59)$$

which is again well known [38]. Therefore, it is seen that the full D dimensional equations reduce to the correct equations in three dimensions. Now we will go on to discuss the important case of $D = 2$.

3.5 Two dimensional gravity

If we naively consider the limit $D \rightarrow 2$ in the D dimensional equations, assuming that $\kappa(D)$ is finite in this limit, we obtain the following results. First, the Poisson equation (3.13) reduces to

$$\nabla^2\phi = 0 \quad (3.60)$$

The above result shows that in two dimensions, the gravitational potential does *not* couple to the matter density ρ . In structure formation, this means that inhomogeneities cannot grow since the perturbed potential φ is not related to δ at all. The second interesting result is that the background Newtonian potential Φ_{FRW} vanishes. This occurs because, referring back to equation (3.18), $\ddot{a} = 0$ for pressureless dust and hence the background potential is zero. Further, the δ equation reduces to

$$\frac{d^2\delta}{da^2} + \frac{2}{a} \frac{d\delta}{da} = \frac{3}{2(1+\delta)} \left(\frac{d\delta}{da} \right)^2 + (1+\delta)(\sigma^2 - 2\Omega^2). \quad (3.61)$$

Linearising the equation as before by dropping the $(\sigma^2 - 2\Omega^2)$ and $(d\delta/da)^2$ terms we obtain

$$\frac{d^2\delta}{da^2} + \frac{2}{a} \frac{d\delta}{da} = 0. \quad (3.62)$$

The solutions to the linearised equation are

$$\delta \propto a^p, \quad p = 0, -1. \quad (3.63)$$

Thus only a constant or the decaying mode is present. This is consistent with the result that the perturbed gravitational potential does not couple to δ . If one considers the STH model, it is easy to see that the growth equation for $R(t)$ reduces to

$$\frac{d^2R}{dt^2} = -\kappa(2)p_{\text{rest}}R \quad (3.64)$$

For, $p_{\text{rest}} = 0$, the solution to the above equation is just $R(t) = B_1t + B_2$ where B_1, B_2 are constants. This is to be expected since there is no gravitational force which can lead to clustering and as a consequence the radius simply grows with time just like the background universe. Thus, if $\kappa(D)$ is *finite* in the limit $D \rightarrow 2$, it is not possible to have gravitational clustering that can grow with time.

We can, however, try some alternative approaches to examine whether it is possible to have a consistent physical picture of growing structures for two dimensional gravity.

One possibility is that instead of assuming $\kappa(D)$ to be finite, let us assume that the expression $(\kappa(D)(D - 2))$ remains finite when $D \rightarrow 2$. This finite value can be fixed, for example, by invoking Gauss's theorem in D dimensions. This gives

$$\kappa(D) = \left(\frac{D-1}{D-2} \right) \frac{2\pi^{D/2} G}{\Gamma[D/2]} \quad (3.65)$$

Thus, $\kappa(D) \rightarrow \infty$ when $D \rightarrow 2$, but the Poisson equation acquires the form

$$\nabla^2 \phi = 2\pi G \rho \quad (3.66)$$

This is, of course, the same form which is obtained by applying Gauss's law in two dimensions. Hence, as in three dimensions, the gravitational potential is determined by the matter density and thus inhomogeneities can in principle grow. There are, however, difficulties with this approach. To begin with, the constant factor $c^4/(2\kappa(D))$ in the action \mathcal{S} in equation(3.1) vanishes for $D = 2$. But this is not too serious a problem. The gravitational part of the action certainly vanishes but because only the variations about the action are of significance this difficulty can be ignored. But a more serious problem arises when the solutions to the Friedmann equation are considered. The solutions for $a(t)$ and $\rho(t)$ in D dimensions are given in equation (3.22). Using equation (3.65), these reduce to,

$$a(t) = \left(\frac{D\pi^{D/2} G C_1}{(D-2)\Gamma[D/2]} \right)^{1/D} t^{2/D} \quad ; \quad \rho(t) = C_1 a^{-D} = \frac{(D-2)\Gamma[D/2]}{D\pi^{D/2} G} t^{-2} \quad (3.67)$$

When $D \rightarrow 2$ then, $a \rightarrow \infty$ and $\rho \rightarrow 0$ irrespective of the dependence on t . This implies that one cannot solve the equations describing the growth of structure in a consistent and non-singular way. Hence, we conclude that it is not possible to

have a theoretical formulation of two dimensional gravity as the Newtonian limit to Einstein's equations in two dimensions.

An alternative that remains is to use the Newtonian fluid equations in D dimensions directly and rewrite them for an expanding background with an *arbitrary* scale factor $a(t)$. Note that $a(t)$ is not obtained from the Friedmann equations and is completely arbitrary. We can superpose the potentials for the background universe and the perturbations in this case as before. The further assumptions we need to make are (i) the potential of the background universe Φ_{bg} is of the form

$$\Phi_{\text{bg}} = -\frac{1}{2} \frac{\ddot{a}}{a} r^2 \quad (3.68)$$

and (ii) the Poisson equation is given by

$$\nabla^2 \phi = \kappa(D) \rho_{\text{bm}} \delta \quad (3.69)$$

where $\kappa(D) = 2\pi^{D/2} G / \Gamma[D/2]$. This form of $\kappa(D)$ is obtained from the use of Gauss's law in D dimensions. We also need to specify how the background density ρ_{bm} depends on time. In analogy with the usual Friedmann equations, we will assume $\rho_{\text{bm}} a^D = C_1$ where C_1 is a constant. This gives an equation for δ with an arbitrary scale factor $a(t)$ as

$$\frac{d^2 \delta}{da^2} + \left(\frac{\ddot{a}a + 2\dot{a}^2}{a\dot{a}^2} \right) \frac{d\delta}{da} - \kappa(D) C_1 \frac{1}{a^D \dot{a}^2} \delta (1+\delta) = \left(\frac{D+1}{D} \right) \frac{1}{1+\delta} \left(\frac{d\delta}{da} \right)^2 + (1+\delta)(\sigma^2 - 2\Omega^2). \quad (3.70)$$

The above equation can be solved in any dimension D if the form of $a(t)$ is given. This gives us a non-singular way to analyse growth of structures in D dimensions, including the case $D = 2$. But in three dimensions we observe that the above equation does not correctly reduce to equation (3.57). We may obtain the correct equation in three dimensions by making an additional ansatz, namely, that

$$\left(\frac{\dot{a}}{a} \right)^2 = \frac{2\kappa(D)}{D} \rho_{\text{bm}}. \quad (3.71)$$

With this, equation (3.70) reduces to

$$\frac{d^2\delta}{da^2} + \left(\frac{6-D}{2a}\right)\frac{d\delta}{da} - \frac{D}{2a^2}\delta(1+\delta) = \left(\frac{D+1}{D}\right)\frac{1}{1+\delta}\left(\frac{d\delta}{da}\right)^2 + (1+\delta)(\sigma^2 - 2\Omega^2) \quad (3.72)$$

Notice that the above equation differs from the earlier equation for δ in D dimensions, equation (3.45), in that there is a factor of $(D-2)$ missing from the coefficient of the $\delta(1+\delta)$ term. Therefore, the above equation does correctly reduce to equation (3.57) since $(D-2)$ equals unity when $D=3$. When $D=2$, equation (3.72) gives

$$\frac{d^2\delta}{da^2} + \frac{2}{a}\frac{d\delta}{da} - \frac{1}{a^2}\delta(1+\delta) = \frac{3}{2(1+\delta)}\left(\frac{d\delta}{da}\right)^2 + (1+\delta)(\sigma^2 - 2\Omega^2) \quad (3.73)$$

On linearising this equation by dropping the $(\sigma^2 - 2\Omega^2)$ term and the nonlinear terms and solving it we get both a growing mode as well as a decaying mode for δ . The solutions are

$$\delta \propto a^q, \quad q = (-1 \pm \sqrt{5})/2 \quad (3.74)$$

(It is interesting to note that one of the power law exponents is the golden ratio).

The Spherical Top Hat (STH) equation in this case turns out to be

$$\ddot{R} = -\frac{GM}{R} + \frac{1}{2}\frac{R}{t^2} \quad (3.75)$$

where M is the constant mass inside a ‘spherical’ shell of radius R . This equation, unfortunately, has no simple analytic solution.

While this procedure leads to nontrivial results, it has many *ad hoc* assumptions and cannot be obtained by taking appropriate limits of Einstein’s theory in a systematic manner. Consequently it cannot be applied to numerical investigations of 2 dimensional gravity with the confidence that the results will have some implications for the three dimensional case.

3.6 Results and Summary

In this chapter we have analysed the case of two dimensional gravitational clustering starting from a formulation of the D dimensional Einstein's equations and taking the proper limits. The system of equations thus arrived at for a $(D + 1)$ dimensional universe has been shown to reduce to the correct equations in three dimensions. But when the $D \rightarrow 2$ limit of these equations is taken, we are forced to conclude that irrespective of the value of $\kappa(D)$, a consistent two dimensional gravity theory in a cosmological context that supports growth of structures cannot be constructed.

If $\kappa(2)$ is assumed to be finite, we observe that the coefficient in Poisson's equation goes to zero thus decoupling the potential from the density. This implies that perturbations do not grow but decay in time due to the expansion of the background spacetime. The alternative which is obtained by using the expression for $\kappa(D)$ given by equation (3.65) gives rise to solutions for the scale factor which are singular and therefore unacceptable.

We have discussed all the ways in which two dimensional gravity may be simulated including an *ad hoc* procedure without a strong foundation which can give non-singular results as far as structure formation scenarios in two dimensions are concerned. The results presented here leads us to conclude that the only way to do a numerical simulation of two dimensional gravity is to simulate infinite 'needles' in a background spacetime expanding in three dimensions and consider the 'particles' in the system to be intersections of the 'needles' with any plane orthogonal to them which is the approach taken in the next chapter.

Chapter 4

Scaling Relations in Two Dimensions

When in doubt use brute force – Ken Thompson

4.1 Gravitational Clustering: Two vs Three Dimensions

A number of attempts have been made in recent years to understand the evolution of constructs like the two point correlation function using certain non-linear scaling relations (NSR) as discussed in chapter 2 ([19],[34],[37]). These studies have shown that the relation between the non-linear and the linearly extrapolated correlation functions is reasonably model independent. This relation divides the evolution of correlation function into three parts [8]: the linear regime, the intermediate regime and the non-linear regime. The evolution in the intermediate regime can be understood in terms of radial collapse around density peaks [37], if it is assumed that the evolution of profiles of density peaks follows the same pattern as an isolated peak. It is customary to invoke the hypothesis of stable clustering [45] to model the non-linear regime. A large number of studies have examined clustering in this regime and the general consensus is that the stable clustering limit does not exist [42].

However, the limited dynamic range of currently available 3-dimensional N-Body simulations poses serious difficulties in investigating this problem in greater detail. It was pointed out [39] that we can circumvent this problem by simulating a two dimensional system, wherein a much higher dynamic range can be achieved. For example, since $160^3 \approx 2048^2$, the computational requirements are the same for a 2D simulation with box size of 2048 and 3D simulation with box size of 160. Assuming that one can reliably use, say, half of box size as *good* dynamic range we have a dynamic range of factor 1000 in 2D against a factor of about 80 in 3D. This allows us to probe higher nonlinearities in 2D compared to 3D. As long as we stick to generic features (like the non-linear scaling relations investigated here) which are independent of dimension, 2D has a definite advantage over 3D. Higher dynamic range is the basic motivation for studying gravitational clustering in two dimensions.

When we go from three to two dimensions, we have, as discussed in chapter 3, two different ways of modeling the system:

- (i) We can consider two dimensional perturbations in a three dimensional expanding universe. Here we keep the force between particles to be $1/r^2$ and assume that all the particles, and their velocities, are confined to a single plane at the initial instant.
- (ii) We can study perturbations that do not depend on one of the three coordinates, i.e., we start with a set of infinitely long straight “needles” all pointing along one axis. The force of interaction falls as $1/r$. The evolution keeps the “needles” pointed in the same direction and we study the clustering in an orthogonal plane. Particles in the N-Body simulation represent the intersection of these “needles” with this plane. In both these approaches the universe is three dimensional and the background is expanding isotropically.

The study of 2-D perturbations (like those due to pancakes, for example) in a 3-D expanding universe faces an operational problem: To begin with, we do not gain the dynamic range if we stick to 3D, even if we consider perturbations in a plane; the force between particles still has to be computed by the solution of Poisson equation in three dimensions. Also, relevance of the interaction of matter outside the plane with these perturbations makes it, essentially, a 3D problem.

Thus we are left with the second possibility. The two dimensional system is the intersection of an orthogonal plane and the “needles” and the force between the “particles” in this plane is given by the solution of the Poisson equation in two dimensions. Such a system is somewhat dichotomous with the background universe expanding isotropically. However, convenience is not the only reason for studying this somewhat strange system — relevant results for the evolution of density profiles around peaks in 2-D have also been computed for this type of a system [18].

Generalization of the NSR to the 2-D system was done using relations for cylindrical collapse by Padmanabhan [37] and we will test these predictions here.

Although the system of infinite needles is appropriate for testing the predictions in the intermediate regime, the same cannot be said for the asymptotic regime. We are dealing with a system that occupies a smaller number of dimensions in the phase space *and* the interaction of the constituents follows a different force law. Therefore, it is difficult to interpret, or carry over, results regarding stable clustering to the full 3-D system.

4.1.1 Non-linear Scaling Relations

The non-linear and the linear correlation functions at two different scales can be related by NSR. The relation between these scales is given by the characteristics

of the pair conservation equation [34]. For the two dimensional system of interest, this equation can be written as [39]

$$\frac{\partial D}{\partial A} - h(A, x) \frac{\partial D}{\partial X} = 2h(A, X), \quad (4.1)$$

Here $D = \log(1 + \bar{\xi})$, $h = -v_p/Hr$ is the scaled pair velocity, $\bar{\xi}(x) = 2x^{-2} \int^x r\xi(r)dr$ is the mean correlation function (ξ is the correlation function), H is the Hubble's constant, $X = \log(x)$ and $A = \log(a)$. The characteristics of this equation are $x^2(1 + \bar{\xi}(x, a)) = l^2$, where x and l are the two scales used in NSR. The self similar models due to Filmore and Goldreich [18] imply that for collapse of cylindrical perturbations the turn around radius and the initial density contrast inside that shell are related as $x_{ta} \propto l/\bar{\delta}_i \propto l/\bar{\xi}_L(l)$. (Here $\bar{\xi}_L$ is the linearly extrapolated mean correlation function). Noting that in two dimensions $M \propto x^2$, we find $\bar{\xi}(x) \propto [\bar{\xi}_L(l)]^2$ in the regime dominated by infall. Stable clustering limit implies $\bar{\xi}_{NL}(a, x) \propto \bar{\xi}_L(a, l)$ [39]. Thus in 2-D the scaling relations are

$$\bar{\xi}(a, x) \propto \begin{cases} \bar{\xi}_L(a, l) & (\text{Linear}) \\ \bar{\xi}_L(a, l)^2 & (\text{Radial Infall}) \\ \bar{\xi}_L(a, l) & (\text{Stable Clustering}) \end{cases} \quad (4.2)$$

A more general assumption compared to stable clustering involves taking $h = \text{constant}$ asymptotically. In a system reaching steady state with both virialisation and mergers contributing to the evolution, one may reach a constant value for h , though it will not be unity if mergers are a dominant phenomenon. (This assumption has been discussed in, for example, [37].) It also allows a larger parameter space to compare simulation results. If $h = \text{constant}$ asymptotically, then $\bar{\xi}(x) \propto \bar{\xi}_L^h(l)$ in this limit. Note that in 3D, the indices for three regimes are 1, 3 and $3h/2$ respectively.

All features of clustering in three dimensions are present here as well. In particular,

- (i) If the asymptotic value of h scales with n such that $h(n+2) = \text{constant}$ then the final slope of the non-linear correlation function will be independent of the initial slope.
- (ii) If NSR exists then it will predict a *specific* index in the intermediate and asymptotic regimes which will depend on the initial power spectrum. In other words, existence of NSR implies that gravitational clustering does not erase memory of initial conditions.
- (iii) It is, however, possible that spectra which are not scale free acquire universal critical indices at which the correlation functions grow in a ‘shape invariant’ manner. This comes about because the growth rate of correlation function varies with the local index and for an index that is not globally constant the correlation functions may ‘straighten out’ by this process.
- (iv) In 3-D clustering, $n = -1$ in the intermediate regime and $n = -2$ in the asymptotic regime [11] are the critical indices. These are the same for clustering in two dimensions.

4.2 Simulations and Results

We carried out a series of numerical experiments to test the ideas outlined above. We used a particle mesh code [9] to simulate power law models. The simulations were done with 1024^2 or 2048^2 particles in order to ensure that we had sufficient dynamic range to study all the three regimes in evolution of non-linear clustering. In particular, it is necessary to use larger simulations for power law spectra with a negative index. Here, we will present results for three models: $n = 1$, $n = 0$ and $n = -0.4$.

All the models are normalized by requiring the linearly extrapolated root mean square fluctuations in density, computed using a Gaussian filter, to be

unity at a scale of 10 grid points at $a = 1.0$. The results we present are for $a = 1, 2$ and 5 for $n = 0$ and $n = 1$, and $a = 1, 2$ and 3 for $n = -0.4$.

A significant source of errors in large simulations is the addition of a small displacement in each step (fraction of a grid length) to a large position (up to 2048 grid lengths). We avoid this problem by using net displacement for internal storage.

We will show the correlation function and the pair velocity only for length scales larger than four grid lengths. We do this to avoid error due to shot noise and other artifacts introduced by various effects at smaller scales. This ensures that errors in our results are acceptably small. (Variations between different realizations give a dispersion of less than 10% in the correlation function.)

In fig.4.2 we have plotted the non-linear correlation function $\bar{\xi}(x)$ as a function of the linearly extrapolated correlation function $\bar{\xi}_L(l)$. Here the scales x and l are related by $x^2(1 + \bar{\xi}) = l^2$. Data for $n = 1$ is represented by circles, that for $n = 0$ by stars and ‘+’ marks the points for $n = -0.4$. Clearly, there are no systematic differences between the three models and the data points trace out a simple curve with three distinct slopes (We have also marked the 2σ errors calculated by averaging over several data sets. The error bars are plotted away from the NSR plot, for visibility and clarity.). The NSR, shown as thick lines, is

$$\bar{\xi}(a, x) = \begin{cases} \bar{\xi}_L(a, l) & \bar{\xi}_L(l) \leq 0.5; \bar{\xi}(x) \leq 0.5 \\ 2\bar{\xi}_L(a, l)^2 & 0.5 \leq \bar{\xi}_L(l) \leq 2; 0.5 \leq \bar{\xi}(x) \leq 8 \\ 4.7\bar{\xi}_L(a, l)^{3/4} & 2 \leq \bar{\xi}_L(l); 8 \leq \bar{\xi}(x) \end{cases} \quad (4.3)$$

The slope in the intermediate regime is as expected. The asymptotic regime has a different slope than that predicted by stable clustering, which is shown as a dashed line. Unlike the observed relations for clustering in three dimensions, the coefficient for the intermediate regime is large. This has important implications for the critical index.

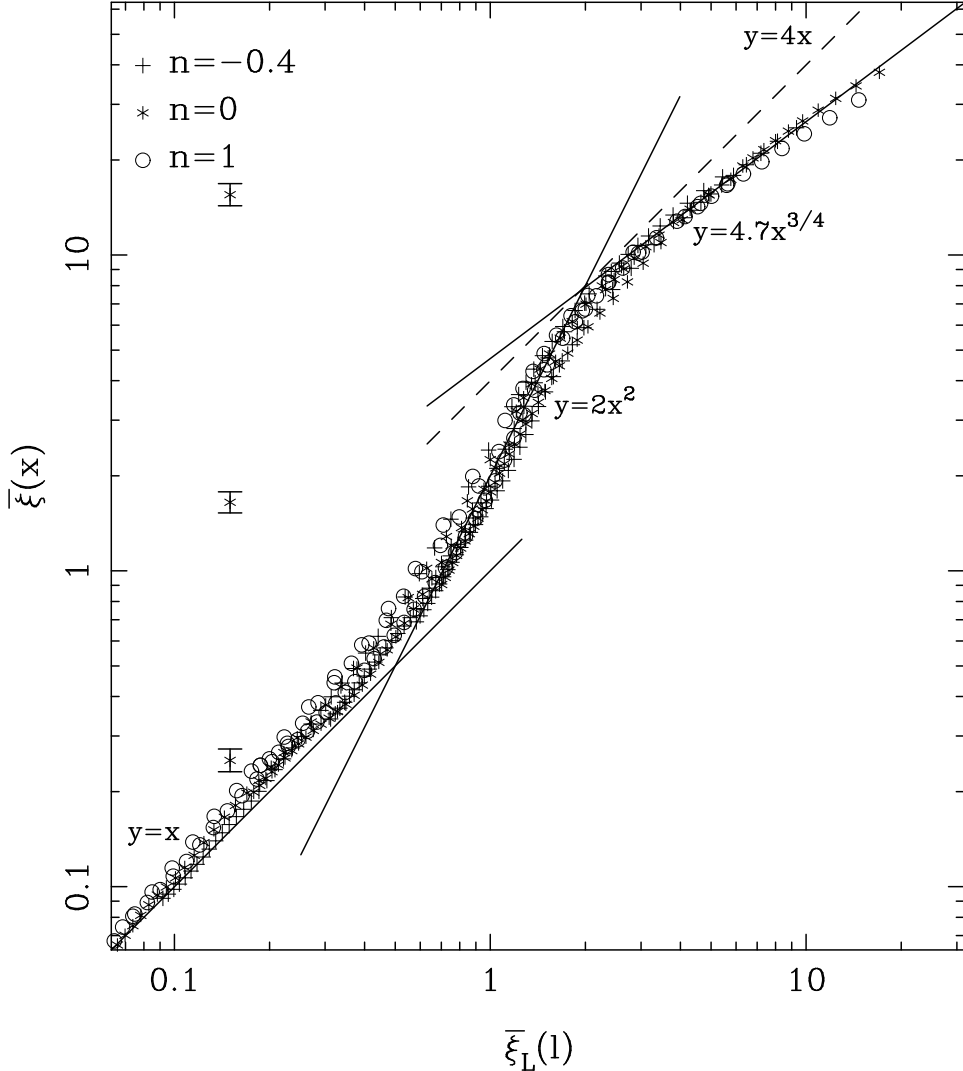


Figure 4.1: This figure shows the non-linear correlation function $\bar{\xi}(x)$ as a function of the linearly extrapolated correlation function $\bar{\xi}_L(l)$. Here the scales x and l are related by $x^2(1 + \bar{\xi}) = l^2$. Data for $n = 1$ is represented by circles, that for $n = 0$ by stars and + marks the points for $n = -0.4$. For each of these models we have plotted data for the three epochs mentioned in the text. The estimated 2σ error bars are shown as vertical lines at three representative values of $\bar{\xi}$ viz. at $\bar{\xi}=15.582$, 1.65 and 0.25 , covering the nonlinear, intermediate and linear regimes. The error bars are shown away from the NSR plot for the sake of visibility. It is clear from this figure that there are no systematic differences between the three models and they trace out a simple curve with three distinct slopes. The slope of the curve in the intermediate regime is same as that predicted by the radial infall model. The stable clustering limit is shown as the dashed line and it is clear that the data points deviate from this curve.

Panels of fig. 4.2 show $\bar{\xi}(x)$ as a function of x/x_{nl} for the three models. These confirm that the slope of $\bar{\xi}(x)$ is consistent with the NSR shown in fig. 4.1. In each of these panels, the slope expected in the stable clustering limit is shown as a dashed line.

As mentioned above, the existence of the NSR (eqn.(4.3)) implies that the slope of the correlation function will depend on the initial spectral index. To this extent, gravitational clustering does not erase memory of initial conditions. However, the differences of slope are significantly reduced by non-linear evolution.

4.3 Summary

Results obtained in this chapter can be summarized as follows:

- (i) We have verified that NSR for the correlation function exist for clustering in 2D in all the three regimes, just like in 3D. This NSR is independent of the power law index – at least for the three indices studied here.
- (ii) In the intermediate regime, the NSR in the form of eqn.(4.3), can be understood in terms of radial infall around peaks. Our simulations verify the predictions [39] for this regime.
- (iii) In the asymptotic regime, our results do *not* agree with the stable clustering hypothesis. The slope of the NSR in the asymptotic regime in fig. 4.1 implies $h = \text{constant}$. We find that, in this regime, $h \simeq 3/4$ for all the models studied here.
- (iv) The existence of NSR implies that the asymptotic slope of the correlation function depends on the initial slope. However, this is strictly true only for pure power law models; for other models it is possible for the spectra to be driven to a universal form. The NSR in the asymptotic regime seems to be linked to the

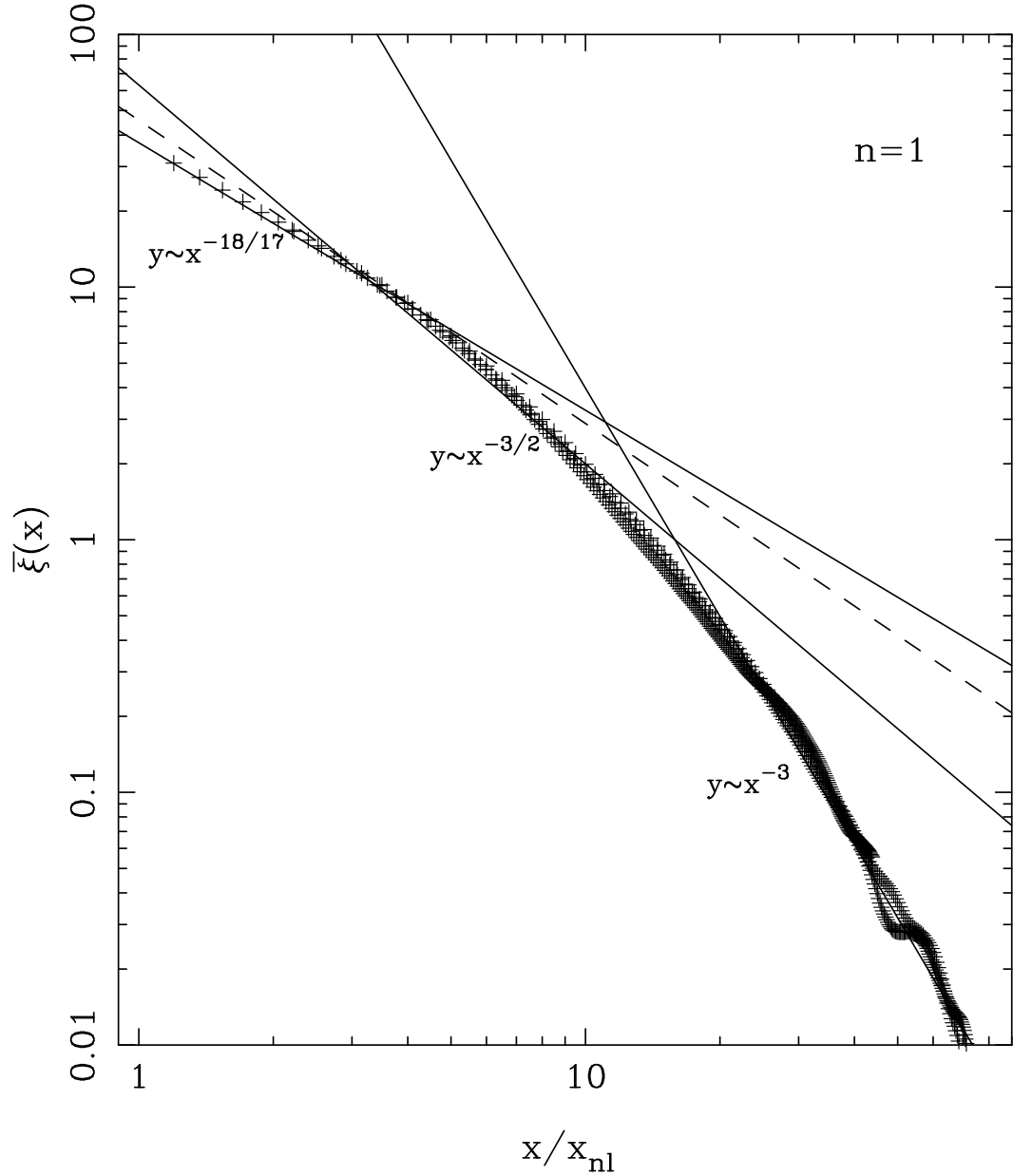


Figure 4.2: The correlation function $\bar{\xi}(x)$ as a function of x/x_{nl} for $n = 1$ model. Here $x_{nl} \propto a^{-2/(n+2)}$. Thick lines mark slopes expected from the non-linear scaling relations shown in fig. 4.1. The dashed line marks the expected slope of the correlation function in the stable clustering limit. The mismatch between the expected slope and the true slope in the intermediate regime may arise from the fact that the assumption of $\bar{\xi} \gg 1$ used in computing the slope is not valid at the lower end of the regime.

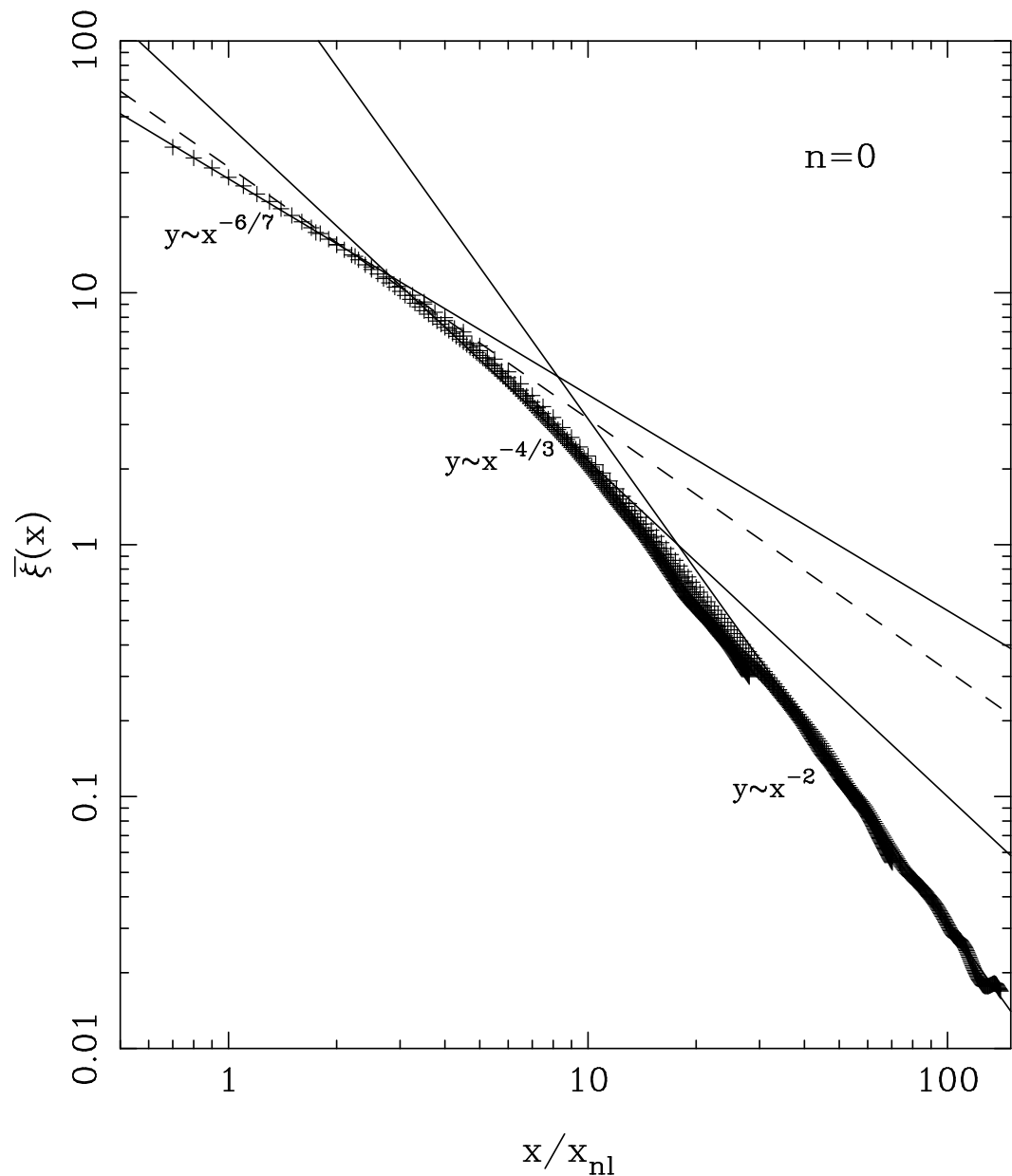
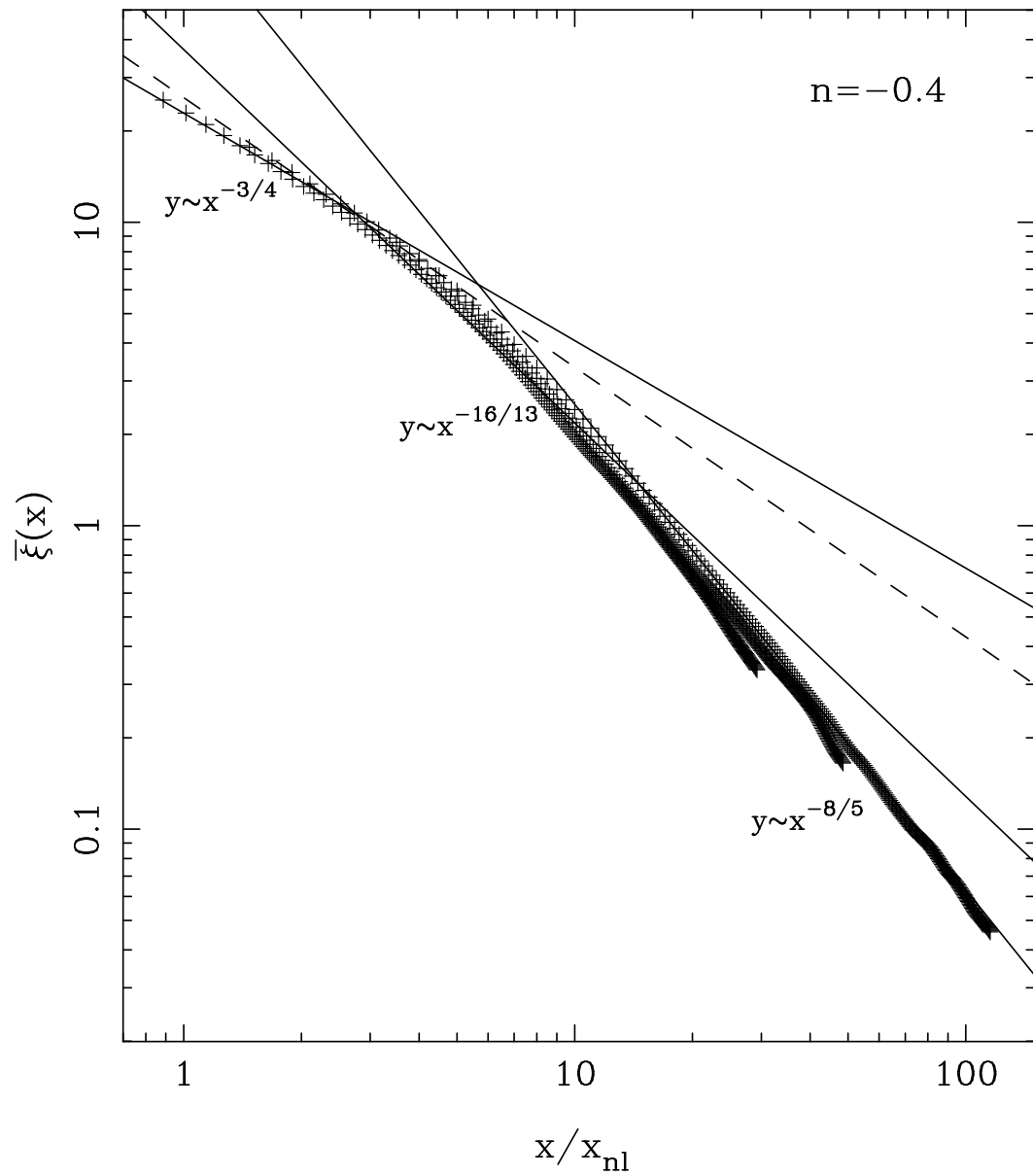


Figure 4.2: Similar plot for $n = 0$.

Figure 4.2: $n = -0.4$.

logarithmic nature of the potential.

A theoretical model for existence of such scaling relations, as mentioned before, was derived on the basis of Spherical Collapse Model. In the next chapter we analyse the physical features of spherical collapse model in detail and derive a physically motivated approach to halting the collapse as opposed to the standard ‘virialization’ argument.

Chapter 5

An improved spherical collapse model

Turbulence is life force. It is opportunity. Let's love turbulence
and use it for change – Ramsay Clark

5.1 Introduction

Analytic modelling of the non-linear phase of gravitational clustering has been a challenging but interesting problem upon which a considerable amount of attention has been bestowed in recent years. The simplest, yet remarkably successful, model for non-linear evolution is the Spherical Collapse Model (SCM, hereafter), which has been applied in the study of various empirical results in the gravitational instability paradigm. Unfortunately, this approach has serious flaws — both mathematically and conceptually. Mathematically, the SCM has a singular behaviour at finite time and predicts infinite density contrasts for all collapsed objects. Conceptually, it is not advisable to model the real universe as a sphere, in spite of the standard temptations to which theoreticians often succumb. The two issues are, of course, quite related, since, in any realistic situation, it is the deviations from spherical symmetry which lead to virialised stable structures getting formed. In conventional approaches, this is achieved by an *ad hoc* method

which involves halting the collapse at the virial radius by hand and mapping the resulting non-linear and linear overdensities to each other. This leads to the well known rule-of-thumb that, when the linear overdensity is about 1.68, bound structures with non-linear overdensities of about 178 would have formed. The singular behaviour, however, makes the actual trajectory of a spherical system quite useless after the turnaround phase — a price we pay for the arbitrary procedure used in stabilizing the system. But the truly surprising feature is that, despite its inherent arbitrariness, the SCM, when properly interpreted, seems to give useful insights into the behaviour of real systems. The Press–Schechter formalism [47], for the abundance of bound structures, uses SCM implicitly; more recently, it was shown that the basic physics behind the non-linear scaling relations (NSR) obeyed by the two point correlation function can be obtained from a judicious application of SCM [37]. These successes, as well as the inherent simplicity of the underlying concepts, make the SCM an attractive paradigm for studying non-linear evolution in gravitational clustering and motivate one to ask: Can we improve the basic model in some manner so that the behaviour of the system after turnaround is ‘more reasonable’ ?

It is clear from very general considerations that such an approach has to address fairly non-trivial technical issues. To begin with, *exact* modelling of deviations from spherical symmetry is quite impossible since it essentially requires solving the full BBGKY hierarchy. Secondly, the concept of a radius $R(t)$ for a shell, evolving only due to the gravitational force of the matter inside, becomes ill-defined when deviations from spherical symmetry are introduced. Finally, our real interest is in modelling the statistical features of the density growth; whatever modifications we make to SCM should eventually tie up with known results for the evolution of, for instance, the two point correlation function. That is, we

have to face the question of how best to obtain the *statistical* properties of the density field from the behaviour of a *single* system.

In this chapter, these problems are addressed in a limited but focussed manner. The deviations from spherical symmetry are tackled by the retention of a term (which is usually neglected) in the equation describing the growth of the density contrast. Working in the fluid limit, we show that this term is physically motivated and present some arguments to derive an acceptable form for the same. The key new idea is to introduce a Taylor series expansion in $(1/\delta)$ (where δ is the density contrast) to model the non-linear evolution. We circumvent the question of defining the ‘radius’ of the non-spherical regions by working directly with density contrasts. Finally, we attempt to make the connection with statistical descriptors of non-linear growth, by using the non-linear scaling relations known from previous work. More precisely, we show that the modified equations predict a behaviour for the relative pair velocity (when interpreted statistically) which agrees with the results of N-body simulations.

The chapter is divided into the following sections. The relevant equations describing the SCM are set out in Section 5.2; we also summarise the physical and *ad hoc* aspects of the SCM here. Next, we recast the equations in a different form and introduce two functions (i) a “virialization term” and (ii) a function $h_{\text{SC}}(\delta)$, whose asymptotic forms are easy to determine. The behaviour of $h_{\text{SC}}(\delta)$ in the presence and absence of the “virialization term” is also detailed here. In Section 5.4, we present the arguments that give the functional forms for the above term over a large range of δ ; we then go on to present the results in terms of a single collapsing body and show how this term stabilizes a collapse which would have otherwise ended up in a singularity in terms of the growth of the density contrast with time. When this term is carried through into the equation for $R(t)$

for a single system, it can be seen the radius reaches a maximum and gracefully decreases to a constant, remaining so thereafter. In the standard SCM, the radius decreases from the maximum all the way down to zero, thereby causing the density to diverge. Section 5.5 summarises the results and discusses their implications.

5.2 The Spherical Collapse Model

The scales of interest in the current work are much smaller than the Hubble length and the velocities in question are non-relativistic; Newtonian gravity can hence be used for the following analysis. We will consider the case of a dust-dominated, $\Omega = 1$ universe and treat the system in the fluid limit as being made up of pressureless dust of dark matter, with a smoothed density, $\rho_m(t, \mathbf{x})$, and a mean velocity, $\mathbf{v}(t, \mathbf{x})$. (This approach, of course, ignores effects arising from shell crossing and multi-streaming; these will be commented on later.) The density contrast, $\delta(\mathbf{x}, t)$ is defined by

$$\rho_m(t, \mathbf{x}) = \rho_b(t)[1 + \delta(\mathbf{x}, t)] \quad (5.1)$$

where ρ_b denotes the smooth background density of matter. We define a velocity field $u^i = v^i/(a\dot{a})$, where v^i is the peculiar velocity (obtained after subtracting out the Hubble expansion) and $a(t)$ denotes the scale factor. Taking the divergence of the field u^i and writing it as

$$\partial_i u_j = \sigma_{ij} + \epsilon_{ijk}\Omega^k + \frac{1}{3}\delta_{ij}\theta \quad (5.2)$$

where σ_{ij} is the shear tensor, Ω^k is the rotation vector and θ is the expansion, we can manipulate the fluid equations [38] to obtain the following equation for δ

$$\begin{aligned} \frac{d^2\delta}{da^2} + \frac{3}{2a} \frac{d\delta}{da} - \frac{3}{2a^2} \delta(1+\delta) &= \\ \frac{4}{3} \frac{1}{(1+\delta)} \left(\frac{d\delta}{da} \right)^2 + (1+\delta)(\sigma^2 - 2\Omega^2) & \end{aligned} \quad (5.3)$$

The same equation can be written in terms of time t as

$$\begin{aligned} \ddot{\delta} - \frac{4}{3} \frac{\dot{\delta}^2}{(1+\delta)} + \frac{2\dot{a}}{a} \dot{\delta} &= \\ 4\pi G \rho_b \delta (1+\delta) + \dot{a}^2 (1+\delta) (\sigma^2 - 2\Omega^2) & \end{aligned} \quad (5.4)$$

This equation turns out to be the same as the one for density contrast in the SCM, except for the additional term in $(1+\delta)(\sigma^2 - 2\Omega^2)$, arising from the angular momentum and shear of the system. To see this explicitly, we introduce a function $R(t)$ by the definition

$$1 + \delta = \frac{9GMt^2}{2R^3} \equiv \lambda \frac{a^3}{R^3} \quad (5.5)$$

where M and λ are constants. Using this relation between δ and $R(t)$, equation (5.4) can be converted into the following equation for $R(t)$

$$\ddot{R} = -\frac{GM}{R^2} - \frac{1}{3} \dot{a}^2 (\sigma^2 - 2\Omega^2) R \quad (5.6)$$

where the first term represents the gravitational attraction due to the mass inside a sphere of radius R and the second gives the effect of the shear and angular momentum.

In the case of spherically symmetric evolution, the shear and angular momentum terms can be set to zero; this gives

$$\frac{d^2R}{dt^2} = -\frac{GM}{R^2} \quad (5.7)$$

which governs the evolution of a spherical shell of radius R , collapsing under its own gravity; M can now be identified with the mass contained in the shell; this is standard SCM.

At this point, it is important to note a somewhat subtle aspect of these equations. The original fluid equations are clearly Eulerian in nature: *i.e.* the time derivatives give the temporal variation of the quantities at a fixed point in space. However, the time derivatives in equation (5.4), for the density contrast δ , are of a different kind. Here, the observer is moving with the fluid element and hence, in this, Lagrangian case, the variation in density contrast seen by the observer has, along with the intrinsic time variation, a component which arises as a consequence of his being at different locations in space at different instants of time. When the δ equation is converted into an equation for the function $R(t)$, the Lagrangian picture is retained; in SCM, we can interpret $R(t)$ as the radius of a spherical shell, co-moving with the observer. The mass M within each shell remains constant in the absence of shell crossing (which does not occur in the standard SCM for reasonable initial conditions) and the entire formalism is well defined. The physical identification of R is, however, not so clear in the case where the shear and rotation terms are retained, as these terms break the spherical symmetry of the system. We will nevertheless continue to think of R as the “effective shell radius” in this situation, *defined by* equation (5.5) governing its evolution. Of course, there is no such ambiguity in the *mathematical* definition of R in this formalism.

Before proceeding further, let us briefly summarize the results of standard SCM. Equation (5.7) can be integrated to obtain $R(t)$ in the parametric form

$$R = \frac{R_i}{2\delta_i}(1 - \cos \theta) \quad (5.8)$$

$$t = \frac{3t_i}{4\delta_i^{3/2}}(\theta - \sin \theta) \quad (5.9)$$

where R_i , δ_i and t_i are the initial radius, initial density contrast and initial time, respectively, with $R_i^3 = (9GMt_i^2/2)(1 + \delta_i)^{-1} \simeq (9GMt_i^2/2)$ for $\delta_i \ll 1$. Given

M , there are only two independent constants, *viz* t_i and δ_i . All the physical features of the SCM can be easily derived from the above solution. Each spherical shell expands at a progressively slower rate against the self-gravity of the system, reaches a maximum radius and then collapses under its own gravity, with a steadily increasing density contrast. The maximum radius, $R_{max} = R_i/\delta_i$, achieved by the shell, occurs at a density contrast $\delta = (9\pi^2/16) - 1 \approx 4.6$, which is in the “quasi-linear” regime. In the case of a perfectly spherical system, there exists no mechanism to halt the infall, which proceeds inexorably towards a singularity, with all the mass of the system collapsing to a single point. Thus, the fate of the shell (as described by equations (5.8) and (5.9)) is to collapse to zero radius at $\theta = 2\pi$ with an infinite density contrast; this is, of course, physically unacceptable.

In real systems, however, the implicit assumptions that (i) matter is distributed in spherical shells and (ii) the non-radial components of the velocities of the particles are small, will break down long before infinite densities are reached. Instead, we expect the collisionless dark matter to reach virial equilibrium. After virialization, $|U| = 2K$, where U and K are, respectively, the potential and kinetic energies; the virial radius can be easily computed to be half the maximum radius reached by the system.

The virialization argument is clearly physically well-motivated for real systems. However, as mentioned earlier, there exists no mechanism in the standard SCM to bring about this virialization; hence, one has to introduce by hand the assumption that, as the shell collapses and reaches a particular radius, say $R_{max}/2$, the collapse is halted and the shell remains at this radius thereafter. This arbitrary introduction of virialization is clearly one of the major drawbacks of the standard SCM and takes away its predictive power in the later stages of evo-

lution. We shall now see how the retention of the angular momentum term in equation (5.6) can serve to stabilize the collapse of the system, thereby allowing us to model the evolution towards $r_{vir} = R_{max}/2$ smoothly.

5.3 The $h_{\text{SC}}(\delta)$ function.

As detailed in the previous section, the primary defect of the standard SCM is the *ad hoc* nature of the stabilization of the shell against its collapse under gravity, which arises on account of the assumption of perfect spherical symmetry, implicit in the neglect of the shear and angular momentum terms. We hence return to equation (5.3), retain the above terms, and recast the equation into a form more suitable for analysis. Using logarithmic variables, $D_{\text{SC}} \equiv \ln(1 + \delta)$ and $\alpha \equiv \ln a$, equation (5.3) can be written in the form (the subscript ‘SC’ stands for ‘Spherical Collapse’)

$$\frac{d^2 D_{\text{SC}}}{d\alpha^2} - \frac{1}{3} \left(\frac{dD_{\text{SC}}}{d\alpha} \right)^2 + \frac{1}{2} \frac{dD_{\text{SC}}}{d\alpha} = \frac{3}{2} [\exp(D_{\text{SC}}) - 1] + a^2 (\sigma^2 - 2\Omega^2) \quad (5.10)$$

It is convenient to introduce the quantity, S , defined by

$$S \equiv a^2 (\sigma^2 - 2\Omega^2) \quad (5.11)$$

which we shall hereafter call the “virialization term”. The consequences of the retention of the virialization term are easy to describe qualitatively. We expect the evolution of an initially spherical shell to proceed along the lines of the standard SCM in the initial stages, when any deviations from spherical symmetry, present in the initial conditions, are small. However, once the maximum radius is reached and the shell recollapses, these small deviations are amplified by a positive feedback mechanism. To understand this, we note that all particles in a

given spherical shell are equivalent due to the spherical symmetry of the system. This implies that the motion of any particle, in a specific shell, can be considered representative of the motion of the shell as a whole. Hence, the behaviour of the shell radius can be understood by an analysis of the motion of a single particle. The equation of motion of a particle in an expanding universe can be written as

$$\ddot{\mathbf{x}}_i + 2\frac{\dot{a}}{a}\dot{\mathbf{x}}_i = -\frac{\nabla\phi}{a^2} \quad (5.12)$$

where $a(t)$ is the expansion factor of the locally overdense “universe”. The $\dot{\mathbf{x}}_i$ term acts as a damping force when it is positive; *i.e.* while the background is expanding. However, when the overdense region reaches the point of maximum expansion and turns around, this term becomes negative, acting like a *negative* damping term, thereby amplifying any deviations from spherical symmetry which might have been initially present. Non-radial components of velocities build up, leading to a randomization of velocities which finally results in a virialised structure, with the mean relative velocity between any two particles balanced by the Hubble flow. It must be kept in mind, however, that the introduction of the virialization term changes the behaviour of the solution in a global sense and it is not strictly correct to say that this term starts to play a role *only after* recollapse, with the evolution proceeding along the lines of the standard SCM until then. It is nevertheless reasonable to expect that, at early times when the term is small, the system will evolve as standard SCM to reach a maximum radius, but will fall back smoothly to a constant size later on.

The virialization term, S , is, in general, a function of a and \mathbf{x} , especially since the derivatives in equation (5.4) are total time derivatives, which, for an expanding Universe, contain partial derivatives with respect to both \mathbf{x} and t separately. Handling this equation exactly will take us back to the full non-linear

equations for the fluid and, of course, no progress can be made. Instead, we will make the *ansatz* that the virialization term depends on t and \mathbf{x} only through $\delta(t, \mathbf{x})$.

$$S(a, \mathbf{x}) \equiv S(\delta(a, \mathbf{x})) \equiv S(D_{\text{SC}}) \quad (5.13)$$

In other words, S is a function of the density contrast alone. This *ansatz* seems well motivated because the density contrast, δ , can be used to characterize the SCM at any point in its evolution and one might expect the virialization term to be a function only of the system's state, at least to the lowest order. Further, the results obtained with this assumption appear to be sensible and may be treated as a test of the *ansatz* in its own framework.

To proceed further systematically, we *define* a function h_{SC} by the relation

$$\frac{dD_{\text{SC}}}{d\alpha} = 3h_{\text{SC}} \quad (5.14)$$

For consistency, we shall assume the *ansatz* $h_{\text{SC}}(a, \mathbf{x}) \equiv h_{\text{SC}}[\delta(a, \mathbf{x})]$. The definition of h_{SC} allows us to write equation (5.10) as

$$\frac{dh_{\text{SC}}}{d\alpha} = h_{\text{SC}}^2 - \frac{h_{\text{SC}}}{2} + \frac{1}{2} [\exp(D_{\text{SC}}) - 1] + \frac{S(D_{\text{SC}})}{3} \quad (5.15)$$

Dividing (5.15) by (5.14), we obtain the following equation for the function $h_{\text{SC}}(D_{\text{SC}})$

$$\frac{dh_{\text{SC}}}{dD_{\text{SC}}} = \frac{h_{\text{SC}}}{3} - \frac{1}{6} + \frac{1}{6h_{\text{SC}}} [\exp(D_{\text{SC}}) - 1] + \frac{S(D_{\text{SC}})}{9h_{\text{SC}}} \quad (5.16)$$

If we know the form of either $h_{\text{SC}}(D_{\text{SC}})$ or $S(D_{\text{SC}})$, this equation allows us to determine the other. Then, using equation (5.14), one can determine D_{SC} . Thus, our modification of the standard SCM essentially involves providing the form of $S(D_{\text{SC}})$ or $h_{\text{SC}}(D_{\text{SC}})$. We shall now discuss several features of such a modeling in order to arrive at a suitable form.

The behaviour of $h_{\text{SC}}(D_{\text{SC}})$ can be qualitatively understood from our knowledge of the behaviour of δ with time. In the linear regime ($\delta \ll 1$), we know that δ grows linearly with a ; hence h_{SC} increases with D_{SC} . At the extreme non-linear end ($\delta \gg 1$), the system “virializes”, *i.e.* the proper radius and the density of the system become constant. On the other hand, the density ρ_b , of the background, falls like t^{-2} (or a^{-3}) in a flat, dust-dominated Universe. The density contrast is defined by $\delta = (\rho/\rho_b) - 1 \sim \rho/\rho_b$ (for $\delta \gg 1$) and hence

$$\delta \propto t^2 \propto a^3 \quad (5.17)$$

in the non-linear limit. Equation (5.14) then implies that $h_{\text{SC}}(\delta)$ tends to unity for $\delta \gg 1$. Thus, we expect that $h_{\text{SC}}(D_{\text{SC}})$ will start with a value far less than unity, grow, reach a maximum a little greater than one and then smoothly fall back to unity. [A more general situation discussed in the literature corresponds to $h \rightarrow \text{constant}$ as $\delta \rightarrow \infty$, though the asymptotic value of h is not necessarily unity. Our discussion can be generalised to this case.]

This behaviour of the h_{SC} function can be given another useful interpretation whenever the density contrast has a monotonically decreasing relationship with the scale, x , with small x implying large δ and vice-versa. Then, if we use a local power law approximation $\delta \propto x^{-n}$ for $\delta \gg 1$ with some $n > 0$, $D_{\text{SC}} \propto \ln(x^{-1})$ and

$$h_{\text{SC}} \propto \frac{dD_{\text{SC}}}{d\alpha} \propto -\frac{d \ln(\frac{1}{x})}{d \ln a} \propto \frac{\dot{x}a}{\dot{a}x} \propto -\frac{v}{\dot{a}x} \quad (5.18)$$

where $v \equiv a\dot{x}$ denotes the mean relative velocity. Thus, h_{SC} is proportional to the ratio of the peculiar velocity to the Hubble velocity. We know that this ratio is small in the linear regime (where the Hubble flow is dominant) and later increases, reaches a maximum and finally falls back to unity with the formation of a stable structure; this is another argument leading to the same qualitative

behaviour of the h_{SC} function.

Note that, in standard SCM (for which $S = 0$), equation (5.16) reduces to

$$3h_{\text{SC}} \frac{dh_{\text{SC}}}{dD_{\text{SC}}} = h_{\text{SC}}^2 - \frac{h_{\text{SC}}}{2} + \frac{\delta}{2} \quad (5.19)$$

The presence of the linear term in δ on the RHS of the above equation causes h_{SC} to increase with δ , with $h_{\text{SC}} \propto \delta^{1/2}$ for $\delta \gg 1$. If virialization is imposed as an *ad hoc* condition, then h_{SC} should fall back to unity discontinuously — which is clearly unphysical; the form of $S(\delta)$ must hence be chosen so as to ensure a smooth transition in $h_{\text{SC}}(\delta)$ from one regime to another.

As an aside, we would like to make some remarks on the nature of the “virialization term”, $S(\delta)$, in a somewhat wider context. As is well-known, gravitational clustering can be described at three different levels of approximation, by different mathematical techniques. The first approach tracks the clustering by following the true particle trajectories; this is what is done, for example, in N-body simulations. This method does not involve any approximation (other than the validity of the Newtonian description at the scales of interest); it is, however, clearly analytically intractable. At the next level, one may describe the system by an one-particle distribution function and attempt to solve the collisionless Boltzmann equation for the distribution function $f(t, \mathbf{x}, \mathbf{v})$; the approximation here lies in the neglect of gravitational collisions, which seems quite reasonable as the time scale for such collisions is very large for standard dark matter particles. Finally, one can treat the system in the fluid limit described by five functions: the density $\rho(t, \mathbf{x})$, mean velocity $\mathbf{v}(t, \mathbf{x})$, and gravitational potential $\phi(t, \mathbf{x})$, thus neglecting multi-streaming effects. Our analysis was based on this level of approximation. The key difference between the last two levels of description lies in the fact that the distribution function allows for the possibility of different particle velocities

at any point in space (*i.e.* the existence of *velocity dispersions*), while the fluid picture assumes a mean velocity at each point. It is also known that the gradients in velocity dispersion can provide a kinetic pressure which will also provide support against gravitational collapse. While a detailed analysis of these terms is again exceedingly difficult, one can incorporate the lowest order effects of the gradient in the velocity dispersion by modifying equation (5.10) to the form

$$\frac{d^2 D_{\text{SC}}}{d\alpha^2} - \frac{1}{3} \left(\frac{dD_{\text{SC}}}{d\alpha} \right)^2 + \frac{1}{2} \frac{dD_{\text{SC}}}{d\alpha} = \frac{3}{2} [\exp(D_{\text{SC}}) - 1] + a^2(\sigma^2 - 2\Omega^2) + f(a, x) \quad (5.20)$$

where $f(a, x)$ contains the lowest order contributions from the dispersion terms.

We can then define

$$S(a, x) = a^2(\sigma^2 - 2\Omega^2) + f(a, x) \quad (5.21)$$

and again invoke the *ansatz* $S(a, x) \equiv S(\delta)$. Note that $S(\delta)$ now contains the lowest order contributions arising from shell crossing, multi-streaming, etc., besides the shear and angular momentum terms, *i.e.* it contains all effects leading to virialization of the system. It is explicitly demonstrated that velocity dispersion terms arise naturally in the “force” equation (for the function $h \equiv -v/\dot{a}x$), derived from the BBGKY hierarchy, and play the same role as the function $S(\delta)$ in the fluid picture. This clearly justifies the above procedure and shows that our approach could have a somewhat larger domain of validity than might be expected from an analysis based on the fluid picture.

5.4 Detailed derivation of equation for h function

The zeroth and first moments of the 2nd BBGKY equation [48] can be combined to obtain the following equation for the dimensionless function $h = -v/\dot{a}x$

$$3h(1 + \bar{\xi})\frac{dh}{d\bar{\xi}} + \frac{h}{2} - h^2 - \frac{3\bar{\xi}}{F} - \frac{9MQe^{-X}}{4\pi F} = h_{\parallel}^2\left(4 + \frac{\partial \ln F}{\partial X}\right) + \frac{\partial h_{\parallel}^2}{\partial X} - 2h_{\perp}^2 \quad (5.22)$$

where we have used the *ansatz*, $h \equiv h(\bar{\xi})$ ([19], [34]). In the above, we have defined

$$\bar{\xi}(x, a) = \frac{3}{x^3} \int_0^x dx \xi(x, a) x^2 \quad (5.23)$$

$$F = \frac{\partial \bar{\xi}}{\partial X} + 3(1 + \bar{\xi}) , \quad X = \ln x \quad (5.24)$$

$$h_{\parallel}^2 = \frac{\Pi}{\dot{a}^2 x^2} , \quad h_{\perp}^2 = \frac{\Sigma}{\dot{a}^2 x^2} \quad (5.25)$$

where Π and Σ are parallel and perpendicular peculiar velocity dispersions ([48],[27]).

Finally, we have assumed that the 3-point correlation function has the hierarchical form ([14], [48])

$$\zeta_{123} = Q(\xi_{12}\xi_{13} + \xi_{13}\xi_{23} + \xi_{12}\xi_{23}) \quad (5.26)$$

and defined

$$M = \int d^3 z [\xi(x) + \xi(z)] \xi(\mathbf{z} - \mathbf{x}) \frac{\cos \theta}{z^2} \quad (5.27)$$

In the non-linear regime, $\bar{\xi} \gg 1$, the stable clustering ansatz yields a scale-invariant power-law behaviour for $\bar{\xi}$ [14], with $\bar{\xi} \propto a^{(3-\gamma)}x^{-\gamma}$, if $h \rightarrow 1$ as $\bar{\xi} \rightarrow \infty$.

In this limit, we have

$$F = (3 - \gamma)\bar{\xi} + 3 \quad (5.28)$$

and

$$\frac{\partial \ln F}{\partial X} = -\gamma \left[1 + \left(\frac{3}{3-\gamma} \right) \left(\frac{1}{\bar{\xi}} \right) \right]^{-1} \quad (5.29)$$

Further, we can write [57] $M = M'x\bar{\xi}^2$, where M' is a constant. Thus, equation (5.22) reduces, in the non-linear regime, to

$$3h\bar{\xi} \frac{dh}{d\bar{\xi}} - h^2 + \frac{h}{2} - \frac{3}{3-\gamma} \left[\frac{3M'}{4\pi} \left\{ \bar{\xi} - \frac{3}{3-\gamma} \right\} + 1 \right] = \\ \left[(4-\gamma) + \frac{3\gamma}{(3-\gamma)\bar{\xi}} \right] h_{\parallel}^2 + \frac{\partial h_{\parallel}^2}{\partial X} - 2h_{\perp}^2 + \mathcal{O}\left(\frac{1}{\bar{\xi}}\right) \quad (5.30)$$

where we have retained terms upto order constant in $\bar{\xi}$. We now assume that h_{\parallel}^2 and h_{\perp}^2 are functions of $\bar{\xi}$ alone, to first order. This yields

$$3h\bar{\xi} \frac{dh}{d\bar{\xi}} - h^2 + \frac{h}{2} - \frac{3}{3-\gamma} \left[\frac{3M'}{4\pi} \left\{ \bar{\xi} - \frac{3}{3-\gamma} \right\} + 1 \right] = \\ G(\bar{\xi}) + \mathcal{O}\left(\frac{1}{\bar{\xi}}\right) \quad (5.31)$$

with

$$G(\bar{\xi}) = \left[(4-\gamma) + \frac{3\gamma}{(3-\gamma)\bar{\xi}} \right] h_{\parallel}^2(\bar{\xi}) - \gamma\bar{\xi} \frac{dh_{\parallel}^2}{d\bar{\xi}} - 2h_{\perp}^2(\bar{\xi}) \quad (5.32)$$

Clearly, if $h \rightarrow 1$ as $\bar{\xi} \rightarrow \infty$, we must have

$$G(\bar{\xi}) = -\frac{3}{3-\gamma} \left[\frac{3M'}{4\pi} \left\{ \bar{\xi} - \frac{3}{3-\gamma} \right\} + 1 \right] - \frac{1}{2} + \mathcal{O}\left(\frac{1}{\bar{\xi}}\right) \quad (5.33)$$

i.e. $G(\bar{\xi}) \approx -9M'\bar{\xi}/4\pi(3-\gamma)$ for $\bar{\xi} \gg 1$.

Since $G(\bar{\xi})$ tends to the above asymptote at late times, the residual part can be expanded in a Taylor series in $1/\bar{\xi}$. Retaining the first two terms of the expansion in equation (5.31), we obtain

$$3h\bar{\xi} \frac{dh}{d\bar{\xi}} - h^2 + \frac{h}{2} + \frac{1}{2} = \frac{A}{\bar{\xi}} + \frac{B}{\bar{\xi}^2} + \mathcal{O}(\bar{\xi}^{-3}) \quad (5.34)$$

This is exactly the same as equation (5.40), with $\bar{\xi}$ replacing δ . $G(\bar{\xi})$ thus plays the same role as $S(\delta)$ in the stabilising of the system against collapse. This

clearly implies that the velocity dispersion terms, h_{\parallel}^2 and h_{\perp}^2 , will contribute to the support term; we are hence justified in writing the virialization term in the more general form

$$S = a^2 (\sigma^2 - 2\Omega^2) + f(a, x) \quad (5.35)$$

where $f(a, x)$ contains contributions from effects arising from shell crossing, multi-streaming, etc.

5.5 The virialization term

We will now derive an approximate functional form for the virialization function from physically well-motivated arguments. If the virialization term is retained in equation (5.6), we have

$$\frac{d^2 R}{dt^2} = -\frac{GM}{R^2} - \frac{H^2 R}{3} S \quad (5.36)$$

where $H = \dot{a}/a$. Let us first consider the late time behaviour of the system. When virialization occurs, it seems reasonable to assume that $R \rightarrow \text{constant}$ and $\dot{R} \rightarrow 0$. This implies that, for large density contrasts,

$$S \approx -\frac{3GM}{R^3 H^2} \quad (\delta \gg 1) \quad (5.37)$$

Using $H = \dot{a}/a = (2/3t)$, and equation (5.5)

$$S \approx -\frac{27GMt^2}{4R^3} = -\frac{3}{2}(1 + \delta) \approx -\frac{3}{2}\delta \quad (\delta \gg 1) \quad (5.38)$$

Thus, the ‘‘virialization’’ term tends to a value of $(-3\delta/2)$ in the non-linear regime, when stable structures have formed. This asymptotic form for $S(\delta)$ is, however, insufficient to model its behaviour over the larger range of density contrast (especially the quasi-linear regime) which is of interest to us. Since $S(\delta)$ tends to the above asymptotic form at late times, the residual part, *i.e.* the part that remains after the asymptotic value has been subtracted away, can be

expanded in a Taylor series in $(1/\delta)$ without any loss of generality. Retaining the first two terms of expansion, we write the complete virialization term as

$$S(\delta) = -\frac{3}{2}(1 + \delta) - \frac{A}{\delta} + \frac{B}{\delta^2} + \mathcal{O}(\delta^{-3}) \quad (5.39)$$

Replacing for $S(\delta)$ in equation (5.10), we obtain, for $\delta \gg 1$

$$3h\delta \frac{dh_{\text{SC}}}{d\delta} - h_{\text{SC}}^2 + \frac{h_{\text{SC}}}{2} + \frac{1}{2} = -\frac{A}{\delta} + \frac{B}{\delta^2} \quad (5.40)$$

[It can be easily demonstrated that the first order term in the Taylor series is alone insufficient to model the turnaround behaviour of the h function. We will hence include the next higher order term and use the form in equation (5.39) for the virialization term. The signs are chosen for future convenience, since it will turn out that both A and B are greater than zero.] In fact, for sufficiently large δ , the evolution depends only on the combination $q \equiv (B/A^2)$. This is most easily seen by rewriting equation (5.3), replacing $S(\delta)$ with the above form. Taking the limit of large δ , *i.e.* $\delta \gg 1$, and rescaling δ to δ/A , we obtain

$$\frac{d^2\delta}{db^2} + \frac{3}{2b} \frac{d\delta}{db} - \frac{4}{3\delta} \left(\frac{d\delta}{db} \right)^2 = -\frac{1}{a^2} + \frac{B}{A^2} \frac{1}{a^2 \delta} \quad (5.41)$$

$$= -\frac{1}{a^2} + \frac{q}{a^2 \delta} \quad (5.42)$$

From the form of the equation it is clear that the constants A and B occur in the combination $q = B/A^2$ and hence the non-linear regime is modelled by a one parameter family for the virialization term.

Equation (5.36) can be written as

$$\ddot{R} = -\frac{GM}{R^2} - \frac{4R}{27t^2} \left[-\frac{27GMt^2}{4R^3} - \frac{A}{\delta} + \frac{B}{\delta^2} \right] \quad (5.43)$$

Using $\delta = 9GMt^2/2R^3$ and $B = qA^2$ we may express equation (5.43) completely in terms of R and t . We now rescale R and t in the form $R = r_{vir}y(x)$ and

$t = \beta x$, where r_{vir} is the final virialised radius [i.e. $R \rightarrow r_{vir}$ for $t \rightarrow \infty$], where $\beta^2 = (8/3^5)(A/GM)r_{vir}^3$, to obtain the following equation for $y(x)$

$$y'' = \frac{y^4}{x^4} - \frac{27}{4}q \frac{y^7}{x^6} \quad (5.44)$$

We can integrate this equation to find a form for $y_q(x)$ (where $y_q(x)$ is the function $y(x)$ for a specific value of q) using the physically motivated boundary conditions $y = 1$ and $y' = 0$ as $x \rightarrow \infty$, which is simply an expression of the fact that the system reaches the virial radius r_{vir} and remains here thereafter. The results

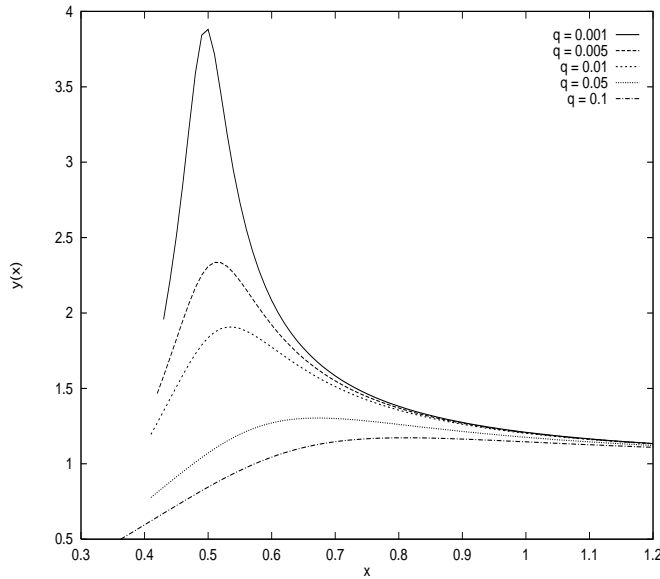


Figure 5.1: $y_q(x)$ for some values of q . The x axis has scaled time, x and the y axis is the scaled radius y .

of numerical integration of this equation for a range of q values are shown in fig. 5.1. As expected on physical grounds, the function has a maximum and gracefully decreases to unity for large values of x [the behaviour of $y(x)$ near $x = 0$ is irrelevant since the original equation is valid only for $\delta \geq 1$, at least]. For a given value of q , it is possible to find the value x_c at which the function reaches its maximum, as well as the ratio $y_{max} = R_{max}/r_{vir}$. The time, t_{max} , at which the system will reach the maximum radius is related to x_c by the relation

$t_{max} = \beta x_c = t_0(1 + z_{max})^{-3/2}$, where $t_0 = 2/(3H_0)$ is the present age of the universe and z_{max} is the redshift at which the system turns around. Figure (5.2) shows the variation of x_c and $y_{max} \equiv (R_{max}/r_{vir})$ for different values of q . The entire evolution of the system in the modified spherical collapse model (MSCM) can be expressed in terms of

$$R(t) = r_{vir} y_q(t/\beta) \quad (5.45)$$

where $\beta = (t_0/x_c)(1 + z_{max})^{-3/2}$. In SCM, the conventional value used for (r_{vir}/R_{max}) is $(1/2)$, which is obtained by enforcing the virial condition that $|U| = 2K$, where U is the gravitational potential energy and K is the kinetic energy. It must be kept in mind, however, that the ratio (r_{vir}/R_{max}) is not really constrained to be *precisely* $(1/2)$ since the actual value will depend on the final density profile and the precise definitions used for these radii. While we expect it to be around 0.5 , some amount of variation, say between 0.25 and 0.75 , cannot be ruled out theoretically. Figure (5.2) shows the parameter (R_{max}/r_{vir}) , plotted as a function of $q = B/A^2$ (dashed line), obtained by numerical integration of equation (5.36) with the *ansatz* (5.39). The solid line gives the dependence of x_c (or equivalently t_{max}) on the value of q . It can be seen that one can obtain a suitable value for the (r_{vir}/R_{max}) ratio by choosing a suitable value for q and vice versa. Using equation (5.14) and the definition $\delta \propto t^2/R^3$, we obtain

$$h_{SC}(x) = 1 - \frac{3}{2} \frac{x}{y} \frac{dy}{dx} \quad (5.46)$$

which gives the form of $h_{SC}(x)$ for a given value of q ; this, in turn, determines the function $y_q(x)$. Since δ can be expressed in terms of x , y and x_c as $\delta = (9\pi^2/2x_c^2)x^2/y^3$, this allows us to implicitly obtain a form for $h_{SC}(\delta)$, determined only by the value of q . Figure (5.3) shows the behaviour of h_{SC} functions obtained by integrating equation (5.16) backwards, assuming that $h_{SC} \rightarrow 1$ as $\delta \rightarrow \infty$. It

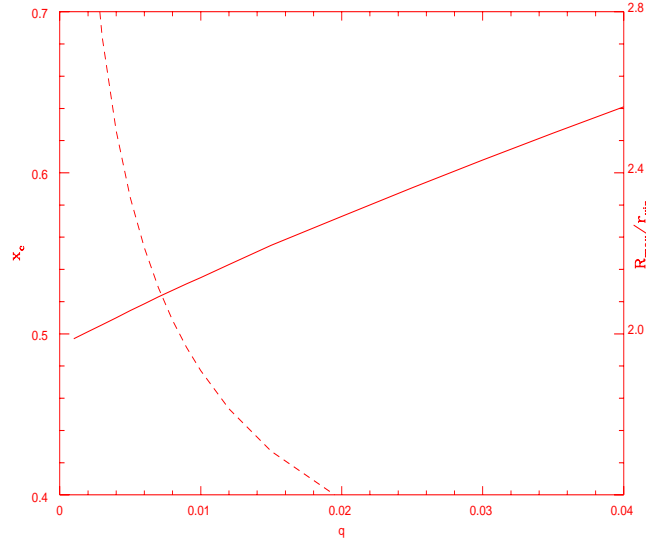


Figure 5.2: The parameters (R_{max}/r_{vir}) (broken line) and x_c (solid line) as a function of $q = B/A^2$. This clearly demonstrates that the single parameter description of the virialization term is constrained by the value that is chosen for the ratio r_{vir}/R_{max} .

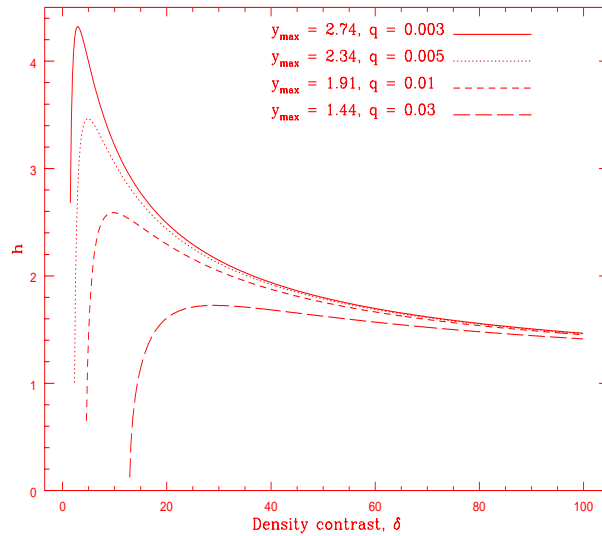


Figure 5.3: The h_{SC} function, obtained for various values of q . The values of q and $y_{max} \equiv R_{max}/r_{vir}$ for the curves are indicated at the top right hand corner. (Further discussion in text)

is seen that all the curves have the same turnaround behaviour expected on the basis of the physical arguments presented in the earlier section.

If the functional form for h_{SC} – determined, say, from N-body simulations – is used as a further constraint, we should be able to obtain the values of q . The major hurdle in attempting to do this is the fact that the available simulation results are given in terms of the averaged two point correlation function, $\bar{\xi}$, and the averaged pair velocity, $h(a, x)$, defined by

$$\bar{\xi} = \frac{3}{r^3} \int_0^r \xi(x, a) x^2 dx ; \quad h(a, x) = -\frac{\langle v(a, x) \rangle}{\dot{a}x} \quad (5.47)$$

where the two-point correlation function ξ is defined as the Fourier transform of the power spectrum, $P(k)$, of the distribution. The results published in the literature assume that $h(a, x)$ depends on a and x only through $\bar{\xi}(a, x)$, that is, $h(a, x) \equiv h[\bar{\xi}(a, x)]$. This assumption has been invoked in several works in the past ([19], [34], [30], [37], [41]) and seems to be validated by numerical simulations. The fitting formula for $h(\bar{\xi})$ can be obtained from related fitting formulas available in the literature [19]. These are, however, statistical quantities and are not well defined for an isolated overdense region. Hence we have to first make the correspondence between $h_{SC}(\delta)$ and $h(\bar{\xi})$, which we do as follows.

It is possible to show by standard arguments [34] that

$$\frac{d\bar{\xi}}{d\alpha} = 3h(1 + \bar{\xi}) \quad (5.48)$$

that is,

$$\frac{dD}{d\alpha} = 3h \quad (5.49)$$

where $D = \ln(1 + \bar{\xi})$ and $\alpha = \ln a$. Equation (5.49) is very similar to equation (5.14), which defines the function $h_{SC}(\delta)$, except for the different definitions of D and D_{SC} in terms of $\bar{\xi}$ and δ respectively. This suggests that one can obtain a

relation between $h_{\text{SC}}(\delta)$ and $h(\bar{\xi})$ by relating the density contrast δ of an isolated spherical region to the two-point correlation function $\bar{\xi}$ averaged over the distribution at the same scale. We essentially need to find a mapping between $\bar{\xi}$ and δ which is valid in a statistical sense.

Gravitational clustering is known to have three regimes in its growing phase, usually called “linear”, “quasi-linear” and “non-linear” respectively. The three regimes may be characterized by values of density contrast as $\delta \ll 1$ in the linear regime, $1 < \delta < 100$ in the quasi-linear regime and $100 < \delta$ in the non-linear regime. The three regimes have different rates of growth for various quantities of interest such as δ , ξ and so on. In the linear regime, it is well known that the density contrast grows proportional to the scale factor, a . This implies that the power spectrum, $P(k) \equiv |\delta_k|^2$ (where δ_k is the Fourier mode corresponding to $\delta(x)$), grows as a^2 . Consequently, $\bar{\xi}$, which is related to $P(k)$ via a Fourier transform, also grows as a^2 , *i.e.* as the square of the density contrast. In the quasi-linear and non-linear regimes, the density contrast does not grow linearly with the scale factor and the relation between δ and $\bar{\xi}$ is not so clearly defined. The quasi-linear regime may be loosely construed as the interval of time during which the high peaks of the initial Gaussian random field have collapsed, although mergers of structures have not yet begun to play an important role. (This idea was used in [37] to model the non-linear scaling relations successfully). If we consider a length scale smaller than the size of the collapsed objects, the dominant contribution to $\bar{\xi}$ (at this scale) arises from the density profiles centered on the collapsed peaks. Using the relation

$$\rho \simeq \rho_b (1 + \bar{\xi}) \quad (5.50)$$

for density profiles around high peaks, one can see that $\bar{\xi} \propto \delta$ in this regime. In

the non-linear regime, δ and $\bar{\xi}$ have the forms $\delta(a, x) = a^3 F(ax)$, $\bar{\xi} = a^3 G(ax)$, where x is a co-moving and $r = ax$ is a proper coordinate. When the system is described by Lagrangian coordinates (which correspond to proper coordinates $r = ax$, *i.e.* at constant r), $\bar{\xi}$ is proportional to δ . Thus, the relation $\bar{\xi} \propto \delta$ appears to be satisfied in all regimes, except at the very linear end. Since we are only interested in the $\delta > 1$ range, we use $\bar{\xi} \approx \delta$ and compare equations (5.48) and (5.14) to identify

$$h_{\text{SC}}(\delta) \approx h(\bar{\xi}) \quad (5.51)$$

It is now straightforward to choose the value of q such that the known fitting function for the h function is reproduced as closely as possible. We use the original function given by Hamilton [19] to obtain the following expression for $h(\bar{\xi})$:

$$h(\bar{\xi}) = \frac{2}{3} \left(\frac{d \ln \mathcal{V}(\bar{\xi})}{d \ln(1 + \bar{\xi})} \right)^{-1} \quad (5.52)$$

where $\mathcal{V}(\bar{\xi})$ is given by the fitting function

$$\mathcal{V}(\bar{\xi}) = \bar{\xi} \left(\frac{1 + 0.0158 \bar{\xi}^2 + 0.000115 \bar{\xi}^3}{1 + 0.926 \bar{\xi}^2 - 0.0743 \bar{\xi}^3 + 0.0156 \bar{\xi}^4} \right)^{1/3} \quad (5.53)$$

Figure (5.4) shows the simulation data represented by the fit (solid line) [19] and the best fit (dashed line), obtained in our model, for $q \simeq 0.02$. We note that the fit is better than 5% for all values of density contrast $\delta \geq 15$. The change in the fit is very marginal if one imposes the boundary condition $h(\delta) \rightarrow 1$ for $\delta \gg 1$, instead of constraining the curves to match at their peaks (for example, the change in the peak height is $\sim 1\%$, if we impose the above condition at $\delta = 10000$).

Figure (5.5) shows the plot of scaled radius $y_q(x)$ vs x , obtained by integrating equation(5.44), with $q = 0.02$. The figure also shows an accurate fit (dashed line)

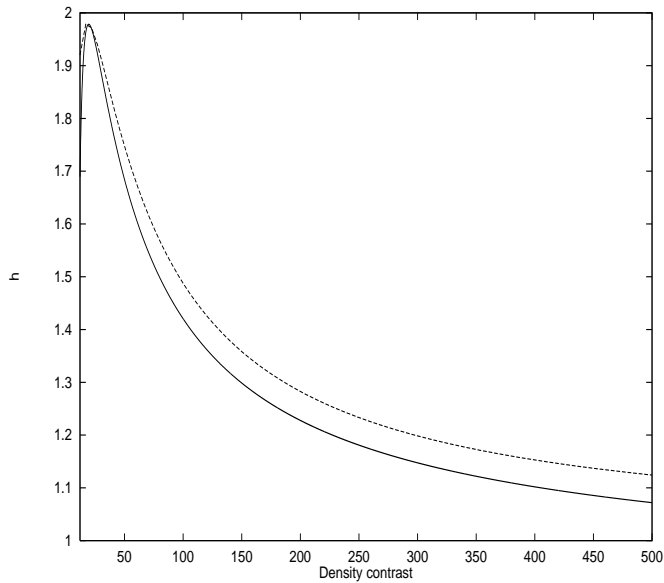


Figure 5.4: The best fit curve for the h function (dashed line) to the simulation data (solid line). The simulation results are obtained from Hamilton [19] and the fit is obtained by adjusting the value of q parameter until the curves coincide.

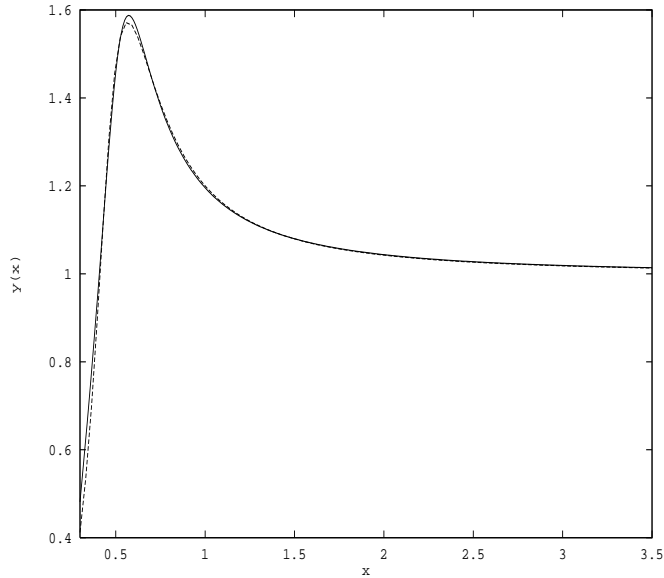


Figure 5.5: Plot of the scaled radius of the shell y_q as a function of scaled time x (solid line) and the fitting formula $y_q = (x + ax^3 + bx^5)/(1 + cx^3 + bx^5)$, with $a = -3.6$, $b = 53$ and $c = -12$ (dashed line) (See text for discussion)

to this solution of the form

$$y_q(x) = \frac{x + ax^3 + bx^5}{1 + cx^3 + bx^5} \quad (5.54)$$

with $a = -3.6$, $b = 53$ and $c = -12$. This fit, along with values for r_{vir} and z_{max} , completely specifies our model through equation (5.45). It can be observed that (r_{vir}/R_{max}) is approximately 0.65. It is interesting to note that the value obtained for the (r_{vir}/R_{max}) ratio is not very widely off the usual value of 0.5 used in the standard spherical collapse model, *in spite of the fact that no constraint was imposed on this value, ab initio, in arriving at this result.* Part of this deviation *may* also originate in the fit which has been used for $h(\bar{\xi})$; Hamilton et al. [19] noticed that objects virialised at $R_{max}/r_{vir} \sim 1.8$, instead of 2, in their simulations.

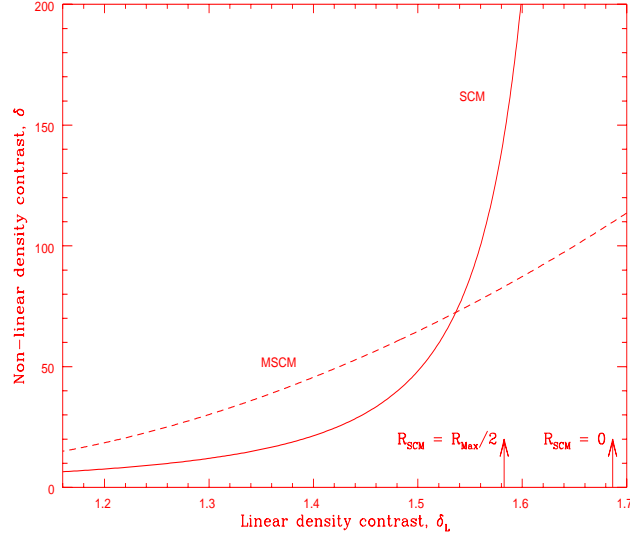


Figure 5.6: The non-linear density contrast in the SCM (solid line) and in the modified SCM (dashed line), plotted against the linearly extrapolated density contrast δ_L .

Finally, figure (5.6) compares the non-linear density contrast in the modified SCM (dashed line) with that in the standard SCM (solid line), by plotting both against the linearly extrapolated density contrast, δ_L . It can be seen (for a given

system with the same z_{max} and r_{vir}) that, at the epoch where the standard SCM model has a singular behaviour ($\delta_L \sim 1.686$), our model has a smooth behaviour with $\delta \approx 110$ (the value is not very sensitive to the exact value of q). This is not widely off from the value usually obtained from the *ad hoc* procedure applied in the standard spherical collapse model. In a way, this explains the unreasonable effectiveness of standard SCM in the study of non-linear clustering.

As mentioned earlier, deviations from spherical symmetry are expected to be small at early epochs and to grow as the system evolves. One would thus expect the two curves of figure (5.6) to approach each other as $\delta \rightarrow 1$ (from above). Further, the curves should overlay in the linear regime ($\delta_L \ll 1$). It can be seen from the figure that the 2 curves *do* approach each other as δ_L reduces towards unity. However, the MSCM has been obtained using a Taylor expansion in $(1/\delta)$; it is clearly *not* applicable for $\delta \ll 1$. Further, the region $\delta > 15$ has been used to fit the function $h(\delta)$ to the data of Hamilton [19]. Hence, one cannot compare the curves in the linear regime.

Figure (5.6) also shows a comparison between the standard SCM and the MSCM in terms of δ values in the MSCM at two important epochs, indicated by vertical arrows. (i) When $R = R_{max}/2$ in the SCM, *i.e.* the epoch at which the SCM *virializes*, $\delta(\text{MSCM}) \sim 83$. (ii) When the SCM hits the singularity, ($\delta_L \sim 1.6865$), $\delta(\text{MSCM}) \sim 110$.

We note, finally, that figure (5.6), which shows the effects of evolution as a mapping from linear to non-linear density contrasts, contains a subtle implicit assumption regarding the definition of the non-linear density contrast. The radius R of a system is not a rigorously defined quantity in the absence of spherical symmetry, and obviously, any argument involving ‘virialization’ precludes strict spherical symmetry. It is, however, a conventional practice to define the ‘radius’,

R , even for a virialized system without strict spherical symmetry. For example, this approach is used to define the density contrast at ‘virialization’ (which has the value, $\delta_{vir} \approx 200$) in the standard SCM. In our model we have an explicit equation for R ; once R and M are given, the non-linear density contrast is a well-defined quantity.

5.6 Results and Summary

It has been shown how the Taylor expansion of a term in the equation for the evolution of the density contrast, δ , in inverse powers of δ , allows us to have a more realistic picture of spherical collapse, which is free from arbitrary abrupt “virialization” arguments. Beginning from a well motivated *ansatz* for the dependence of the “virialization” term on the density contrast we have shown that a spherical collapse model will gracefully turn around and collapse to a constant radius with $\delta \sim 110$ at the same epoch when the standard model reaches a singularity. Figure (5.5) shows clearly that the singularity is avoided in our model due to the enhancement of deviations from spherical symmetry, and consequent generation of strong non-radial motions.

We derive an approximate functional form for the virialization term starting from the physically reasonable assumption that the system reaches a constant radius. This assumption allows us to derive an asymptotic form for the virialization term, with the residual part adequately expressed by keeping only the first and second order terms in a Taylor series in $(1/\delta)$. It is shown that there exists a scaling relation between the coefficients of the first and second order terms, essentially reducing the virialization term to a one parameter family of models.

The form of the h function published in the literature, along with a tentative mapping from δ to $\bar{\xi}$, in the non-linear and quasi-linear regimes, allow us to further

constrain our model, bringing it in concordance with the available simulation results. Further, it is shown that this form for the virialization term is sufficient to model the turnaround behaviour of the spherical shell and leads to a reasonable numerical value for density contrast at collapse.

There are several new avenues suggested by this work.

- (i) The assumption $h_{\text{SC}} \rightarrow 1$, $R \rightarrow r_{\text{vir}}$ is equivalent to “stable clustering”, in terms of the statistical behaviour. Since stable clustering has so far not been proved conclusively in simulations and is often questioned, it would be interesting to see the effect of changing this constraint to $h \rightarrow \text{constant}$ for $t \rightarrow \infty$.
- (ii) The technique of Taylor series expansion in $(1/\delta)$ seems to hold promise. It would be interesting to try such an attempt with the original fluid equations and (possibly) with more general descriptions.
- (iii) It must be stressed that we used the $\delta - \bar{\xi}$ mapping — possibly the weakest part of our analysis, conceptually — only to fix a value of q . We could have used some high resolution simulations to actually study the evolution of a realistic overdense region. We conjecture that such an analysis will give results in conformity with those obtained here.
- (iv) Finally, the curves of figure (5.6) can be used to describe the spatial distribution of virialised haloes ([30],[52]). It would be interesting to investigate how things change when the MSCM is used in place of the standard spherical collapse model.

In the next chapter we shall approach the problem of structure formation from a completely different point of view, namely that of Quasi Steady State Cosmology (QSSC).

Chapter 6

Structure formation in QSSC

Just because everything is different doesn't mean anything
has changed – Paradoxial quotations

6.1 Introduction

The Quasi-Steady State Cosmology (QSSC) was first proposed in 1993 and explored further by Fred Hoyle, Geoffrey Burbidge and Jayant Narlikar in a series of papers ([20],[21],[22],[23],[24]). The QSSC offers an alternative to the commonly accepted big bang cosmology, and the above work claims to provide a singularity-free cosmological model, which is consistent with the data on discrete source populations, can explain the production of light nuclei as well as the spectrum and anisotropy of the microwave background. Because the dynamical and physical conditions in this cosmology are considerably different from those in the standard cosmology, the theoretical reasoning required to understand what is observed may differ too. In short, one may not simply lift a theoretical line of reasoning from standard cosmology and expect to apply it to the same problem in the QSSC.

One of the outstanding problems in modern big bang cosmology is the problem of formation of large scale structure in the universe. The standard approach consists in starting with prescribed primordial fluctuations of spacetime geome-

try and matter density, evolving them through an inflationary era, having them interact with nonbaryonic dark matter, then carrying out N-body simulations of interacting masses which may eventually form into groups to be identified with large scale structures like galaxies, clusters, superclusters and voids, etc. Although a lot of this work has gone into cosmology textbooks ([45],[36]), it is a fair comment to say that no unique and generally acceptable structure formation scenario has yet emerged in standard cosmology.

The problem of structure formation poses a challenge in the QSSC also and it should be viewed against the background of the above standard approach. As we shall see in Section 6.2, the QSSC does not have an era when the baryonic matter density in the universe was $\sim 10^{81}$ times its present value, as it was in the big bang cosmology in the immediate post-inflation era. Thus the growth of fluctuations in the form of gravitational instabilities will not be similar in this cosmology to that in the big bang cosmology.

Recently the gravitational stability of the QSSC models against small perturbations was examined in detail in a paper by Banerjee and Narlikar [12]. They found the cosmological solution to be stable and thus there was no net growth in density fluctuations. The model is basically oscillatory and perturbations of density and metric grow only to a finite amount during the contraction phase and then decay during the expansion phase. These authors concluded that gravitational instability alone cannot lead to formation of structures in the QSSC. Instead, explosive matter creation in the so-called *minibangs* is expected to be the principal cause of forming structures. In this chapter we try to understand the pattern of formation and growth of structures in the QSSC though numerical simulations by using a simplified toy model.

The organization of this chapter is as follows: In section 6.2 we briefly review

the basic theory of QSSC. The numerical toy model will be introduced in section 6.3. Section 6.4 is devoted to computing the two point correlation function for the distributions arising in the toy model and its comparison with observations. In section 6.5 we summarise the results by highlighting the success of this approach and indicating how it can be further improved.

6.2 The Basic Theory of the QSSC

The basic formulation of the QSSC is via the Machian theory of gravity first proposed by Hoyle and Narlikar ([25],[26]) in which the origin of inertia is linked to a long range scalar interaction between matter and matter. Specifically, the theory is derivable from an action principle with the simple action:

$$\mathcal{A} = - \sum_a \int m_a ds_a, \quad (6.1)$$

where the summation is over all the particles in the universe, labeled by the index a , the mass of the a th particle being m_a . The integral is over the world line of the particle, ds_a representing the element of proper time of the a th particle.

The mass itself arises from interaction with other particles. Thus the mass of particle a at point A on its worldline arises from all other particles b in the universe:

$$m_a = \sum_{b \neq a} m_{(b)}(A), \quad (6.2)$$

where $m_{(b)}(X)$ is the contribution of inertial mass from particle b to any particle situated at a general spacetime point X . The long range effect is Machian in nature and is communicated by the scalar mass function $m_{(b)}(X)$ which satisfies the conformally invariant wave equation

$$\square m_{(b)} + \frac{1}{6} R m_{(b)} + m_{(b)}^3 = N_{(b)}. \quad (6.3)$$

Here the wave operator is with respect to the general spacetime point X . R is the scalar curvature of spacetime and the right hand side gives the number density of particle b . The field equations are obtained by varying the action with respect to the spacetime metric g_{ik} . The important point to note is that the above formalism is conformally invariant. In particular, one can choose a conformal frame in which the particle masses are constant. If the constant mass is denoted by m_p , the field equations reduce to

$$R^{ik} - \frac{1}{2}g^{ik}R + \Lambda g^{ik} = -\frac{8\pi G}{c^4}[T^{ik} - f(C^iC^k - \frac{1}{4}g^{ik}C^lC_l)], \quad (6.4)$$

where c is the speed of light and C is a scalar field which arises explicitly from the ends of broken world lines, that is when there is creation (or, annihilation) of particles in the universe. The constant f denotes the coupling of the C -field to spacetime. Thus the divergence of the matter tensor T^{ik} need not always be zero, as the creation or annihilation of particles is compensated by the non-zero divergence of the C -field tensor in Eq.(6.4). The quantities G (the gravitational constant) and Λ (the cosmological constant) are related to the large scale distribution of particles in the universe. Thus,

$$G = \frac{3\hbar c}{4\pi m_p^2}, \quad \Lambda = -\frac{3}{N^2 m_p^2}, \quad (6.5)$$

N being the number of particles within the cosmic horizon.

Note that the signs of the various constants are determined by the theory and not put in by hand. For example, the constant of gravitation is positive, the cosmological constant negative and the coupling of the C -field energy tensor to spacetime is negative.

6.2.1 Matter Creation

The action principle tells us that matter creation is possible at a given spacetime point provided the ambient C -field satisfies the equality $C_i C^i = m_p^2$ at that point. In normal circumstances, the background level of the C -field will be *below* this level. However, in the strong gravity obtaining in the neighbourhood of compact massive objects, the value of the field can be locally raised. This leads to creation of matter along with the creation of negative C -field energy. The latter also has negative stresses which have the effect of blowing the spacetime outwards (as in an inflationary model) with the result that the created matter is thrown out in an explosion. Qualitatively, the creation and ejection proceeds along the following lines.

The process normally begins by the creation of the C -field along with matter in the neighbourhood of a compact massive object. The former, being propagated by the wave equation, tends to travel outwards with the speed of light, leaving the created mass behind. However, as the created mass grows, its gravitational redshift begins to assert itself, and the C -field gets trapped in the vicinity of the object. As its strength grows, its repulsive effect begins to manifest itself, thus making the object less and less bound and unstable. Finally, a stage may come when a part of the object is ejected from it with tremendous energy. It is thus possible for a parent compact mass to eject a bound unit outwards. This unit may act as a center of creation in its own right.

We shall refer to such pockets of creation as *minibangs* or *mini-creation events* (MCEs). A spherical (Schwarzschild type) compact matter distribution will lead to a spherically symmetric explosion whereas an axi-symmetric (Kerr type) distribution would lead to jet-like ejection along the symmetric axis. Because of the conservation of angular momentum of a collapsing object, it is expected that the

latter situation will in general be more likely.

In either case, however, the minibang is *nonsingular*. There is no state of infinite curvature and terminating worldlines, as in the standard big bang, nor is there a black hole type horizon. The latter because the presence of the C -field causes the collapsing object to bounce outside the event horizon.

6.2.2 The Cosmological Solution

The feedback of such minibangs on the spacetime as a whole is to make it expand. In a completely steady situation, the spacetime will be that given by the de Sitter metric. However, the creation activity passes through epochs of ups and downs with the result that the spacetime also shows an oscillation about the long term steady state. Sachs [49] has computed the general solutions of this kind and the simplest such solution with the line element given by

$$ds^2 = c^2 dt^2 - S^2(t)[dr^2 + r^2(d\theta^2 + \sin^2\theta d\phi^2)], \quad (6.6)$$

where c stands for the speed of light has the scale factor given by

$$S(t) = e^{t/P} \left[1 + \eta \cos \frac{2\pi\tau(t)}{Q} \right]. \quad (6.7)$$

The constants P and Q are related to the constants in the field equations, while $\tau(t)$ is a function $\sim t$ which is also determined by the field equations. We shall, however, use the approximation $\tau(t) = t$ which is adequate for the approach used in this chapter. The parameter η may be taken positive and is less than unity. Thus the scale factor never becomes zero: the cosmological solution is without a spacetime singularity. The form of the scale factor, $S(t)$, in the metric (6.6) is shown in Figure 6.1.

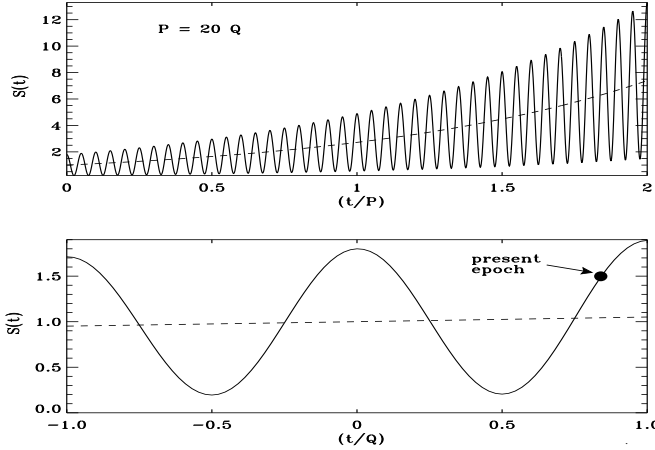


Figure 6.1: The scale factor $S(t)$ of the QSSC in the upper panel against t to show how several oscillatory cycles of short period Q are accommodated in the longer e -folding time P of the exponential expansion. In the lower panel are sketched a few oscillations on an expanded timescale with our present epoch marked.

6.2.3 Observational Checks

Hoyle ([21],[22]) have shown that the above cosmology gives a reasonably good fit to the observations of discrete source populations, such as the redshift-magnitude relation, radio source count, angular diameter-redshift relation and the maximum redshifts so far observed, with the choice of the following set of parameters:

$$P \approx 20Q, \quad Q \approx 4.4 \times 10^{10} \text{ yrs}, \quad \eta = 0.8, \quad \Lambda = -0.3 \times 10^{-56} \text{ cm}^{-2}, \quad t_0 = 0.7Q.$$

Of these, the last is the present epoch of observation. It is not essential that the model should have only these parameteric values. Indeed, the parameter space is wide enough to make the model robust. Moreover, the fitting of observations to theory does not require postulating ad hoc evolution which is commonly necessary in the case of standard cosmology.

The above framework thus outlines a cosmological model without a beginning and without an end, in which a de Sitter type exponential expansion, character-

ized by a very long time scale P , is superposed with finite size oscillations of a shorter time scale Q . Each cycles are statistically identical in their physical properties. In this sense the universe is ‘quasi-steady’. We next see how structures might grow and proliferate in such a universe.

6.3 A Toy Model for Formation of Structures

In an attempt to understand how structures may possibly grow and distribute in space we have carried out the following numerical experiment in two as well as three dimensional space. We describe the $2D$ case first and detail the $3D$ versions subsequently.

6.3.1 2D-Simulations

A large number of points ($N \sim 10^5 - 10^6$), each one representing a mini-creation event, is distributed randomly over a unit square area . The average nearest-neighbour distance for such a distribution will then be $(1/\sqrt{N})$. Now suppose that in a typical mini-creation event, each particle generates another neighbour particle at random within a distance, $d = x/\sqrt{N}$ in $2D$. Here, the number x is a fraction between 0 and 1 . We shall call x the separation parameter. As explained in section 6.2.1, the above denotes an ejected piece lying at a distance $\leq d$ from the original compact object.

The sample area is then uniformly stretched by a linear factor $\sqrt{2}$ to represent expansion of space. We now have the same density of points as before, i.e., $2N$ points over area of 2 units. From this enlarged square remove the periphery so as to retain only the inner unit square. This process thus brings us back to the original state but with a different distribution of an average N points over a unit square. This process is repeated n times . Here the number of iterations, n , plays

the role of “time” as in the standard models of structure formation. The number distribution of points evolves as the ‘creation process’ generates new points near the existing ones. We will refer to each point as a ‘particle’ or ‘unit’.

Not surprisingly, soon after, i.e., after $n = 3 - 4$ iterations of the above procedure, clusters and voids begin to emerge in the sample area and create a *Persian Carpet* type of patterns. As the experiment is repeated, voids grow in size while clusters become denser. Figure 6.2 illustrates a typical numerical simulation. It shows that expansion coupled with creation of matter is a natural means of generating voids and clusters. But what of the filaments ? Here we

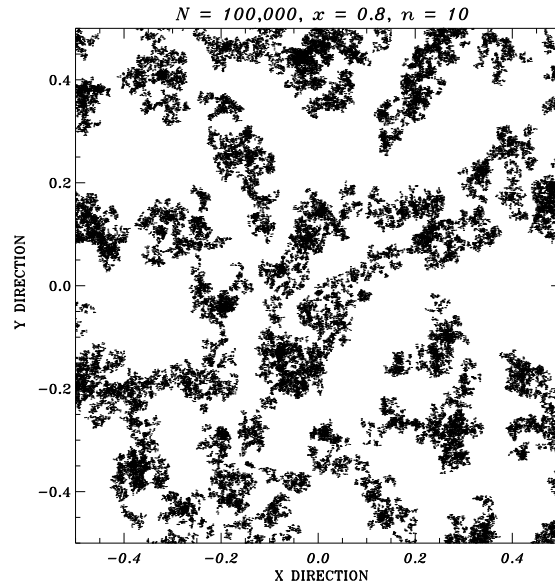


Figure 6.2: A cluster-void distribution generated in the 2D toy model for $N = 100,000$ initially randomly distributed particles, with typical separation parameter $x = 0.8$, and the number of iterations $n = 10$. Each particle resembles a galaxy. For further discussion see the text.

recall that the creation process near a typical compact massive object will not be isotropic if the mass is spinning. Matter will be preferentially ejected along the axis of spin. To build this effect into the above simulation we adopt the following algorithm.

We assume that in a typical $n > 2$ iteration, the creation of the new neighbour unit C around a typical unit B is not entirely random, but, instead, related to the previous history of creation of B from an earlier generation unit A . So the direction BC is broadly aligned with the direction AB in which B itself was ejected. Typically this is ensured by assuming that the ejection is at a random angle in the forward semicircle as explained in Figure 6.3. We will refer to this as *aligned ejection*, as opposed to the *isotropic ejection* of Figure 6.2. Physically

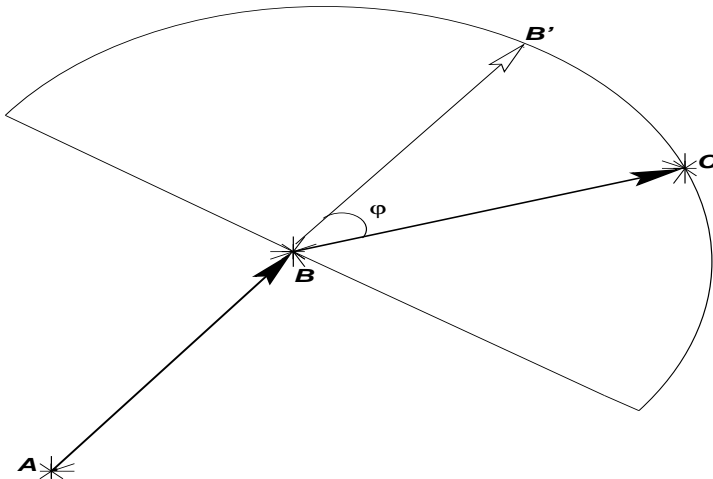


Figure 6.3: Schematic procedure for creating units in aligned direction for $n > 2$. Particle A is a representative of first generation units which are distributed randomly. B is a representative of the second generation units, being created in a random direction. Point C represents a third generation unit which has been created in the half plane lying away from A off the line perpendicular to AB . BC therefore makes an acute angle, φ , with the line ABB' .

this means that the unit B ejected by A retains ‘memory’ of its origin through its spin which is more or less aligned with the spin of A . Which is why when it ejects a unit C , it is more or less aligned with the earlier ejection direction AB .

Although this algorithm does not demand strict alignment, it is interesting to note that the filamentary structure grows along with voids as n increases. Features generated in this way have very suggestive similarities with the observed

large scale structure as shown in a typical simulation of Figure 6.4. We have also investigated the result of restricting the secondary ejection to a narrower angle, e.g, by keeping the angle φ of Figure 6.3 in the range $(-\pi/4, \pi/4)$. Not surprisingly we find the filamentary structure more pronounced in such a case. In general, we may argue that the higher the angular momentum per unit mass of the compact object causing ejection, the narrower is the angle of ejection, the greater is the alignment and hence more pronounced the filamentary structure. Figure 6.5 shows a typical two dimensional gravitational clustering simulation

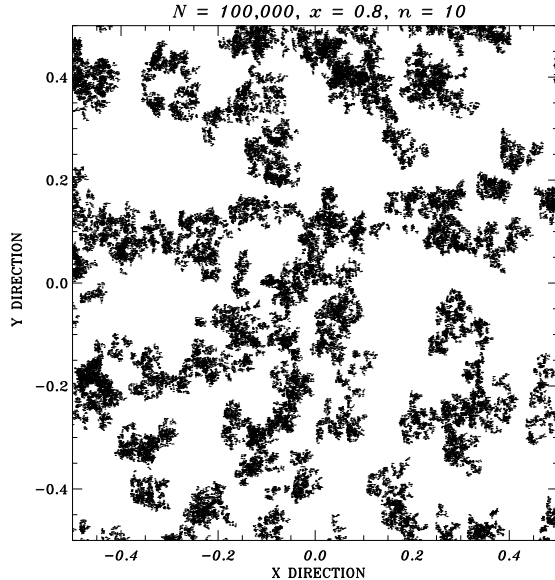


Figure 6.4: A computer simulated filament-void distribution with $n(> 2)$ iterations of aligned ejections having new points following the rule of Figure 6.3, for the same parameters of Figure 6.2.

data in standard big bang cosmology.

It can be seen that both compact and extended structures are present in both the approaches to structure formation. Since there is no observational data with which comparisons can be made in two dimensions we shall henceforth deal with the 3D simulations only.

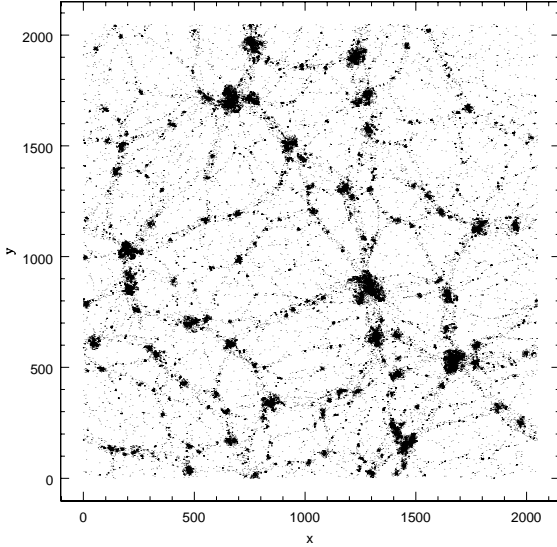


Figure 6.5: A power law 2D simulation in the standard big bang cosmology for power index, $n = -0.4$ of density fluctuations.

6.3.2 3D-Simulations

The 3D simulation is similar, with the necessary modifications for the higher dimensionality. Thus we start with a unit cube with N points distributed at random within it, the typical interpoint distance being $(1/\sqrt[3]{N})$. Creating a new near neighbour for each particle by the same rule as in the 2D case, we need to expand each edge of the cube by the factor $\sqrt[3]{2}$. We next apply the same algorithm favouring aligned ejection, suitably modified for 3D. To compare the three dimensional distributions with the observed distributions made up from redshift surveys, we need to take a thin inside slice of the cube perpendicular to one of its edges and examine the distribution of points therein. Before making such a comparison, however, we will first apply 3D-simulations within the framework of the QSSC.

6.3.3 Simulations of QSSC Cycles

To bring the toy model closer to the reality of the QSSC, we proceed as follows. We expect the creation activity to be confined largely to a narrow era around a typical oscillatory minimum, when the C -field is at its strongest. By considering the number density of collapsed massive objects at one oscillatory minimum of QSSC to be f , the number density at the next oscillatory minimum would fall to $f \exp(-3Q/P)$, if no new massive objects were added. Thus to restore a steady state from one cycle to the next,

$$\alpha f \equiv [1 - \exp(-3Q/P)]f \sim (3Q/P)f, \quad (6.8)$$

masses must be created anew. In other words, a fraction $(3Q/P)$ of the total number of massive objects must duplicate themselves in the above fashion.

Notice that, unlike the old steady state theory which had new matter appearing continuously, we have here discrete creation, confined to epochs of minimum of scale factor. The ‘steady-state’ is maintained from one cycle to next. Which is why the above addition αf is required at the beginning of each cycle. Therefore, instead of creating a new neighbour particle around each and every one of the original set of N particles, we do so only around αN of these points chosen randomly, where the fraction α is as defined in (6.8). Likewise, the sample volume is homologously expanded by the factor $\exp(3Q/P)$ only instead of by factor 2. We choose the inner cube as before. Figure 6.6 shows the simulated distributions in cubical slices for isotropic as well as aligned ejections. After a few iterations clusters and voids begin to appear, with the case for aligned ejections showing filaments. For a comparison, see an actually observed distribution of galaxies from a redshift survey in Figure 6.7. In the above approximation we have assumed that the creation activity is concentrated at the oscillatory minima. It

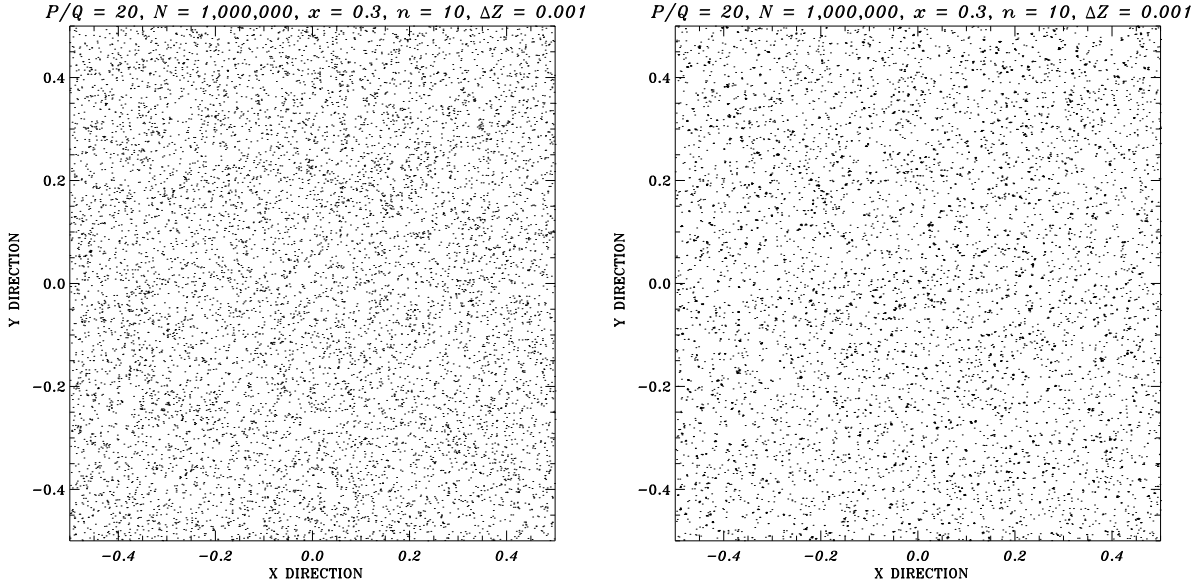


Figure 6.6: A 3-dimensional version, adapted for the QSSC with $N = 1,000,000$, $x = 0.3$, $n = 10$, and $P/Q = 20$. Slice thickness in the Z direction is $\Delta Z = 0.001$. Evidently, voids are seen separated by filamentary structures. The left panel is for the case of isotropic distribution of particles, whereas the right panel shows the case of aligned ejections.

could be extended over an appreciable part of the oscillatory period, in which case one would see large scale structure in the radial direction as seen from an observer. We have not modified an algorithm to cover such cases, but feel that this should be investigated, especially since the recent analysis of the redshift-magnitude relation for supernovae has generated interest in the QSSC models of this kind [13].

6.4 The Two Point Correlation Functions

Although visual inspection of Figures 6.6 and 6.7 suggests that the simulation is proceeding along the right lines, a *quantitative* measure of the cluster-void distribution will help in comparing simulations with reality.

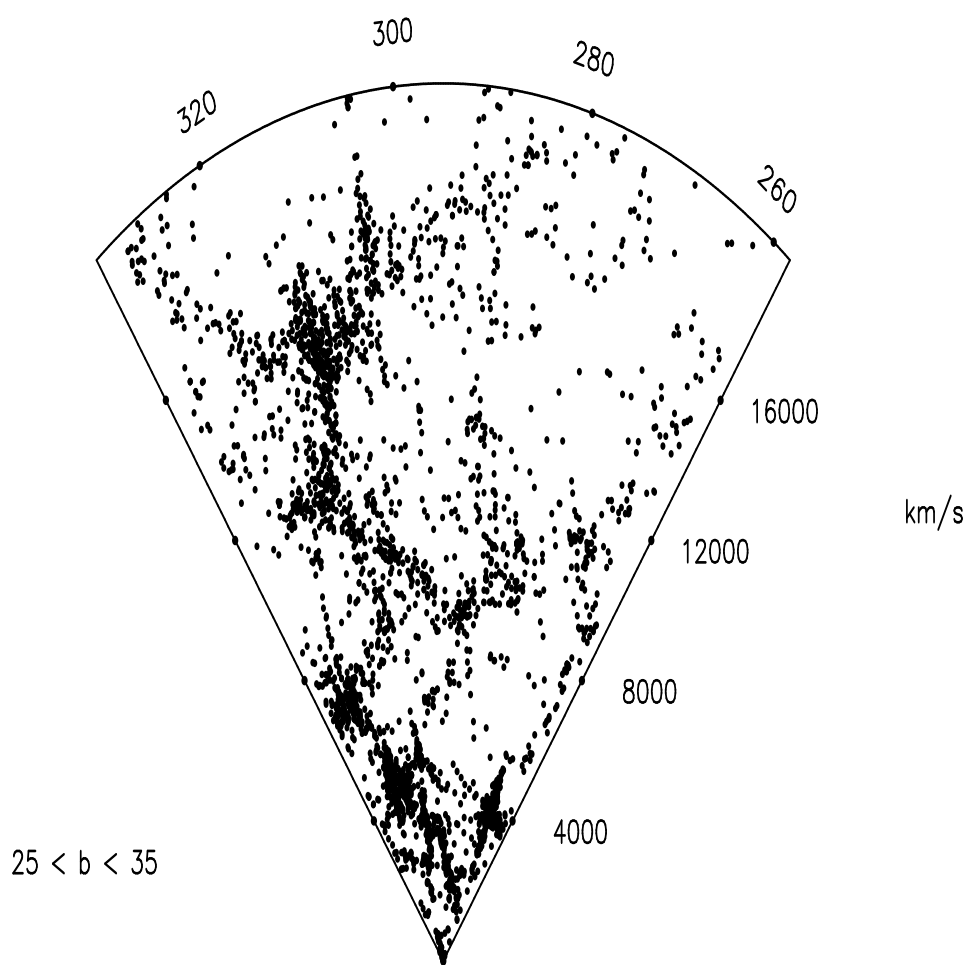


Figure 6.7: A FLAIR redshift survey in the direction of Hydra-Centaurus[54]

The dimensionless autocorrelation function

$$\xi(r) = \langle [\rho(\mathbf{r}) - \langle \rho \rangle][\rho(\mathbf{r}_1 + \mathbf{r}) - \langle \rho \rangle] \rangle / \langle \rho \rangle^2, \quad (6.9)$$

where $\langle \rho \rangle$ is the average density in the volume, is one convenient measure of such irregularities in the space distribution. Typically, different classes of objects cluster at different characteristic lengths. To fix ideas in the present model, we will look at distribution of clusters of galaxies. Observationally, it is believed that the two point correlation function for cluster distribution obeys the following scaling law:

$$\xi_{cc}(r) = \left(\frac{r}{r_0} \right)^{-\gamma}, \quad (6.10)$$

with $\gamma \simeq 1.8$ and $r_0 = 25h^{-1}$ Mpc, where the Hubble constant at the present epoch is taken to be $100h$ kms $^{-1}$ Mpc $^{-1}$. In order to quantify the issues of formation of structures in this scenario we have taken the following measures.

It is known that instead of having a smooth distribution of matter on large scales, the observed universe has structures of typical sizes of a few tens of megaparsecs . These “structures” are regions of density considerably higher than the background density, with the maximum density contrast $\delta = (\delta\rho(r)/\langle \rho \rangle)$ going from order unity (in the case of clusters) to a few thousand (in the case of the galaxies).

Any process which generates structures must be able to produce to the zeroth order , entities whose density contrast is of such magnitude and with the property that on larger and larger distance scales, the density contrast becomes less significant. This is to ensure that on a large enough scale the universe is homogeneous.

Given this prescription for generating structures without gravitational dynamics, we first ensured that the visual impression created by the cluster sim-

ulations did imply that as the number of iterations were increased the number of high density regions also increased. In the initial configuration one expects to find regions of high density arising only because of the Poisson noise. In the later “epochs” after a few iterations, however, we expected and did find that the variation of the one point distribution function for density ($\rho / \langle \rho \rangle$) with $\langle \rho \rangle$ the average density in the volume, showed a steady and significant increase in the the number of high and intermediate density regions, as is expected in a clustering scenario. We further observed that the value of maximum density also increased as a function of the number of iterations, which in this experiment corresponds to “time”. The density field has been generated on a grid placed into the simulation volume using the algorithm of cloud in cell.

Our simulations show the growth of structures through rise in the density maximum as a function of number of iterations. The aligned ejection mode leads to faster clustering than the isotropic one.

One must also examine the dependence of this “growth” on another important parameter in this prescription, namely the typical maximum separation between a creation site and the unit which is created. This was indicated by the parameter x in our earlier discussion.

Again our studies investigate results of the structure formation algorithm when the parameter x is changed. We find that higher densities are achieved when this distance (in units of boxsize) is made smaller. This is intuitively expected.

In the QSSC case, clustering is stronger in the early epochs for the isotropic ejection model, although at a later stage the density function for the aligned ejection model catches up and ultimately exceeds the rate for the isotropic case.

The next quantitative measure that we computed from these data set was

the two point correlation function. The following figures summarise the results of these computations. It can be seen that the observationally obtained power law dependence of the two point correlation function $\xi(r) = (r_0/r)^{1.8}$ can be obtained provided a sufficient number of iterations has been performed, *i.e.*, a sufficient length of “time” has elapsed.

Figure 6.8 shows the two point correlation function for the case of the QSSC based model. As “time” goes on, the slope of the correlation function gets closer and closer to -1.8 . From the value of the X-axis intercept of the two point correlation function it is possible to get a rough estimate of the size of the structures in units of the size of our simulation box. From our results we have estimated that the size of the structures formed is approximately $\beta = 0.15 - 0.3$ times the boxsize. If one sets these values equal to the observationally accepted value of r_0 , one can get a better physical sense of the results. If we set, $\beta = 0.3$, say, and $r_0 = 25h^{-1}$ Mpc, then the linear size of the simulation box would be $\sim 84h^{-1}$ Mpc.

The above exercise is an attempt to relate our toy model to a realistic cosmological scenario. The model per se talks of a ‘dimensionless’ box containing N points. With the above identification, we have 10^5 points in a volume of $(84h^{-1})^3$ (Mpc) 3 . Let us assign a mass of $10^n M_\odot$ to each point. We then get a cosmological smoothed out density of

$$\rho = \frac{10^{n+5} M_\odot}{(84h^{-1})^3 (Mpc)^3} = 0.6h \times 10^{n-12} \rho_c \quad (6.11)$$

where ρ_c is the critical density of the universe. Thus we get the density parameter $\Omega = 0.6h \times 10^{n-12}$. Setting this equal to unity (the QSSC does not have any limit on baryonic matter either from deuterium abundance or from CMBR anisotropy) we get for $h = 0.6$, a typical mass as $1.5 \times 10^{13} M_\odot$, suitable for a cluster.

Of course, as the above exercise shows, the results can be scaled up/down by rescaling the simulation parameters and thus are independent of the ‘absolute’ size of the box. A more detailed dynamical theory of the creation process will tell us how to relate the absolute size of clustering to the theoretical parameters.

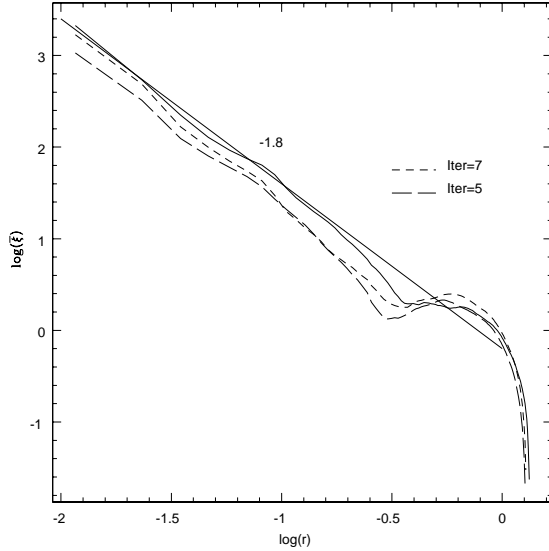


Figure 6.8: The two point correlation function for the QSSC based model. Here, $N = 100,000$ and $x = 0.3$. As “time” goes on, the curve approaches more and more closely the slope of -1.8 . The solid curve shows the result after 10 iterations.

6.5 Results and Summary

It must be stressed that these results are to be viewed as a preliminary report on a new scheme for generating structures in the Quasi Steady State Cosmology and quite a lot of follow up work has to be put into refining the model, so as to arrive at the values of the various parameters (chosen so far in an empirical way) from a deeper theoretical standpoint. Whatever the details of the creation process, the QSSC has repeated oscillations. We are trying to understand with

the help of probability theory and stochastic processes, how clustering develops through such an iterative programme.

The primary statistical indicator we have used in our analysis is the two point correlation function $\bar{\xi}(r)$. In order to further examine the statistical properties of the particle distribution, one must investigate the behaviour of higher moments and other quantities such as the “shape statistics”. Work analyzing the higher moments, scaling relations , shape statistics etc using algorithms such as counts in cells, is in progress.

However, the problem of formation of large scale structure being a complex one, it is desirable to keep the theoretical options open in the underlying cosmology. At the risk of stating the obvious, we should contrast the present approach from the standard approach to structure formation in the big bang cosmology. In the standard approach primordial fluctuations are postulated to begin with and their growth is studied under the effect of the gravitational field. Here, the main process which generates structures in the universe is the creation of matter around MCEs rather than gravitational instability. Our computer simulations show very clearly that the filament-cluster-void pattern observed in large scale structure can be generated simply from a creation algorithm. To what extent gravitational effects will further influence this picture remains to be seen. Although we have given preliminary ideas in subsection 6.2.1, a more detailed cosmogonic theory is also needed to tell us how coherent objects are ejected by mini-creation events.

The success of the present toy model, however, holds out hope for a better understanding of structure formation via this alternative route.

Chapter 7

Conclusions

I may not have gone where I intended to go, but I think I have ended up where I intended to be – Douglas Adams

In the previous chapters we have established some new and important results in the field of nonlinear gravitational clustering and have shown that it is possible to gain insights into the role of gravity in clustering and consequent formation of large scale structure. The coherent theme presented in this work dealt with existence and models for the universal aspects of gravitational clustering, via various mechanisms. We also critically examined the role of gravity in structure formation theories by studying alternate models for structure formation, thus taking an open minded approach to the problem.

We are led to the conclusion that there are universal phenomena in gravitational clustering and we have analysed the reason behind their existence to some extent, analytically and semi analytically. In chapter 2 we established the existence of *approximately* invariant profiles for two point correlation function which evolved in a manner similar to linear growth, at all scales. It was also shown that this universal form is related to the fixed point phenomena in power transfer, which is already well known in literature. The connection between these forms “units of nonlinear universe” and the universal nonlinear scaling relation proposed by Hamilton and others is also clearly established. Numerical verifica-

tion of these results required high resolution N body simulations, which in turn led to analysis of two dimensional gravity in the next chapter.

The next chapter tried to understand this result better by trying to understand the analytic framework underlying 2D simulations. In this work we have concluded that two dimensional structure formation simulations in an expanding background requires that we model it as parallel “infinite needles” with particles defined by the intersection of a plane orthogonal to these needles. We developed a $(D+1)$ dimensional model of structure formation and have discovered that all the other approaches to 2D gravity violate either physical or consistency constraints.

In the next chapter we have probed this connection further by addressing the existence of such Nonlinear Scaling Relations in two dimensions. Two dimensional simulations provided us with much higher resolution so that this question could be addressed in detail. We have conclusively shown that although such a relation does exist in two dimensions as well, the behaviour at nonlinear end indicated that the clusters do not display the stable clustering behaviour as expected from 3D simulations. Thus the slope at the nonlinear end for the scaling relation is not unity as would have been expected from a model based on standard stable clustering behaviour, contrary to some of the results claimed in literature. On the other hand, the results obtained supported the existence of a generalised ‘stable clustering’ that had been predicted earlier.

We followed the trail of results and attempted to understand stable clustering and late time behaviour of clustering systems in the universe in more detail. This led to a detailed analysis of the behaviour of single cluster without making the usual additional assumptions about strict spherical symmetry and so on. A careful modelling of the asymmetries that are generated during the collapse phase of a density perturbation allowed us to derive a completely natural (as opposed to

the *ad hoc*) procedure for stabilisation of a spherically collapsing system which was consistent with the usual results. However our results differed quantitatively from the values obtained in the standard spherical collapse model. This allowed us to establish the connection between the shear and vorticity terms in the equations and the averaged pairwise velocity ratio function which is a measure of stable clustering.

A critical examination of the role of gravity led us to investigate structure formation in Quasi Steady State Cosmology. The results of this investigation into a toy model without gravity (just expansion and creation of matter) indicate that it is possible to model some quantitative aspects of structure formation, such as the index of the two point correlation function by this process which is consistent with the accepted values. The visual images also reveal a clear cluster and void network which develops from a uniform distribution of particles. Statistical indicators such as minimal spanning trees which examine essentially all moments of the distribution reveal the growth of clustering in a manner comparable to growth of clustering in standard scenarios. Thus we have established that the observed two point correlation function with a slope of -1.8 can be obtained even in a model without gravitationally induced clustering.

The analysis of dark matter gravitational clustering process has led to the following results established in this thesis. There exist generic aspects to gravitational clustering the most notable being the existence of fixed points in the way power is transferred from large scales to small scales. This transfer of power leads to scaling laws for statistical quantities such as two point correlation functions which are to a great degree independent of background cosmology and the matter power spectra. These scaling laws whose existence enable us to study late time behavior of the system easily have been vindicated in numerous simulations both

in three and two dimensions. These two dimensional simulations which were intended to explore generic behavior of gravitational clustering led to a complete theoretical analysis of gravity in two dimensions which leads to greater coherence in the theoretical framework.

It remains an open problem to explain and understand how the actual particle motion in the simulation volume is connected with power transfer and with the existence of fixed points in evolution of these quantities. Some work which addresses the issue has indicated that the growth of power in small scales are caused by matter flows from large distances, essentially the central peaks gathering in the matter particles which flow along the regions of shocks or ‘caustics’ in the initial field. Thus the final configurations are connected to the initial Gaussian random field which are generated in inflationary scenarios for example.

It can be observed that the final structures that are formed at late times tend to be spherical (when they are not tidally disrupted or have significant amounts of angular momentum). The existing spherical collapse models suffer from the *ad hoc* nature of the mechanism used to halt the spiraling collapse. A more rigorous analysis of spherical collapse model, including the amplification of asymmetries in the system in the collapsing phase leads to different thresholds for formation of collapsed structures with respect to the standard spherical model upon which theories such as the Press Schechter formalism is based. A study of this ‘virialisation’ process is important in modeling the formation of clusters of galaxies and in analyzing quantities such as mass functions and their evolution.

These mass functions provide a quantitative measure of the dark matter wells in which the baryons can settle, cool and fragment and form the myriad structures that are observed. Connecting the observations with the semi empirical models of galaxy formation available currently as well as simulating the complete formation

scenario from dark matter to clusters and galaxies is the fundamental program of structure formation theories in the standard model.

This work is expected to lead us to a comprehensive model for baryonic structures. It is necessary to understand further the transfer of power in detail to explore generic features of gravity. This involves understanding second order effects which may be modelled by approximation schemes such as Zeldovich approximation. It is possible to separate the particles into categories based on their net displacement and compute the contributions to the power spectrum from each category. This avenue must be explored to understand the details of connections between particle motion and power transfer.

Subsequent to the formation of these clusters at high peaks at early times, the baryonic structures form a population of super massive stars, which serve as nuclei for galaxies at late times. A complete model for structure formation should be able to compute the initial star formation as well as the formation and propagation of radiation and ionization fronts in the neutral medium. This initial population of stars will lead to formation of super massive black holes and quasars and trigger of further star formation which may reionize the universe at a later epoch, leaving a signature on the cosmic microwave background.

In parallel with this, an alternative cosmological structure formation scenario explored in this thesis is the quasi steady state cosmology. In studying this model and attempting to understand the observational data in the light of this model, we were led to a greater understanding of the standard model itself and a set of stringent tests that may be designed to distinguish between the many cosmologies. A large number of statistical measures, such as minimal spanning trees, fractal dimension, cluster mass functions, measures of shapes and orientations etc are used as discriminators between models which leads to a larger array of tests of the

standard model *per se* which may cast further light on the formation processes. This model also brought to light an interesting question regarding power law profiles for two point correlation function which was generated even in a model devoid of gravitational clustering.

Existence of other universal aspects of gravity, such as density and potential profiles and their functional forms is another avenue which requires further exploration and is connected to the conclusions arrived at in this thesis.

As the observational data drives us toward the era of precision cosmology, it will be possible to analyse these universal aspects in greater detail by comparing simulation models convolved with observational and instrument effects with maps of the sky which is expected to expose much of the weaknesses as well as reveal the strengths of the current paradigms of cosmology and structure formation.

Bibliography

- [1] Smoot G.F. et al., Ap.J **396**,(1992).
- [2] Bennet C.L et al., Ap.J **464**,(1996).
- [3] Perlmutter S. et al., Ap.J **517**,(1990).
- [4] Bertschinger E., Ap.JS **58**,1985
- [5] Berentzen I. et al., **astro-ph/0301300**,(2003).
- [6] Alimi J.M., Bouchet F.R., Pellat R., Sygnet J.F. and Moutarde F., Ap.J **354**,(1990).
- [7] J.S.Bagla, S. Engineer and T. Padmanabhan,Ap.J **498**,(1998).
(<http://xxx.lanl.gov/astro-ph/9707330>)
- [8] Bagla J.S. and Padmanabhan T. *Proceedings of the sixth Asia Pacific regional Meeting of the IAU, ed. V.K.Kapahi et al,* Special supplement to the Journal of Astronomy and Astrophysics 16, **77**,(1995).
- [9] Bagla J.S. and Padmanabhan T., Pramana-J.Phys **42**,(1996).
- [10] Bagla J.S and Padmanabhan T., MNRAS, (1997).
- [11] Bagla J.S. and Padmanabhan T., MNRAS **286**, 1023,(1997).
- [12] Banerjee, S. K., & Narlikar, J. V., Ap.J **487**, 69,(1997).

- [13] Banerjee, S. K., Narlikar, J. V., Hoyle, F., Burbidge, G. & Sandage, A. preprint,(1999).
- [14] Davis, M. and Peebles, P. J. E., Ap.J.S **34**, 425,(1977).
- [15] Deser S., Jackiw R. and t'Hooft G., Annals of Phys. **152**,(1984).
- [16] S. Engineer, Nissim Kanekar and T. Padmanabhan, MNRAS **314**, (2000). (<http://xxx.lanl.gov/astro-ph/9812452>)
- [17] S.Engineer,
K.Srinivasan, T. Padmanabhan,Ap.J **512**,(1999). (<http://xxx.lanl.gov/astro-ph/9805192>)
- [18] Filmore J.A. and Goldreich P. Ap.J **281**, 1,(1984).
- [19] Hamilton A.J.S., Kumar P., Lu E. and Mathews A., Ap.J **374**,L1, (1991).
- [20] Hoyle, F., Burbidge, G., & Narlikar, J. V., Ap.J **410**, 437,(1993).
- [21] Hoyle, F., Burbidge, G., & Narlikar, J. V., MNRAS **267**, 1007,(1994).
- [22] Hoyle, F., Burbidge, G., & Narlikar, J. V., A&A **289**, 729,(1994).
- [23] Hoyle, F., Burbidge, G., & Narlikar, J. V., Proc. Roy. Soc. A **448**, 191,(1995).
- [24] Hoyle, F., Burbidge, G., & Narlikar, J. V., MNRAS **277**, L1,(1995).
- [25] Hoyle, F., & Narlikar, J. V., Proc. Roy. Soc. London, A **282**, 191,(1964).
- [26] Hoyle, F., & Narlikar, J. V., Proc. Roy. Soc. London, A **294**, 138,(1996).
- [27] Kanekar, N, Ap.J,**512**, astro-ph:9812203,(1999).

- [28] Landau L. and Lifshitz E., *Classical Theory of Fields* (Pergamon Press),(1975).
- [29] McClelland J. and Silk, J., Ap.J **217**, 331,(1977).
- [30] Mo H.J.,Jain B. and White S.D.M., MNRAS **276**, L25,(1995).
- [31] Munshi D., Chiang L., Coles P. and Melott A.L., astro-ph/9707259,(1997).
- [32] Navarro J.F, Frenk C.S and White S.D.M, Ap.J **462**, 563,(1996).
- [33] A.Nayeri, S.Engineer, J.V.Narlikar and F. Hoyle, Ap.J **525**,(1999).
- [34] Nityananda R. and Padmanabhan T, MNRAS,**271**, 976,(1994).
- [35] Padmanabhan,T.,Physics Reports,**188**, 285,(1990).
- [36] Padmanabhan T., *Structure Formation in the Universe* (Cambridge University Press),(1994).
- [37] Padmanabhan T.,MNRAS,**278**, L29,(1996).
- [38] Padmanabhan, T.,*Cosmology and Astrophysics - through problems*, Cambridge University Press, Cambridge, (1996).
- [39] Padmanabhan T.,*Proceedings of 36th Herstmonceux Conference, Edited by Ofer Lahav, E.Terlevich and R.Terlevich*, Cambridge University Press,(1996).
- [40] Padmanabhan. T,*Proceedings of ICGC-95 held at IUCAA, Pune, India, Edited by S. Dhurandhar and T. Padmanabhan*, Kluwer,(1997).
- [41] T. Padmanabhan and S. Engineer,Ap.J **493**,(1998).
[\(http://xxx.lanl.gov/astro-ph/9704224\)](http://xxx.lanl.gov/astro-ph/9704224)

- [42] Padmanabhan T., Cen R., Ostriker J.P. and Summers F.J., Ap.J **466**, 604,(1996).
- [43] Peacock J.A and Dodds S.J., MNRAS **267**, 1020,(1994).
- [44] Peacock J.A and Dodds S.J., MNRAS **280**, L19,(1996).
- [45] Peebles P.J.E., *Large Scale Structure of the Universe*, Princeton Univ. Press, Princeton, NJ,(1980).
- [46] Peebles, P. J. E., *Principles of physical cosmology*, Princeton University Press, Princeton, New Jersey,(1993).
- [47] Press, W. H. & Schechter, P., Ap.J **187**, 425-438,(1974).
- [48] Ruamsuwan, L. & Fry, J. N., Ap. J, **396**,416,(1992).
- [49] Sachs, R., & Narlikar, J. V., & Hoyle, F., A&A **313**, 703,(1996).
- [50] Sathyaprakash B.S., Sahni V., Munshi D., Pogosyan D. and Melott A.L., MNRAS **275**,(1995).
- [51] Shandarin S.F. and Zeldovich Ya. B., Rev. Mod. Phys. **61**,(1989).
- [52] Sheth, R. K., MNRAS, **300** 1057,(1998).
- [53] Sheth R. and Jain B., MNRAS,**285** 231,(1997).
- [54] Raychaudhury, Somak, Colless, M., & Hola, R., Proceedings of the 35th Herstmonceux Conference on *Wide-Field Spectroscopy and the Distant Universe*, Cambridge 1994, World Scientific.
- [55] Tamman, G.A, Second International Conference on Dark Matter in Astro and Particle Physics (DARK98), Heidelberg, Germany, July 20-25, (1998).

- [56] Valinia A., Shapiro P.R., Martel H. and Vishniac E.T., Ap.J **479**,(1997).
- [57] Yano, T. and Gouda, N., Ap.J **487**, 473,(1997).
- [58] Zeldovich Y.B, A&A **5**,(1970).